AN ABSTRACT OF THE THESIS OF

Ill-Keun Rhee for the degree of Doctor of Philosophy in Electrical and Computer Engineering presented on February 23, 1990.

Title: Nonlinear Approach to the Direction Finding Problem in Array Processing

Redacted for Privacy

Abstract approved: _____

Ronald R. Mohler

In sonar or radar array processing, one of the most important objectives is to estimate the angles of incidence of distant source signals in a noisy environment. The standard eigenstructure-based method, which is known to yield high resolution spectral estimates for solving the direction finding problem, relies on the assumption that additive sensor noises are white Gaussian processes that are spatially uncorrelated between sensors. In the cases of correlated noise fields, non-Gaussian noises, highly correlated source signals, relatively low signal-to-noise (S/N) ratio, and/or very closely located source signals, direction finding performance based on the standard eigenstructure algorithm is severely degraded.

For this study, the (ordinary) nonlinear second-order method (SOM) and revised nonlinear SOM, along with the

generalized eigenstructure algorithm, which decorrelates correlated noise fields with known or estimated noise correlation coefficients, are discussed.

Ordinary and revised SOMs produce new data sequences, or "second-order signals", by auto-convolution of the original data sequences that were corrupted by additive noises on the sensor array. By reference to appropriate algebraic calculations, an eigenstructure orthogonality relationship, which is similar to the classical first-order method (FOM) that deals directly with original data sequences, is derived.

It is also demonstrated that the revised SOM can be used more effectively than the (ordinary) SOM in conjunction with an FOM, such as multiple-signal classification (MUSIC) or many of its subsequent variations, to accommodate troublesome cases such as closely located multiple (coherent) sources, limited numbers of sensors, correlated Gaussian noises lacking information on the noise correlation coefficients, non-Gaussian noises, and a low S/N ratio. Based on computer simulation, examples of analysis and estimations for the direction finding problems in several environments are provided.

Furthermore, the theoretical derivations of the S/N ratios for the FOM and SOM, as well as the threshold S/N ratios for very closely spaced multiple sources and a

statistical consideration of the computer simulation results, are presented.

Nonlinear Approach to the Direction Finding Problem in Array Processing

by

Ill-Keun Rhee

A THESIS

submitted to

Oregon State University

in partial fulfillment of
the requirements for the
degree of

Doctor of Philosophy

Completed February 23, 1990

Commencement June 1990

APPROVED:

Redacted for Privacy

Professor of Electrical and Computer Engineering in charge of major

Redacted for Privacy

Head of Department of Electrical and Computer Engineering

Redacted for Privacy

Dean of Graduate School

Date thesis is presented February 23, 1990

Typed for Ill-Keun Rhee

Acknowledgements

"· · · the truth shall make you free."
(St. John 8:32)

I wish to express my gratitude to my major professor R. Mohler for his support, guidance and friendship during each stage of this work. I also thank professors R. Engelbrecht, W. Kolodziej, A. Pacut and R. Burton for serving on my committee and their helpful comments. Special thanks are extended to Mr. S. K. Park and Mr. H. Rolnik for their helpful discussions and friendships.

I would also like to thank my wife In-Kyeong and my daughter Misoo, for their unending love, encouragement and patience. Finally, sincere appreciation and love are extended to my father General Joon-Soo Rhee, my mother Jung-Soon, my brother Hyeong-Keun, and my sister Eun-Sook for their many sacrifices, invaluable encouragement and support.

The research leading to this dissertation was supported by the Office of Naval Research under Grant number N00014-81-0814.

Table of Contents

Table of Contents (continued)

Chapter Page

List of Figures

List of Figures (continued)

List of Figures (continued)

List of Figures (continued)

List of Figures (continued)

List of Figures (continued)

List of Tables

List of Tables (continued)

Nonlinear Approach to the Direction Finding Problem In Array Processing

CHAPTER 1

INTRODUCTION

Array processing is concerned with processing received data that has been contaminated by noises from a spatially distributed array of sensors. One of the primary goals of passive sonar or radar array processing is to estimate the intensity of a signal in a given noisy environment as a function of the frequency and wavenumber vector, or of the angles of incidence of distant source signals. This takes the form of a parameter estimation problem and is similar in many respects to spectral estimation processes. Therefore, the directions of distant source signals can be extracted by the identification of the sharpest peaks of the spatial frequency power spectrum of received signals with additive noises on the sensor array. A number of spectral estimation techniques [9,14,17,21,38,43] for solution of the direction finding problem have been developed over the last decade and more.

On the other hand, in recent years, several authors [2,3,7,18,29,32,39,45] have adapted standard eigenstructure-based methods, which are known to yield high resolution estimates even when the source signals are partially coherent, to the direction finding problem. The significance of source signal coherence may evolve from signal reverberation (e.g., underwater acoustics) or from jamming.

The second chapter of this study includes a consideration of the first-order method (FOM), defined as a method for the direct accommodation of the original data received from the sensor array. The signal and noise model used for solution of the direction finding problem in array processing is described. Since finite data samples and limited numbers of sensors in an array impose limitations upon resolution of the multiple source directions, the resolution limits which provide the general criterion for most direction-finding methods developed to this date are then discussed and a classical Bartlett spectrum, an auto-regressive (AR) spectral estimate, and a maximum likelihood (ML) spectral estimate are described as examples of spectral estimation methods in order to compare them with the standard eigenstructure-based method, which utilizes eigenvectors corresponding to the smallest eigenvalues (in the noise subspace) of the received-data covariance matrix (or the periodogram spectrum). Examples of the Bartlett, ML, and

AR spectra are provided, with performance comparisons. The well-known multiple signal classification (MUSIC) technique is shown as an example of the FOM, using a standard eigenstructure algorithm which is suitable to situations of low S/N ratio and closely spaced source signals, in comparison to the methods previously considered. In addition, comparisons are made for the MUSIC, and other spectral estimation methods considered, focusing on their resolution capabilities. The standard eigenstructure algorithm requires that the additive sensor noises are spatially white Gaussian and uncorrelated from sensor to sensor. However, there are practical situations where the noise fields can be strongly correlated and a generalized eigenstructure algorithm, which decorrelates correlated noise fields, is introduced. This algorithm can be applied to most direction finding techniques for which the noise correlation coefficient is known or can be accurately estimated. Examples are provided to demonstrate the validity of this generalized eigenstructure algorithm.

In theory, the eigenstructure algorithm offers the determination of the number of source signals from a multiplicity of the smallest eigenvalues of the spatial array covariance matrix. In a practical sense, however, the spatial array covariance matrix is unknown [28] and the covariance matrix must be estimated from a finite sample size. This results in the differentiation of

eigenvalues with probability one, thus making it difficult to determine the number of source signals merely by examination of eigenvalues obtained from the estimated received-data covariance matrix. To conclude this chapter, the information theoretic criteria proposed in Akaike's [1] information criterion (AIC) and Schwartz-Rissanen's [34,41] minimum description length (MDL) method are used to correctly determine the number of source signals. (Computer simulation results for these information theoretic criteria are provided.)

From a practical point of view, the situation, in which noise fields are spatially correlated without information on the noise correlation coefficients, can be met. Chapter 3 includes a discussion of the second-order method (SOM), initially developed by Bugnon and Mohler [4]. This method accommodates "second-order signals" by auto-convolution of the received original data sequences on the sensor array in order to cope with troublesome situations such as a very low signal-to-noise (S/N) ratio and/or closely spaced source signals. Bugnon, Mohler, and Rhee [5] have shown that the (ordinary) SOM can be applied successfully to the cases of not only (partially) correlated noises between sensors, without knowledge of the noise-correlation coefficient, but also non-Gaussian noises like uniformly distributed random noises. A new SOM, or "revised SOM", is introduced, based upon use of a new covariance matrix that gives more accurate and sharper

peaks than the ordinary SOM in the instances of closely located multiple (correlated) sources, limited numbers of sensors, correlated Gaussian noises with or without noise correlation coefficient information, non-Gaussian noises, and/or low S/N ratios. SOMs do not compete with, but rather can be combined with, most FOMs to improve source direction estimation. A spatial smoothing method [33,42] can be then combined with the (ordinary) and revised SOMs to resolve the direction finding problem for totally coherent source signals and correlated sensor noises.

In Chapter 4 the FOM, (ordinary) SOM and revised SOM are compared, providing concrete examples, including single source detection with uncorrelated/correlated sensor noises at a low S/N ratio and the resolution capabilities of the uncorrelated/correlated, closely spaced, multiple source signals with Gaussian as well as non-Gaussian noises.

In Chapter 5, the degree to which the SOM is superior to the FOM with respect to the S/N ratio is discussed. Also, threshold S/N ratios expressions for the FOM and SOM are derived for situations when multiple sources are closely spaced. These quantified results readily indicate that the SOM resolves closely spaced multiple sources better than the FOM. Simulation results are obtained by conducting several runs, comparing the theories for the threshold S/N ratios. In addition, the envelopes in which the SOM can resolve multiple source

directions better than the FOM are demonstrated for both equipowered and non-equipowered sources. Also, the Estimation of Signal Parameter via Rotational Invariance Techniques (ESPRIT) [27,37] is introduced and compared with the SOM, briefly. The modified direction finding scheme, which makes the array covriance matrix hermitian Toeplitz by taking average values of diagonal and off-diagonal elements of the sample array covariance matrix where those matrix element values are practically all different, can somewhat improve the resolution of multiple source directions.

Lastly, this study is summarized and conclusions are presented in Chapter 6.

Symbols and Notation

$*$ Complex conjugate transpose

$\otimes$ Convolution operator

Δ Delta product performing a component to component multiplication of two matrices

λ Wavelength

ρ Correlation coefficient of sensor noises

T Transpose of the matrix or vector

c Speed of planewave propagation

D Sensor spacing

F Fourier transform operator

f_o Center frequency of the planewave

f_s Temporal sampling Frequency

M Number of sources

N Number of data points

Q Number of sensors

$[S/N]_f$ Signal-to-noise ratio for the first-order method

$[S/N]_s$ Signal-to-noise ratio for the second-order method

CHAPTER 2

FIRST-ORDER DIRECTION FINDING METHODS

In this chapter, several first-order methods for finding the directions of source signals arriving at sensor arrays are discussed. To solve the direction finding problem, the signal and noise model array processing must first be derived.

2.1 Signal and Noise Model

First, the problem of resolving the arrival directions of multiple source signals incident to a sensor array in the presense of background noise is considered.

When the M source signals are impinging on the uniform linear array with Q sensors from directions $\{\theta_1, \theta_2, \cdots, \theta_M\}$, signals received at the ith sensor can be expressed as

$$r_i(t) = \sum_{l=1}^{M} s_l(t-(i-1)(D/c)\sin\theta_l) + x_i(t) , \qquad (2-1)$$

where

$s_l(\cdot)$ = signal emitted by the lth source,

θ_l = direction angle of the lth source, and

$x_i(t)$ = additive noise at the ith sensor, and $x(1)$, $x(2)$, ..., $x(N)$ are independent and identically distributed (i.i.d.) .

For one-dimensional plane wave sources (Fig. 2-1), the characteristics of which are discussed in Appendix A, Eq.(2-1) can be written as

$$r_i(t) = \sum_{l=1}^{M} \exp\{j\omega_o t - jk_l x_{ki}\} + x_i(t) \quad , \tag{2-2}$$

where

$k_l = (\omega_o/c)D \sin\theta_l = k_o D \sin\theta_l$ (the normalized spatial frequency or angular wavenumber with respect to the x-axis), and (2-3)

$x_{ki} = (i - 1)$. (2-4)

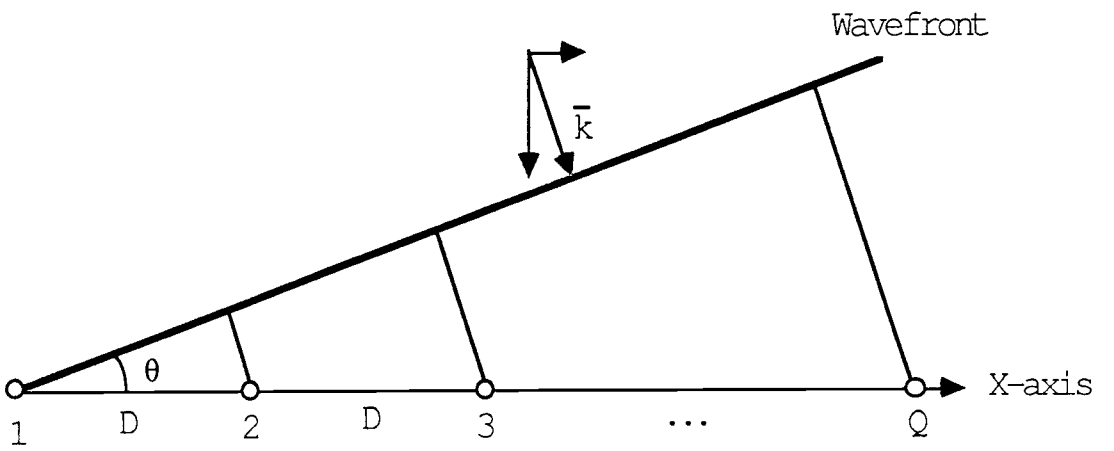

Fig. 2-1 Configuration for a plane wave impinging on the sensor array.

Generally, the plane wave sources can be expressed in three dimensions (Fig. 2-2) as

$$r_i(t) = \sum_{l=1}^{M} \exp\{j\omega_o t - \mathbf{k}^T\mathbf{r}\}, \qquad (2\text{-}5)$$

where

$\mathbf{k}^T = [k_x \; k_y \; k_z]$

$= (\omega_o D/c)\,[(\sin\theta_l)(\sin\phi_l), (\cos\theta_l)(\sin\phi_l), (\cos\phi_l)]$ (the normalized wave-number vector), and

$\mathbf{r}^T = [x_k \; y_k \; z_k]$ (the positional vector).

Fig. 2-2 shows the graphical description of the plane wave, in which the plane surface perpendicular to the direction of $\mathbf{k}$ is referred to as the wavefront.

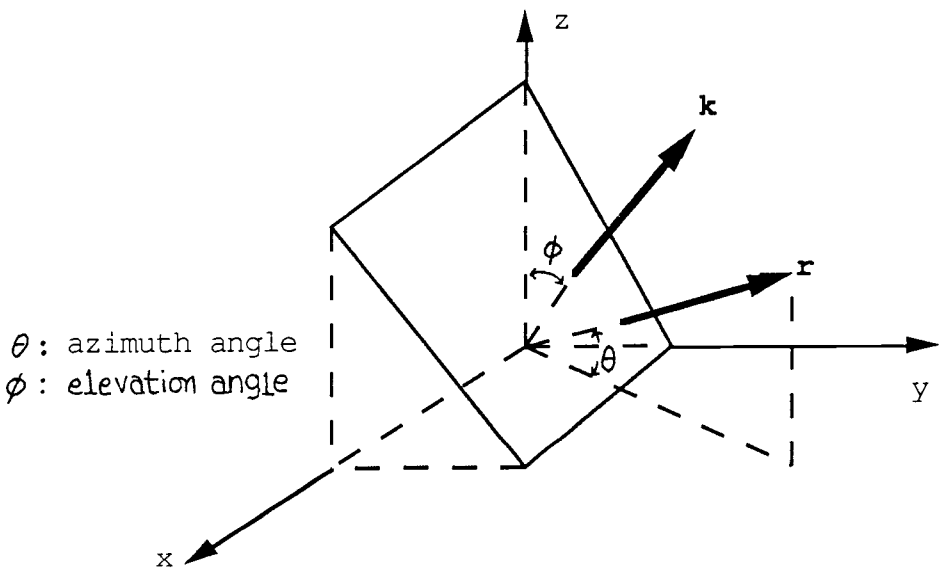

Fig. 2-2 Three-dimensional plane wave.

In this study, for the sake of simplicity, we consider only one-dimensional cases, such as Eqs.(2-2),

(2-3), and (2-4), are considered, unless otherwise noted. To obtain the received-data from the sensor array, the signals are sampled according to both temporal and spatial sampling theorems, i.e., to avoid temporal and spatial aliasing effects arising from the time and space sampling processes, the temporal sampling frequency f_s must be greater than or equal to twice the center frequency f_o of the plane wave. In the same manner, the spatial sampling frequency $(1/D)$ should be greater than or equal to twice the spatial frequency of the wave $(1/\lambda)$, where λ is the wavelength equal to $(2\pi/k)=(c/f_o)$. Thus, we have the sampling time

$$T_s = (1/f_s) \leq (1/(2f_o)), \tag{2-6}$$

and

$$D \leq (\lambda/2) = (1/2)(c/f_o) . \tag{2-7}$$

Furthermore, since the magnitude of $(\sin\theta_1)$ is less than one, from Eqs.(2-3) and (2-4) the sampling condition forces k_1 to lie within the Nyquist interval $(-\pi \leq k_1 \leq \pi)$. Then rewriting Eq.(2-2) as

$$r_i(t) = \sum_{1=1}^{M} s_1(t) \exp\{-j\omega_o(i-1)(D/c)\sin\theta_1\} + x_i(t) \tag{2-8}$$

and letting

$$\omega_{i1} = \omega_o(i-1)(D/c)\sin\theta_1 , \tag{2-9}$$

the received signals on the sensor array can be expressed

in the vector form:

$$\mathbf{r}(t) = \sum_{l=1}^{M} \mathbf{a}(\theta_l) s_l(t) + \mathbf{x}(t), \tag{2-10}$$

or

$$\mathbf{r}(t) = \mathbf{A}_1 \mathbf{s}(t) + \mathbf{x}(t), \tag{2-11}$$

where

$$\mathbf{r}^T(t) = [r_1(t), r_2(t), \ldots, r_Q(t)], \tag{2-12}$$

$$\mathbf{s}^T(t) = [s_1(t), s_2(t), \ldots, s_M(t)], \tag{2-13}$$

and

$$\mathbf{x}^T(t) = [x_1(t), x_2(t), \ldots, x_Q(t)]; \tag{2-14}$$

and where $\mathbf{A}_1$ is a $Q \times M$ direction matrix of the FOM whose columns are directional-vectors, expressed as

$$\mathbf{a}^T(\theta_l) = [1, \exp(-j\omega_{21}), \ldots., \exp(-j\omega_{Ql})]. \tag{2-15}$$

If the source signals are modeled as stationary (zero-mean) stochastic processes they are assumed to possess a positive definite matrix **P**. On the other hand, if the source signals are modeled as deterministic signals with zero-sample mean, then it is assumed that

$$\mathbf{P} = (1/N) \sum_{t=1}^{N} \mathbf{s}(t)\mathbf{s}^*(t) \ , \quad \text{for large } N \tag{2-16}$$

is exist and is positive definite <persistent excitation condition>.

Assuming that the additive noises are zero-mean and uncorrelated to the source signals, the following sample array covariance matrix, corresponding to Eq.(2-11), is given by:

$$\mathbf{R} = \mathbf{A}_1\mathbf{P}\mathbf{A}_1^* + E[\mathbf{x}(t)\mathbf{x}^*(t)], \qquad (2\text{-}17)$$

where the noise sample covariance matrix approaches to true noise covariance matrix for large N.

For two jointly stationary random signals $u_i(t)$ and $u_j(t)$ are called uncorrelated if $\rho_{ij}=0$, correlated if $0<|\rho_{ij}|<1$, and coherent if $\rho_{ij}=1$, where

$$\rho_{ij} = E[u_i(t)u_j^*(t)]/(E[|u_i(t)|^2]E[|u_j(t)|^2])^{1/2}.$$

On the other hand, for the deterministic signals, ρ_{ij} can be expressed as

$$\rho_{ij} = |P_{ij}|^2/(P_iP_j) \quad \text{for large } N,$$

where

$$P_{ij} = (1/N)\sum_{t=1}^{N} u_i(t)u_j^*(t) \ ,$$

$$P_i = (1/N)\sum_{t=1}^{N} |u_i(t)|^2 \ , \qquad \text{and} \quad P_j = (1/N)\sum_{t=1}^{N} |u_j(t)|^2 \ .$$

Note that if the sources are uncorrelated with respect to each other, the source covariance matrix $\mathbf{P}$ is diagonal and nonsingular; if the sources are correlated, then $\mathbf{P}$ is nondiagonal and nonsingular. Coherent sources make $\mathbf{P}$ nondiagonal, but singular.

If the noises are uncorrelated between sensors and have the constant variances σ^2, then

$$\mathbf{R} = \mathbf{A}_1\mathbf{P}\mathbf{A}_1^* + \sigma^2\mathbf{I}_Q \,, \tag{2-18}$$

where $\mathbf{I}_Q$ is the $Q \times Q$ identity matrix.

2.2 Resolution Limit

In the case of a limited number of data sequences and a limited number of sensors, the resolution capability is one of the key issues in contemporary direction-finding estimation. In this section, the broadly accepted resolution criterion initiated by Rayleigh [31] is considered. As a rule, for temporal (spatial) spectral analysis, the spectral resolution limit is approximately the reciprocal of the signal observation time (effective aperture of the array), i.e.,

$$T_e B_e = 1$$

where T_e is the temporal (spatial) observation time and B_e is the temporal (spatial) bandwidth. This relationship is called the time-bandwidth product (TBP). Modification of the relationship required for random signal cases has been explained by Marple [25]. However, the TBP does not explicitly quantify the capability of resolving a spectral response due to two or more signals. As a result, a number of proposed definitions of resolution have appeared in the literature, most of which concern the capability of

resolving the desired angles of two adjacient sinusoids. These definitions rely on some measure of how close the two sinusoids may be before their spectral responses are indistinguishable. High resolution direction-finding methods effectively extrapolate the measured signal beyond its observed interval. This effectively makes T_e larger, while B_e becomes smaller and the resolution is correspondingly improved.

The following example provides a specific illustration of the resolution limit of a plane wave in array processing. Consider a plane wave with a center frequency f_o and the normalized spatial frequency $k_n=(\omega_o/c)D\sin\theta$. It follows, then, that

$$s(x,t) = \exp(j\omega_o t - jk_n x) \quad , \quad 0 \le x \le Q-1$$

where Q represents the number of sensors. Taking a spatial Fourier transform of $s(x,t)$,

$$S(k,t) = \sum_{x=0}^{Q-1} \exp(j\omega_o t - jk_n x)\exp(jkx)$$

$$= \exp(j\omega_o t) \sum_{x=0}^{Q-1} \exp\{j(k-k_n)x\}$$

$$= \exp(j\omega_o t)\left[\frac{1-\exp[j(k-k_n)Q]}{1-\exp[j(k-k_n)]}\right]$$

$$= \exp(j\omega_o t)\exp[j(k-k_n)(Q-1)/2]\left[\frac{\sin[(k-k_n)Q/2]}{\sin[(k-k_n)/2]}\right].$$

The magnitude of the spectrum of $s(x,t)$ is depicted in Fig. 2-3. Its resolution capability, expressed in terms of normalized spatial frequency, is limited to the width

$$\Delta k = (2\pi/Q).$$

Furthermore, by letting $\Delta k = (2\pi D/\lambda)\Delta\theta$, the approximate resolution limit of the direction angles can be obtained as $\Delta\theta = (\lambda/(QD))$, or $\Delta\theta = (2/Q)$, if $D = (\lambda/2)$.

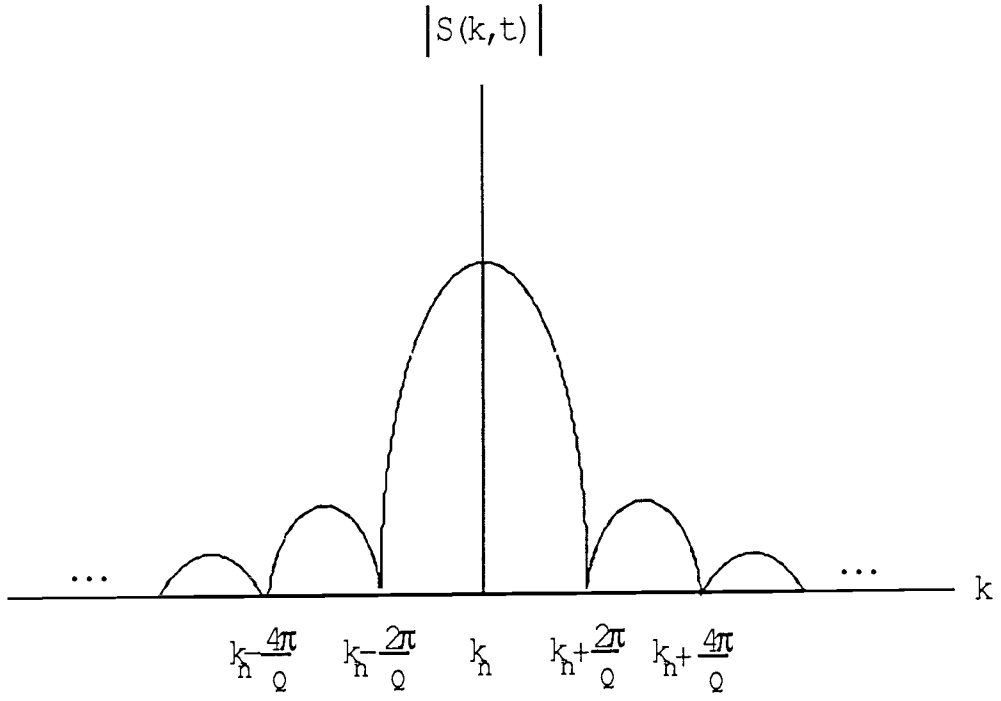

Fig. 2-3 Magnitude of spatial spectrum of a complex sinusoidal wave incident on the array with Q sensors.

2.3 Classical Bartlett, Auto-regressive, and Maximum-likelihood Spectral Estimation Methods

As one of the first-order spectral estimation methods, first, consider the classical Bartlett spectral estimate, which is a typical example of the Fourier method. The Bartlett method takes the spatial Fourier transform of the windowed array covariance function to obtain the classical Bartlett spectrum,

$$\hat{D}(\theta) = \sum_{i=-Q}^{Q} W_B(i) R_i \exp(jkx_i), \tag{2-19}$$

where

$$k = (\omega_o/c) D \sin\theta , \tag{2-20}$$

$$x_i = (i - 1) ,$$

$$R_{i=m-n+1} = E[r_m(t) r_n^*(t)], \quad i,m,n = 1,2,\ldots,Q , \tag{2-21}$$

and $W_B(i)$ is the Bartlett window, defined as

$$W_B(i) = \begin{cases} (1/(Q+1))(Q+1-|i|), & -Q \le i \le Q \\ 0 & \text{elsewhere} . \end{cases} \tag{2-22}$$

With respect to the directional-vector of Eq. (2-15), the array covariance matrix can then be expressed as

$$\mathbf{R} = \sum_{l=1}^{M} \sum_{m=1}^{M} E[s_l s_m^*] \mathbf{a}(\theta_l) \mathbf{a}^*(\theta_m) + E[\mathbf{x}\mathbf{x}^*] . \tag{2-23}$$

Assuming that between themselves the sources are incoherent and the sensor noises are spatially uncorrelated with constant variances σ^2, Eq. (2-23) can be rewritten as

$$\mathbf{R} = \sum_{I=1}^{M} E[s_I s_I^*]\mathbf{a}(\theta_I)\mathbf{a}^*(\theta_I) + \sigma^2\mathbf{I} \ . \qquad (2\text{-}24)$$

Then introducing the Q x 1 searching vector $\mathbf{a}(\theta)$ as

$$\mathbf{a}^T(\theta) = [1, \exp(-jkx_2), \ldots, \exp(-jkx_Q)] \ , \qquad (2\text{-}25)$$

Eq. (2-19) can be expressed as

$$\hat{D}_{BT}(\theta) = \mathbf{a}^*(\theta)\mathbf{R}\mathbf{a}(\theta) \qquad (2\text{-}26)$$

by neglecting the scaling factor $(1/(Q+1))$.

Two additional spectral estimates [8,26,30,38] can be considered. The auto-regressive (AR) estimate, also known as maximum entropy (ME) or Burg's spectral estimate, takes the form

$$\hat{D}_{AR}(\theta) = \left[|\mathbf{a}^*(\theta)\mathbf{R}^{-1}\mathbf{u}_o|^2 \right]^{-1} , \qquad (2\text{-}27)$$

where $\mathbf{u}_o^T = [1,0,0,\cdots,0]$, which is the unit vector composed of one followed by $Q-1$ zeros.

The second spectral estimate example of the spectral estimate is the maximum-likelihood (ML), or minimum variance (MV), estimate expressed as

$$\hat{D}_{MV}(\theta) = \left[\mathbf{a}^*(\theta)\mathbf{R}^{-1}\mathbf{a}(\theta) \right]^{-1} . \qquad (2\text{-}28)$$

The AR and MV estimates work very well so long as the S/N ratios are fairly high. For multiple source signals, the resolvability properties of the AR and MV estimates improve when both the S/N ratios and the number of sensors increase if the desired angles of source signals impinging on the sensor array are well separated from each other (i.e., satisfying the Rayleigh resolution limit by more than $(2/Q)$ [rad]).

As shown in the following example, at the desired angles the AR spectral estimate exhibits sharper peaks than the Bartlett spectral estimate.

Example 2.1 Figs. 2-4 and 2-5 represent the resolution limits of the Bartlett method with three and five sensors, respectively. It can easily be seen that the Rayleigh resolution limit improves as the number of sensors is increased.

Fig. 2-6 shows the Bartlett, ML, and AR spectral estimates as given in Eqs.(2-26), (2-27), and (2-28), respectively, for two pure sinusoidal waves at $\theta_1 = 15^\circ$ and $\theta_2 = 55^\circ$ with five sensors, where additive sensor noises are white Gaussian and uncorrelated between sensors, at S/N = 16.9 dB. It may be observed that the AR spectrum has sharper and deeper spectral peaks than the Bartlett and the ML spectra. Maintaining S/N = 16.9 dB, the number of sensors decreased to three in Fig. 2-7, in which

it may be obsersed that all spectra tend to worsen. In particular, the Bartlett spectrum cannot resolve the two peaks. The effect of decreasing the S/N ratio is shown in Fig. 2-8, in which all spectra again worsen as the S/N ratio is changed decreased to 10.9 dB. In all three cases, Figs. 2-6, 2-7, and 2-8, the AR spectrum is shown at best solution for resolving the direction-angles of multiple sources.

Finally, Figs. 2-9 and 2-10 indicate how the AR resolution capabilities of the single source and two source signals, respectively, change in terms of the number of sensors. From both figures it is easily shown that the resolution increases with an increase in the number of sensors.

The apparent resolution of the MV spectral estimate is poorer than that of the AR estimate, but is better than the classical Bartlett method. Cox [10] has quantified the resolution capability of the MV method. While other studies have related that the AR spectral estimate clearly justifies the statement that the MV estimate shows less resolution than the AR estimate. Burg [6] showed the relationship between AR and MV spectral estimates takes the form

$$[D_{MV}]^{-1} = (1/Q) \sum_{k=1}^{Q} [D_{AR}]^{-1} ,$$

i.e., the reciprocal of the MV spectral estimate is equal

to the average of the reciprocals of the AR spectral estimates from 1 to Q. The lower resolution of the MV spectral estimate relative to the AR estimate observed is, in practical terms, due to the averaging effect of the AR spectra of the least resolution for a small number of sensors, mixed with the AR spectra of the highest resolution for a large number of sensors. For large data records, the variance of the MV spectral estimate has been observed empirically to be less than an AR spectral estimate of identical number of sensors [23]. Moreover, the relationships between resolution, the number of sensors, the S/N ratio and the bias for the estimates considered above have been firmly established [23,24,38].

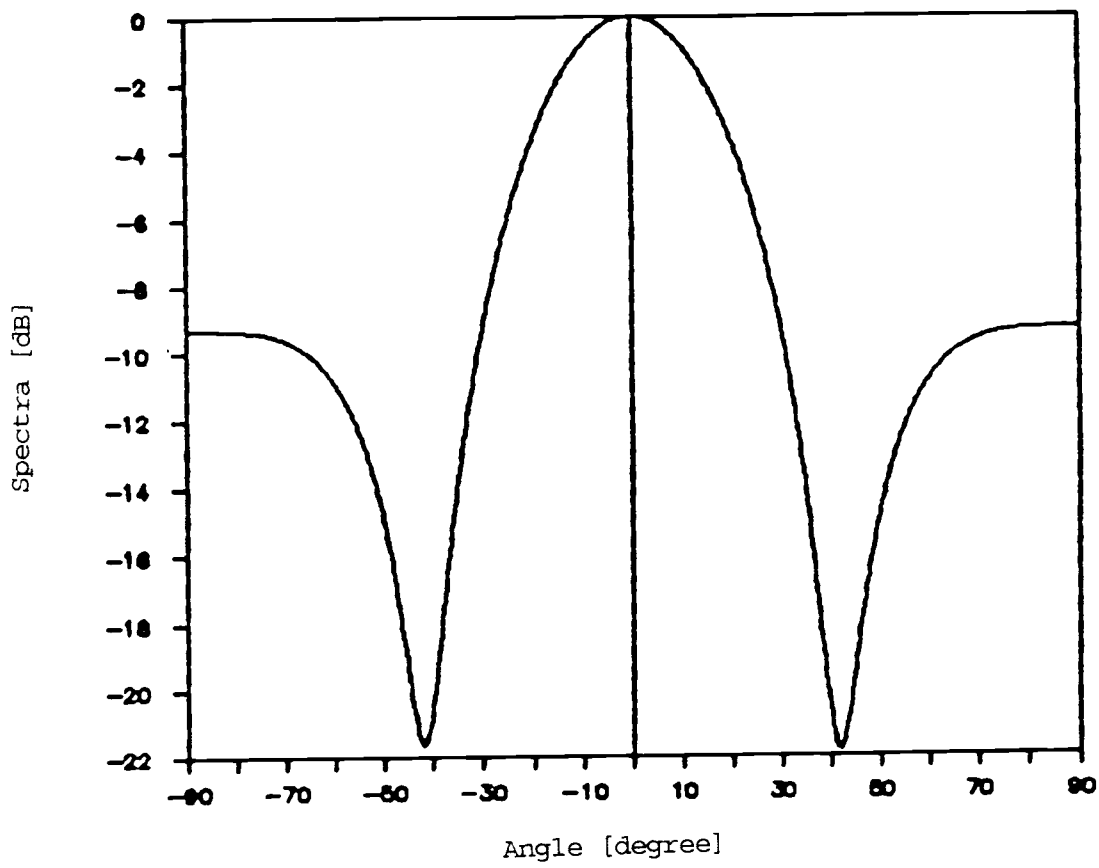

Fig.2-4. Bartlett Spectrum with 3 Sensors at S/N=16.9 dB.

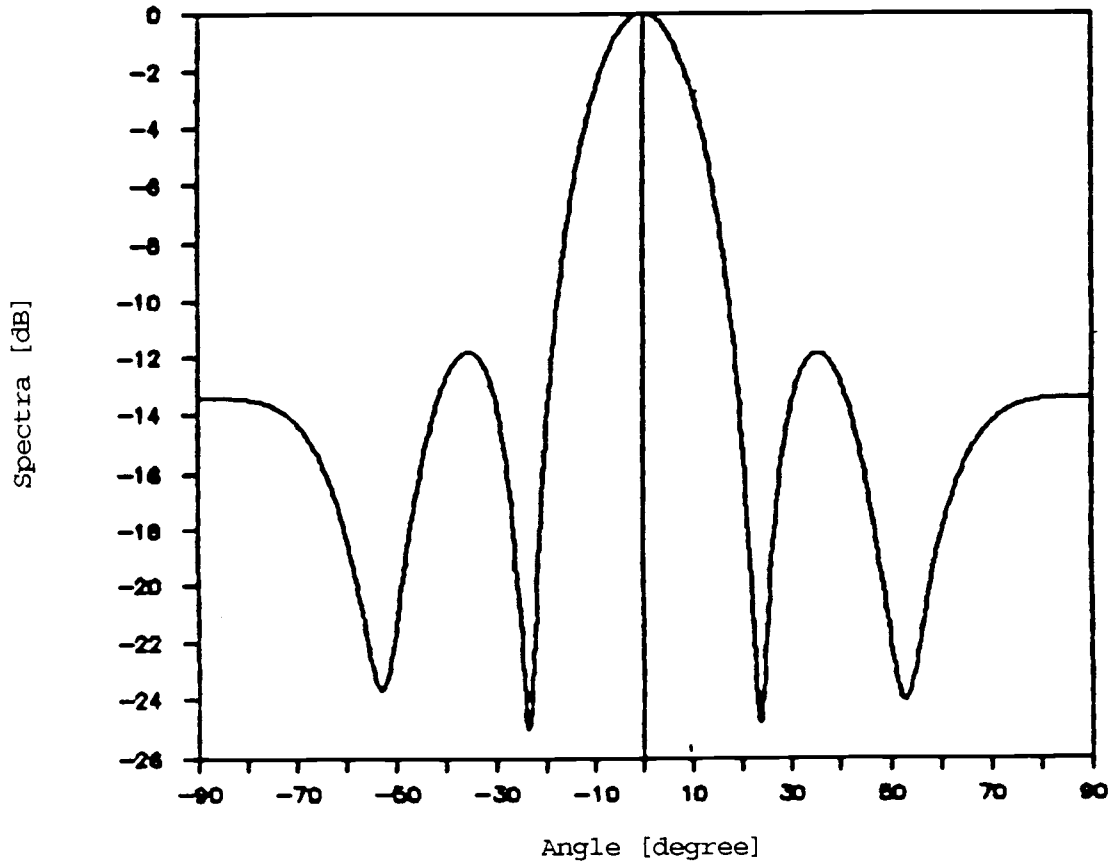

Fig.2-5. Bartlett Spectrum with 5 Sensors at S/N=16.9 dB.

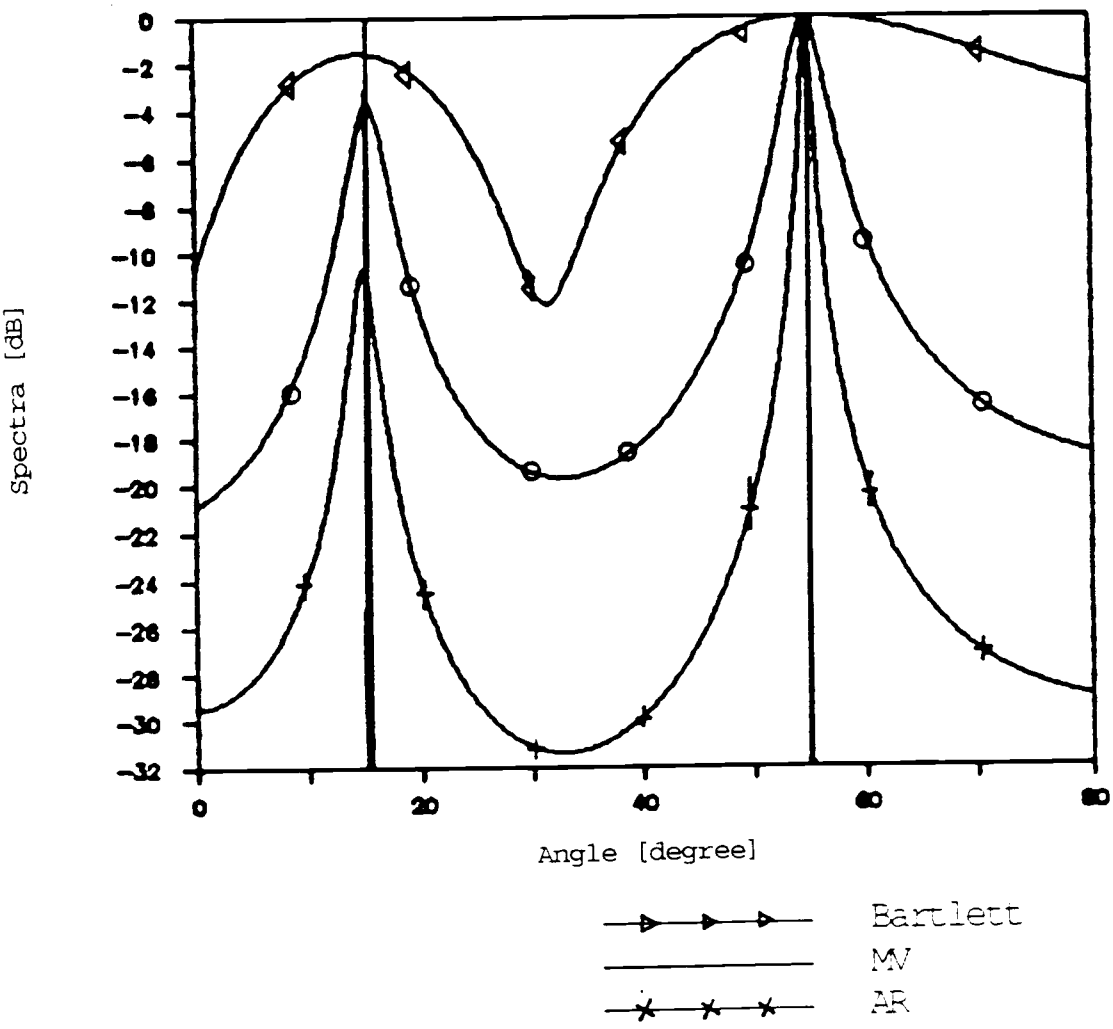

Fig.2-6. Bartlett, MV, and AR Spectra of Two Sources, θ_1=15°, θ_2=55°, with 5 Sensors at S/N=16.9 dB.

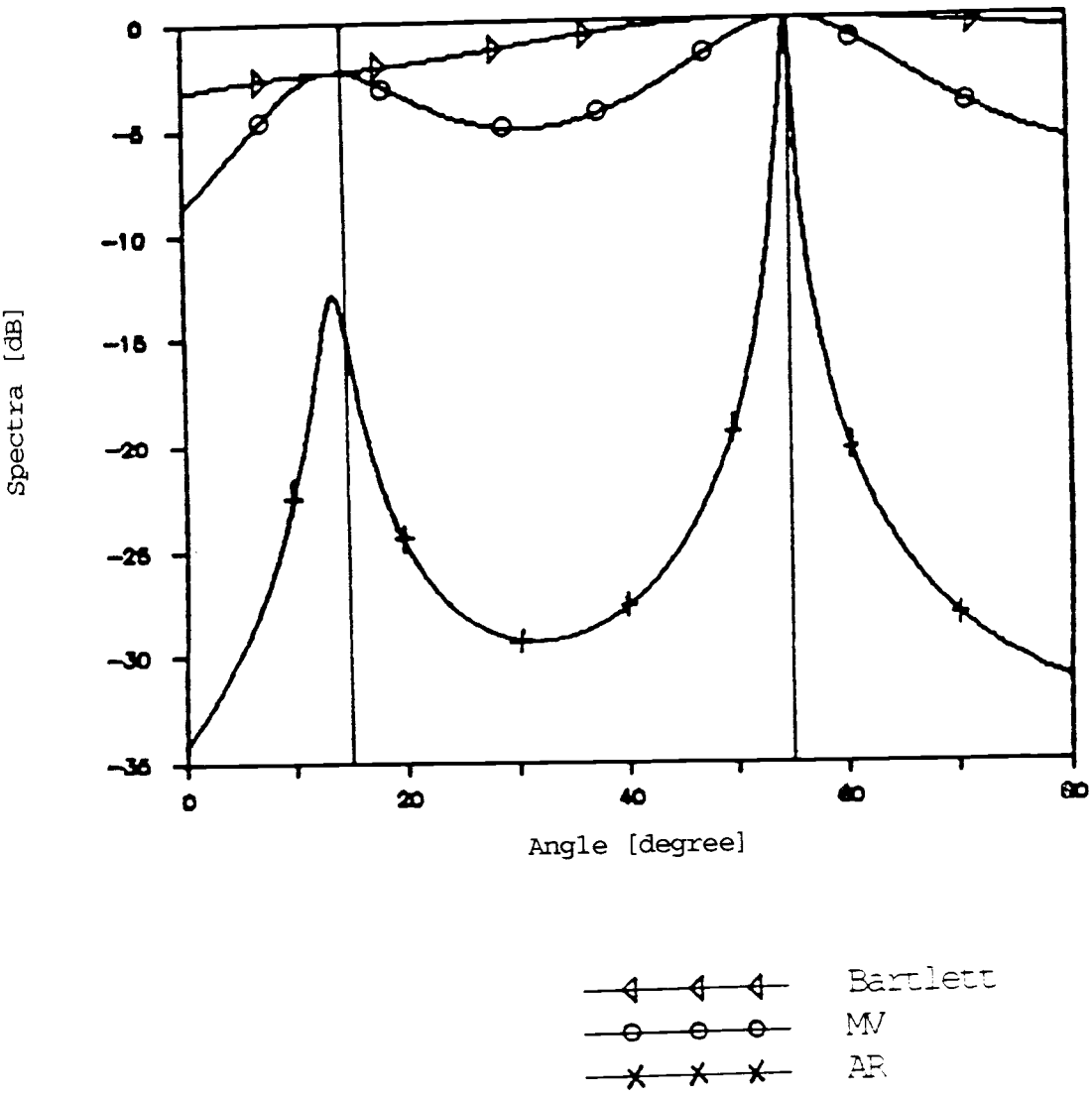

Fig.2-7. Bartlett, MV, and AR Spectra of Two Sources, θ_1=15°, θ_2=55°, with 3 Sensors at S/N=10.9 dB.

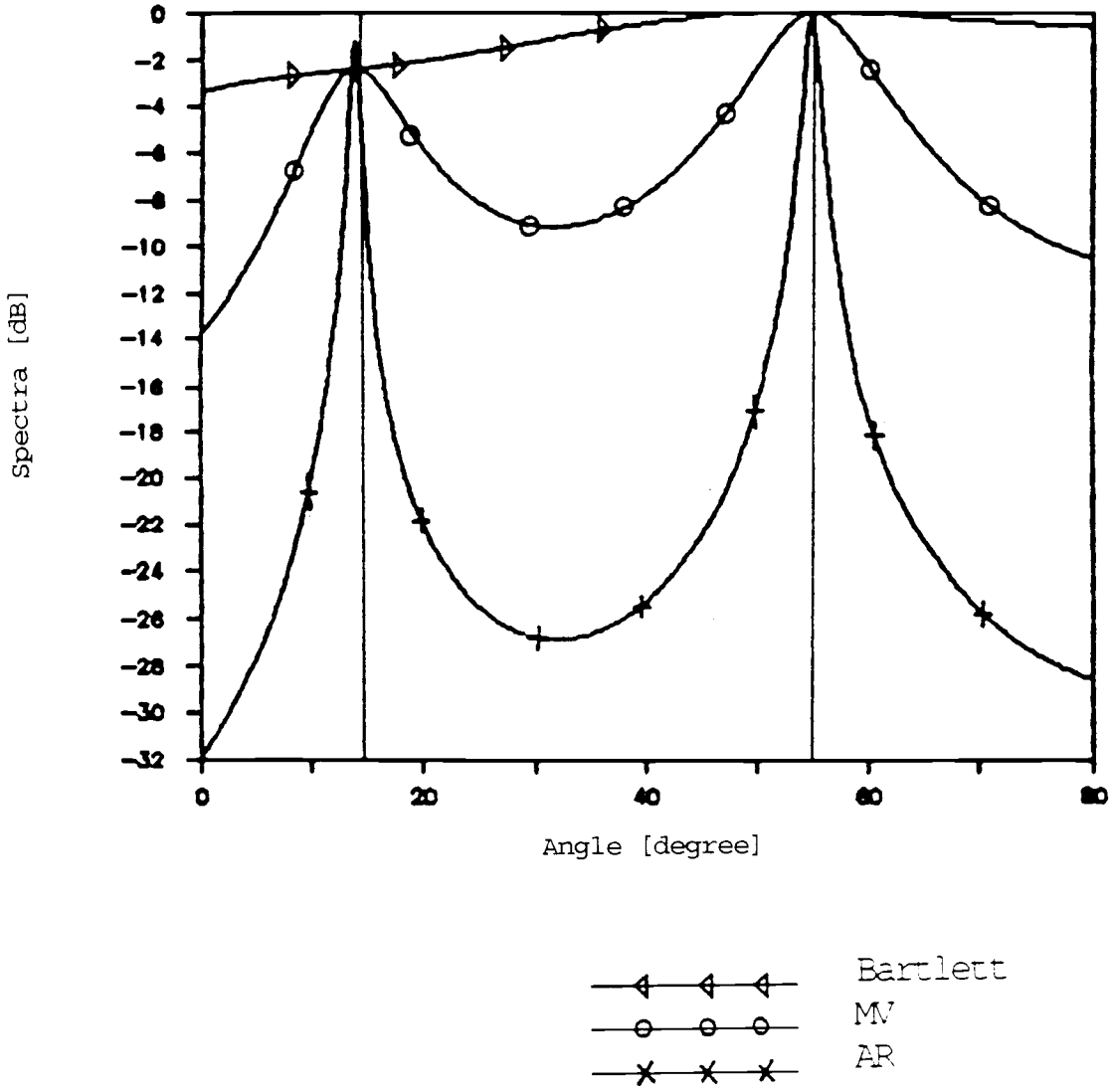

Fig.2-8. Bartlett, MV, and AR Spectra of Two Sources, θ_1=15°, θ_2=55°, with 3 Sensors at S/N=16.9 dB.

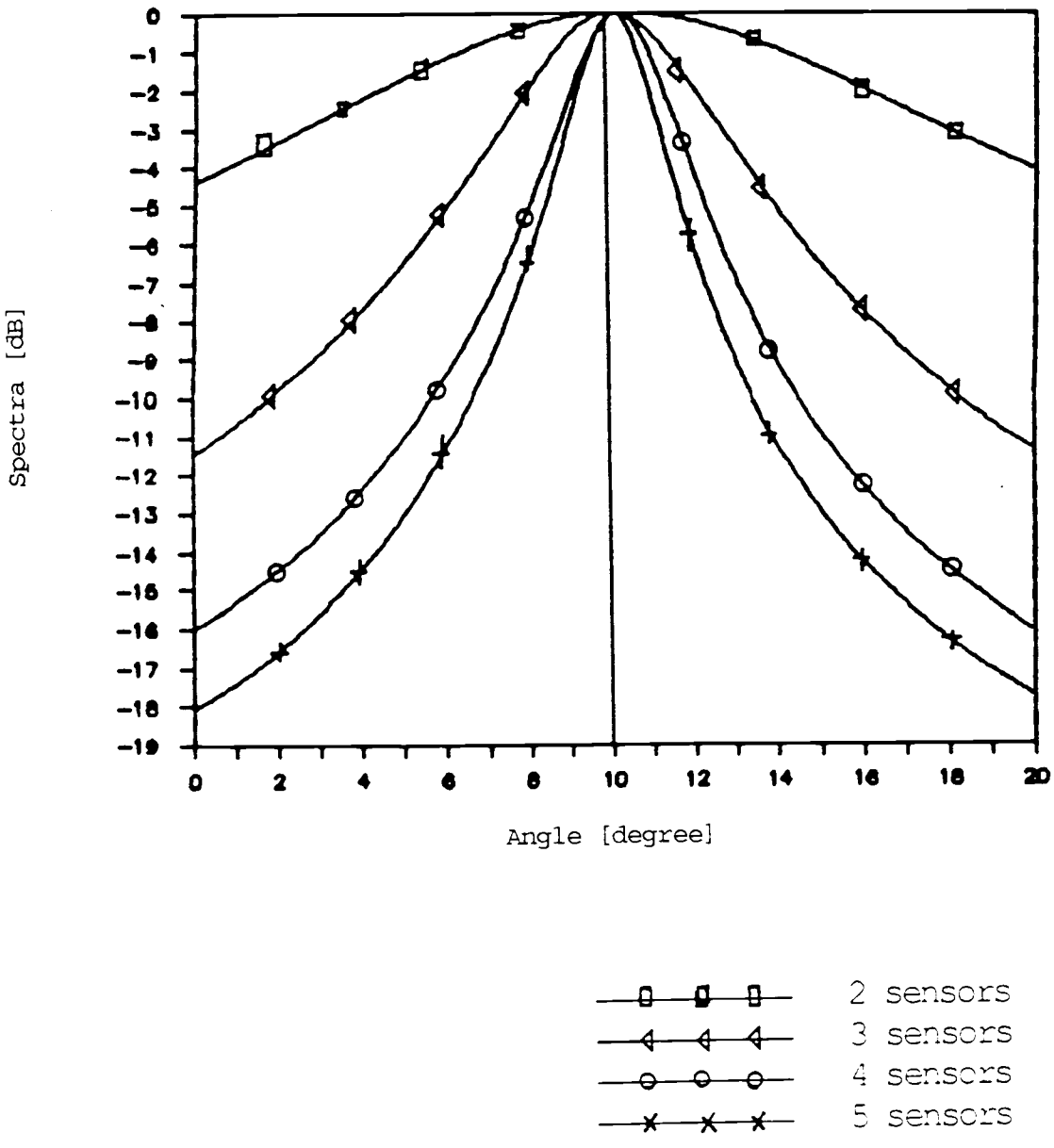

Fig.2-9. AR Spectra of Single Source at 10° with 2, 3, 4, and 5 Sensors at S/N=3 dB.

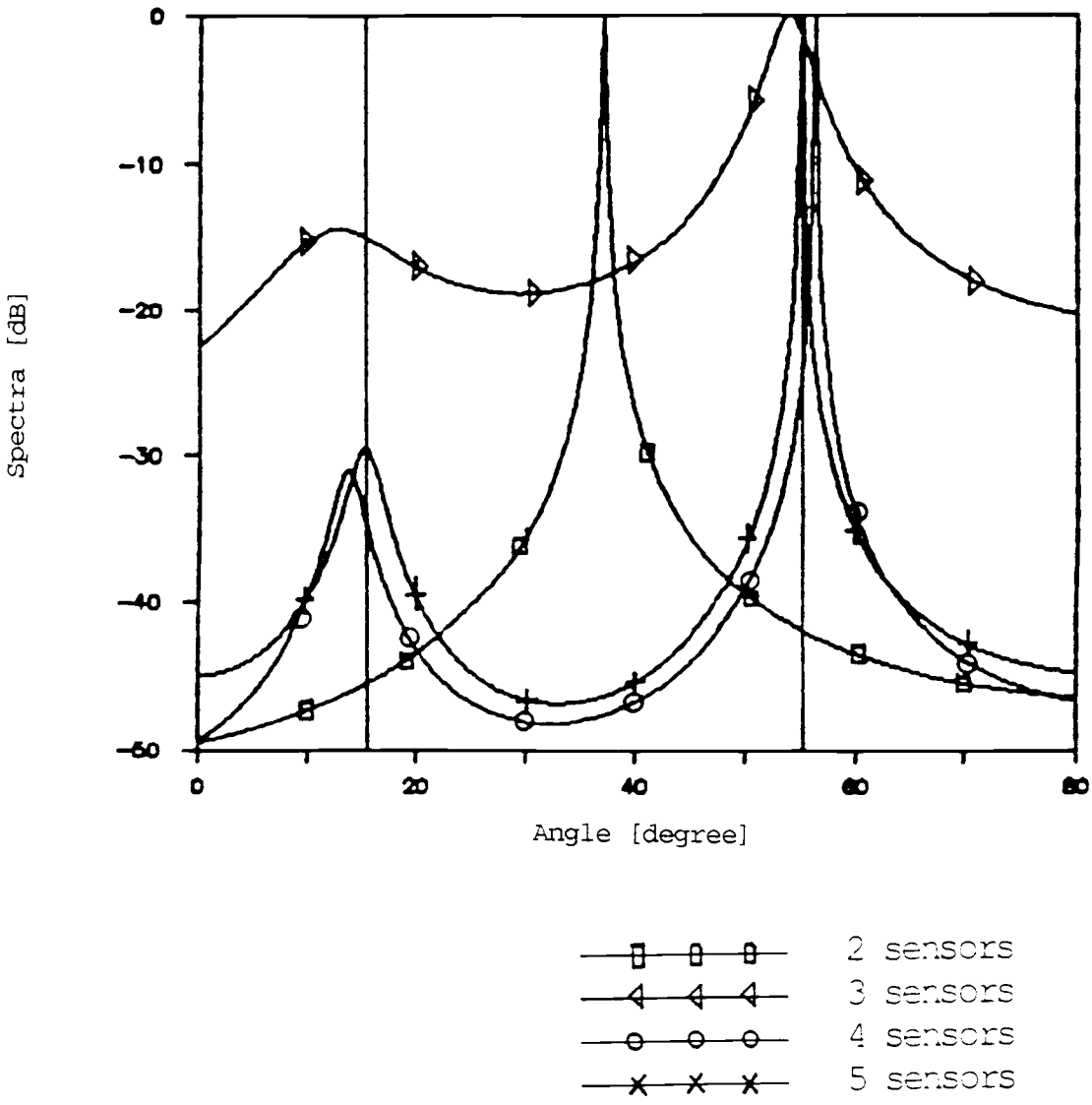

Fig.2-10. AR Spectra of Two Sources at θ_1=15° and θ_2=55° with 2, 3, 4, and 5 Sensors at S/N=3 dB.

2.4 Multiple Signal Classification Method Based on Standard Eigenstructure Algorithm

The eigenstructure-based methods for the direction-finding problem are known to yield better resolution and more desirable angle estimation characteristics than such spectral techniques as the AR or MV, especially at the lower S/N ratios, in which the latter techniques often fail to resolve closely spaced sources. The principal idea of such eigenstructure-based methods as the multiple signal classification (MUSIC) method is the division of the information in a spatial array covariance matrix into two vector subspaces, one of which is a signal subspace and the other a noise subspace. In this section, Schmidt's [10,33] MUSIC method is considered as a typical example of a FOM. This MUSIC method is subsequently used to compare the direction-finding performances with SOMs.

For the M plane wave source signals incident on the uniform linear array with Q sensors from directions $\{\theta_1, \theta_2, \cdots, \theta_M\}$, as considered in section 2.1, the $Q \times Q$ spatial sample array covariance matrix was derived in Eq.(2-16):

$$\mathbf{R} = \mathbf{A}_1\mathbf{P}\mathbf{A}_1^* + E[\mathbf{X}\mathbf{X}^*].$$

For spatially uncorrelated noises with constant variances σ^2, $\mathbf{R}$, as in Eq.(2-18), was determined to be

$$\mathbf{R} = \mathbf{A}_1\mathbf{P}\mathbf{A}_1^* + \sigma^2\mathbf{I}_Q.$$

The following theorem can then be applied to solve the direction finding problem.

Theorem 2.1 (Standard Eigenstructure Algorithm (SEA))

Let $\{\varepsilon_1>\varepsilon_2>\ldots>\varepsilon_Q\}$ and $\{\mathbf{v}_1,\mathbf{v}_2,\ldots,\mathbf{v}_Q\}$ be the eigenvalues and the corresponding eigenvectors of $\mathbf{R}$ given by Eq.(2-18), where $\mathbf{A}_1$ is the $Q \times M$ Vandermonde matrix with rank M ($M<Q$). So long as the $M \times M$ matrix $\mathbf{P}$ is nonsingular, the following is true:

i) the minimum eigenvalue of $\mathbf{R}$ is σ^2 with multiplicity $Q-M$, i.e.,

$$\varepsilon_{M+1} = \varepsilon_{M+2} = \cdots = \varepsilon_Q = \sigma^2 ;$$

ii) the eigenvectors associated with the minimal eigenvalues are orthogonal to the column span of the matrix $\mathbf{A}_1$, i.e.,

$$\{\mathbf{v}_{M+1}, \mathbf{v}_{M+2}, \cdots, \mathbf{v}_Q\} \perp \{\mathbf{a}(\theta_k), \quad k = 1,2,\ldots,M\}$$

where $\mathbf{a}(\theta_k)$ is the kth column vector of $\mathbf{A}_1$ as expressed in Eqs.(2-9) and (2-15).

Proof 2.1

i) Since $\mathbf{A}_1$ has a rank of M and $\mathbf{P}$ is a positive definite matrix, $\mathbf{A}_1\mathbf{P}\mathbf{A}_1^*$ is non-negative with rank equal to M. Therefore, the matrix $\mathbf{R}$ in Eq.(2-18) is positive definite. Since $\{\varepsilon_1>\varepsilon_2>\cdots>\varepsilon_Q\}$ and $\{\mathbf{v}_1,\mathbf{v}_2,\cdots,\mathbf{v}_Q\}$

are the eigenvalues and corresponding eigenvectors of the positive definite matrix $\mathbf{R}$, i.e., $\mathbf{R}\mathbf{v}_i = \varepsilon_i \mathbf{v}_i$, $i = 1,2,\cdots,Q$, then

$$[\mathbf{A}_1\mathbf{P}\mathbf{A}_1^* + \sigma^2\mathbf{I}]\,[\mathbf{v}_1,\mathbf{v}_2,\ldots,\mathbf{v}_Q]$$

$$= \begin{bmatrix} \varepsilon_1 & 0 & \cdot & \cdot & 0 \\ 0 & \varepsilon_2 & 0 & \cdot & 0 \\ \cdot & \cdot & \cdot & \cdot & \cdot \\ 0 & \cdot & 0 & & \varepsilon_Q \end{bmatrix} [\mathbf{v}_1,\mathbf{v}_2,\ldots,\mathbf{v}_Q]$$

or

$$[\mathbf{A}_1\mathbf{P}\mathbf{A}_1^*]\,[\mathbf{v}_1,\mathbf{v}_2,\ldots,\mathbf{v}_Q]$$

$$= \begin{bmatrix} \varepsilon_1-\sigma^2 & 0 & \cdot & \cdot & 0 \\ 0 & \varepsilon_2-\sigma^2 & 0 & \cdot & 0 \\ \cdot & \cdot & \cdot & \cdot & \cdot \\ \cdot & \cdot & \varepsilon_M-\sigma^2 & \cdot & \cdot \\ \cdot & \cdot & \cdot & \varepsilon_{M+1}-\sigma^2 & \cdot \\ \cdot & \cdot & \cdot & \cdot & 0 \\ 0 & \cdot & \cdot & 0 & \varepsilon_Q-\sigma^2 \end{bmatrix} [\mathbf{v}_1,\mathbf{v}_2,\ldots,\mathbf{v}_Q].$$

Since $\mathbf{A}_1\mathbf{P}\mathbf{A}_1^*$ has the rank of M with M non-zero eigenvalues, the $(Q-M)$ ε_i must be equal to σ^2 in order that both sides of the equation have identical ranks (M). For the non-negative definite matrix $\mathbf{A}_1\mathbf{P}\mathbf{A}_1^*$, the ε_i with values equal to σ^2 must be the smallest

within these terms. Thus, it can be seen that

$$\varepsilon_{M+1} = \varepsilon_{M+2} = \cdots = \varepsilon_Q = \sigma^2 .$$

The vector space corresponding to the minimal eigenvalues σ^2 is then called the noise subspace, along with the vector space associated with the signal subspace of the rest of the eigenvalues.

ii) Using the full rank property of $\mathbf{A}_1$ and $\mathbf{R}$, and defining $\mathbf{V}_n = [\mathbf{v}_{M+1}, \mathbf{v}_{M+2}, \cdots, \mathbf{v}_Q]$, which spans the noise subspace of $\mathbf{R}$, each with the identical minimal eigenvalues σ^2, it is easily seen that the linearly independent column vectors of the matrix $\mathbf{A}_1$ is orthogonal to the subspace $\mathbf{V}_n$. □

Thus the desired direction angles of the source signals will be associated with the peaks of the function, according to Theorem 2.1,

$$\hat{D}_{\text{MUSIC}} = \left[\mathbf{a}^*(\theta) \left(\sum_{k=M+1}^{Q} \mathbf{v}_k \mathbf{v}_k^* \right) \mathbf{a}(\theta) \right]^{-1} \qquad (2\text{-}32)$$

where $\mathbf{a}(\theta)$ is the $Q \times 1$ searching vector, as defined in Eq. (2-25).

Unlike the spectral estimates discussed in the previous section, D_{MUSIC} does not represent the true signal power associated with each direction angles, but the peaks of D_{MUSIC} guaranteedly corresponds to the true direction angles so long as the ensemble average $\mathbf{R}$ of the sample

array covariance matrix is exactly known along with uncorrelated noises between sensors. Eq.(2-32) also implies required minimum number of sensors should be at least one more than the total number of sources present (i.e., $Q \geq M+1$).

Note that now the eigenstructure-based methods retain only the information in the signal subspace eigenvectors, i.e., they form only a rank M approximation to **R**, thereby excluding the contribution of power in the noise subspace components. As a result, these eigenstructure-based methods effectively enhance the S/N ratio and yield high resolution direction-finding assignments in array processing. Moveover, the eigenstructure algorithm offers the effect of obtaining the value of the noise variance.

The following example clearly indicates the value of the proposed MUSIC method based upon the standard eigenstructure algorithm in comparision to the methods considered in section 2.3. Unless otherwise stated, 256 data samples will be used for computer simulations, throughout this study.

Example 2.2 The resolution capability of the MUSIC method, compared with the spectral estimation methods introduced in section 2.3, is considered for two plane waves buried in spatially uncorrelated Gaussian noises.

Fig. 2-11 compares the MUSIC method and the Bartlett, MV, and AR methods for two sources at $\theta_1 = 15^\circ$ and $\theta_2 = 55^\circ$ with three sensors at S/N = 10.9 dB. It is clear that the MUSIC method based on the standard eigenstructure algorithm, is more reliable than either the AR, MV, or Bartlett methods, although the AR method appears to be competitive in the case of both a high S/N ratio and well-separated source signals (i.e., greater than the Rayleigh resolution limit).

However, from Figs. 2-12 and 2-13 it may be seen that the resolution performance of the AR spectrum abruptly worsens, in comparision to the MUSIC method, as the S/N ratio is decreased. As a result, the AR spectrum cannot resolve the two peaks at S/N = -5.9 dB, while the MUSIC method clearly accomplishes (Fig. 2-13).

Fig. 2-14 reflects a test performed to determine how well the four direction-finding methods resolve the direction angles when the two source signals are closer at a fairly high S/N ratio. In this case, only the MUSIC method resolves the two peaks at 15° separation with S/N = 16.9 dB. Moreover, the more samples that are taken, the better the resolution obtained with the MUSIC method (Fig. 2-15). Note that, as seen in Fig. 2-15, even the MUSIC cannot resolve the two source signals for $N = 128$.

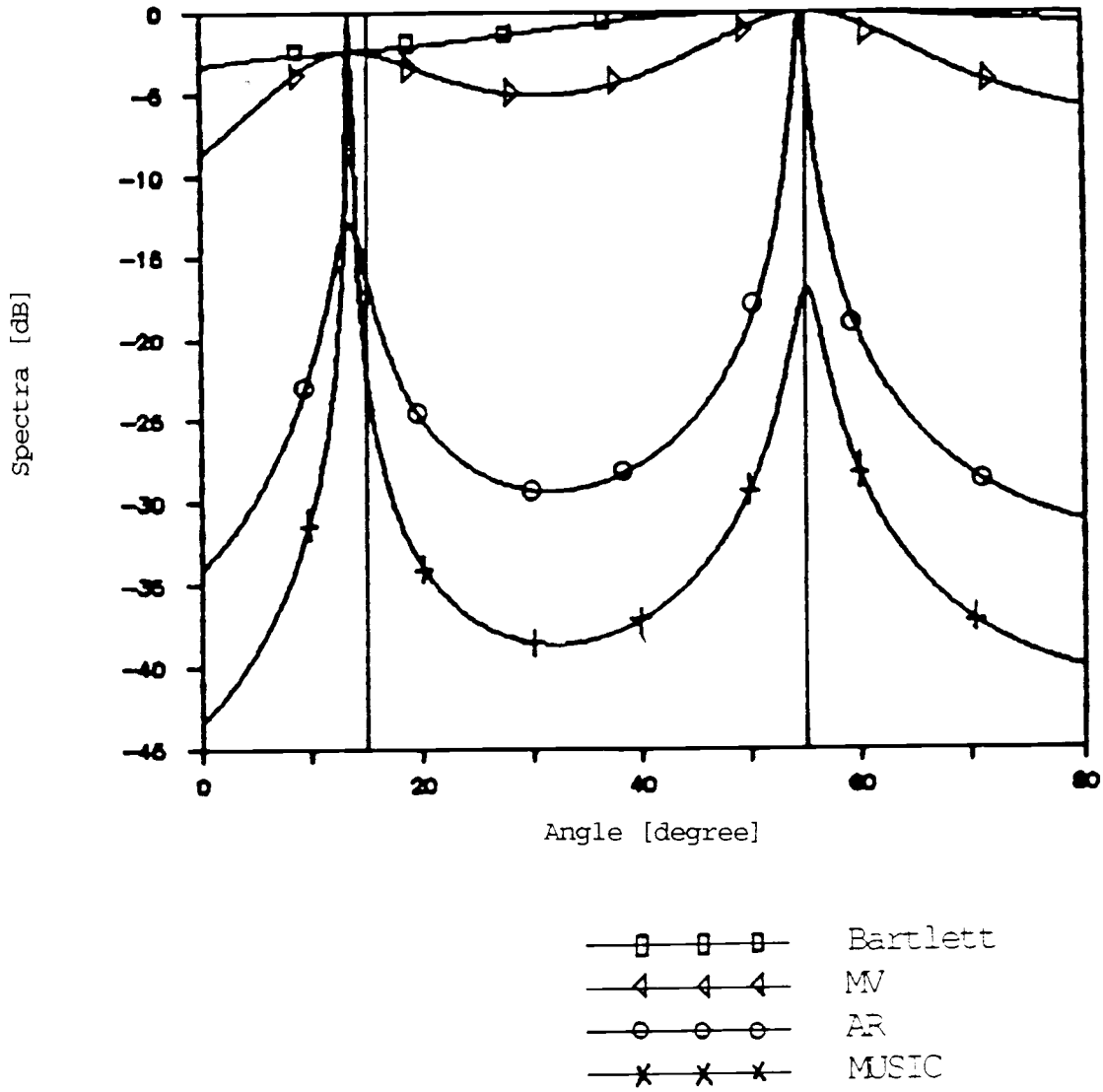

Fig.2-11. MUSIC, Bartlett, MV, and AR Spectra of Two Sources, θ_1=15°, θ_2=55°, with 3 Sensors at S/N=10.9 dB.

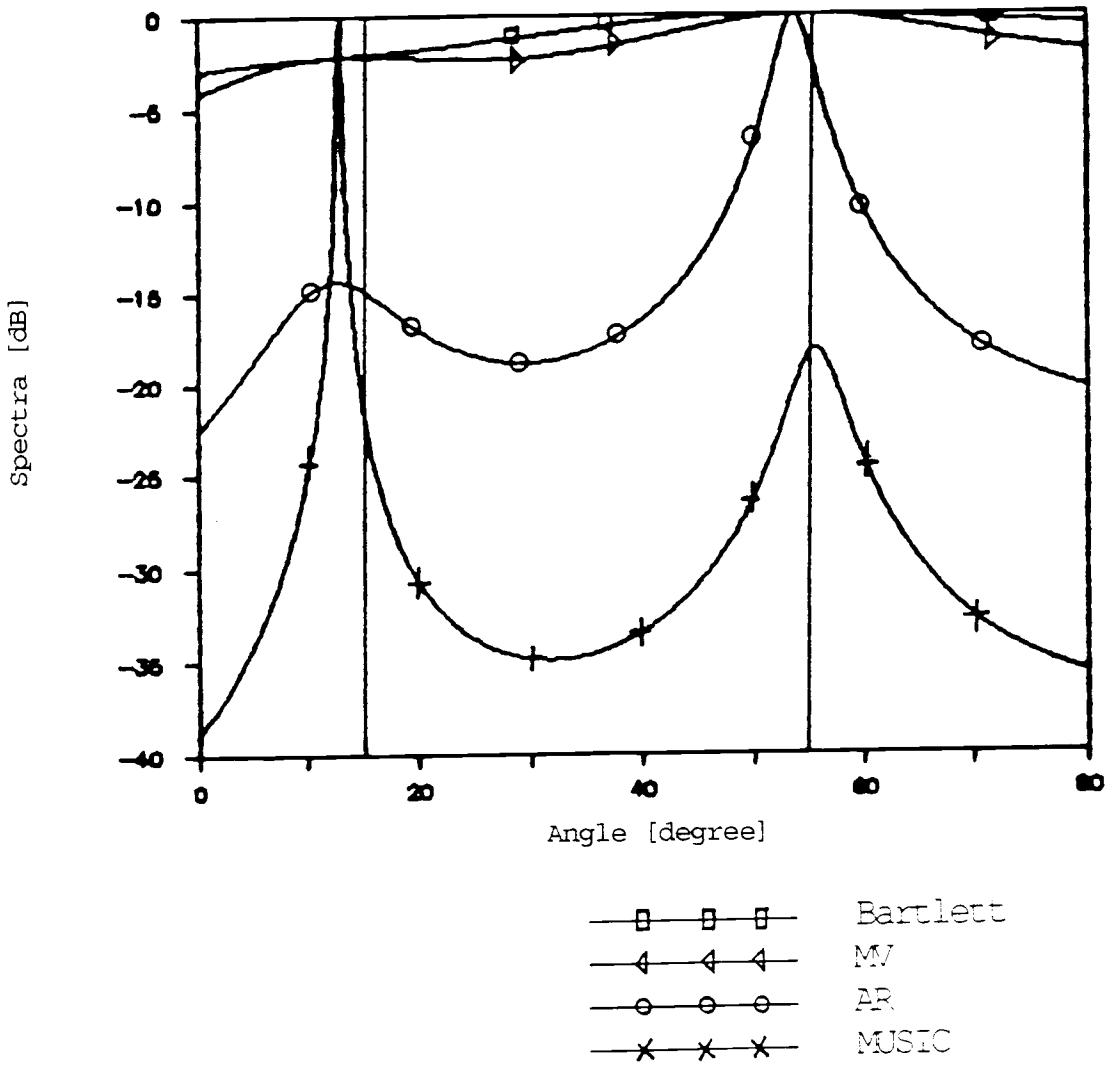

Fig.2-12. MUSIC, Bartlett, MV, and AR Spectra of Two Sources, θ_1=15°, θ_2=55°, with 3 Sensors at S/N=3 dB.

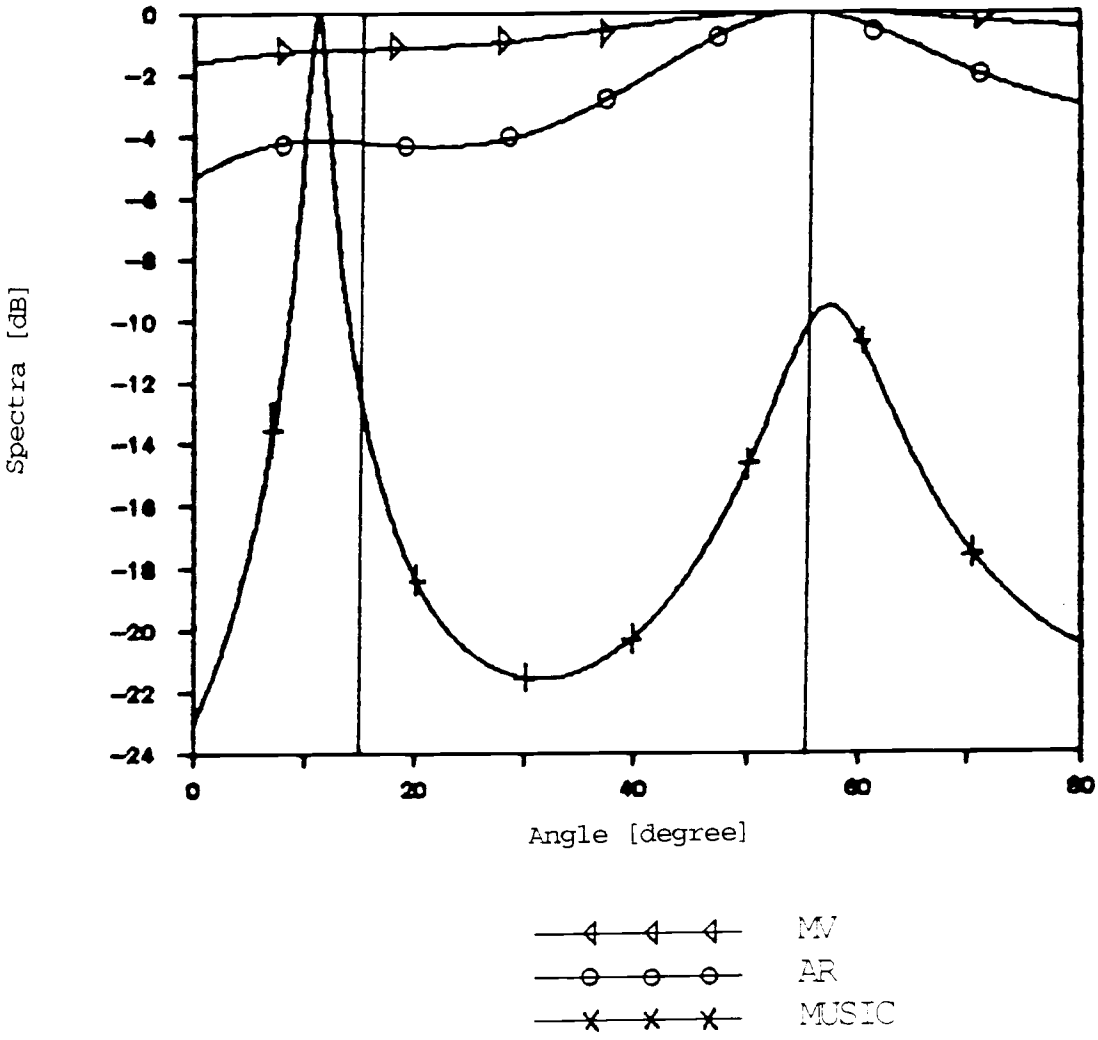

Fig.2-13. MUSIC, MV, and AR Spectra of Two Sources, θ_1=15°, θ_2=55°, with 3 Sensors at S/N=-5.9 dB.

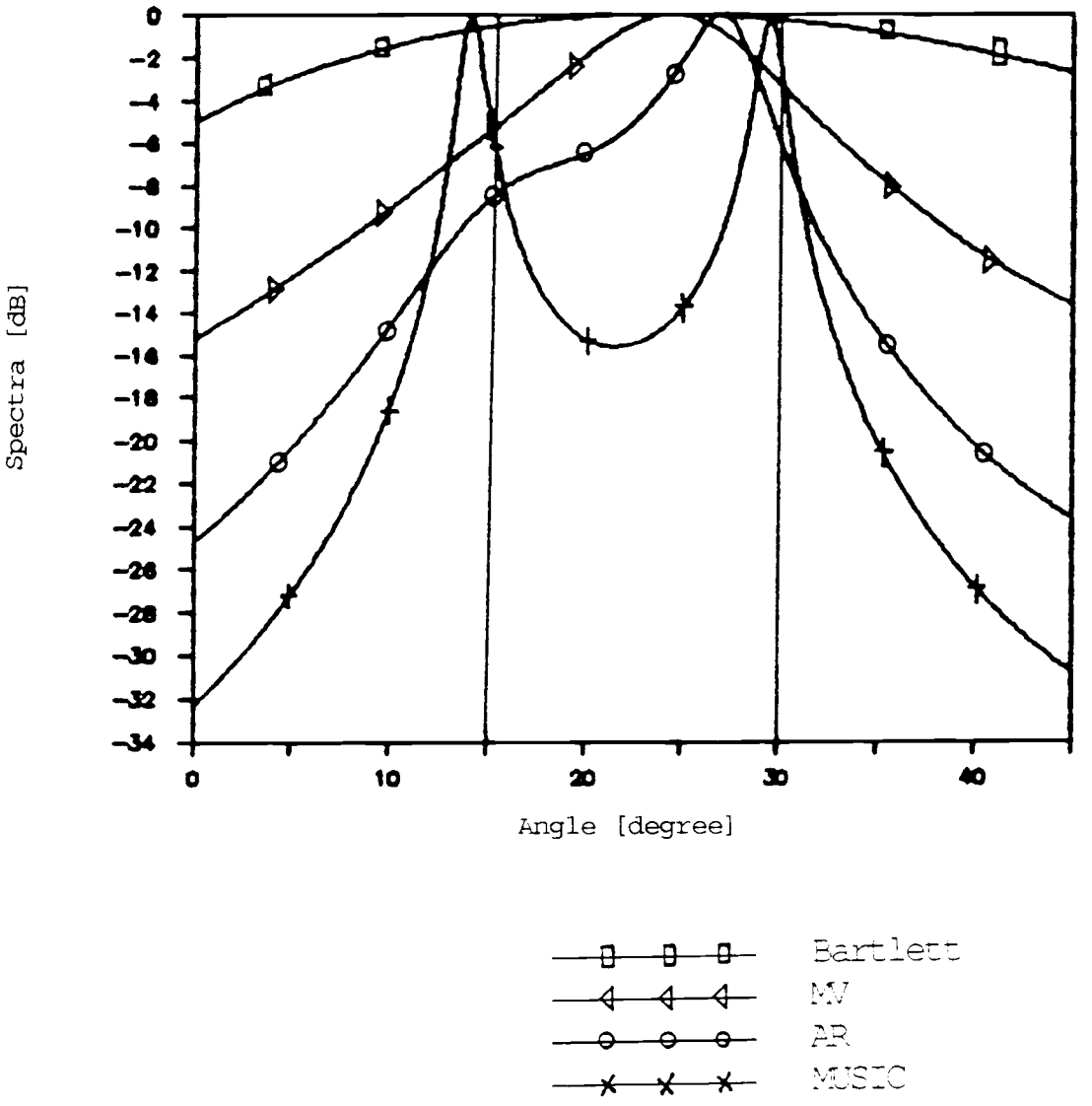

Fig.2-14. MUSIC, Bartlett, MV, and AR Spectra of Two Sources, θ_1=15°, θ_2=30°, with 3 Sensors at S/N=16.9 dB.

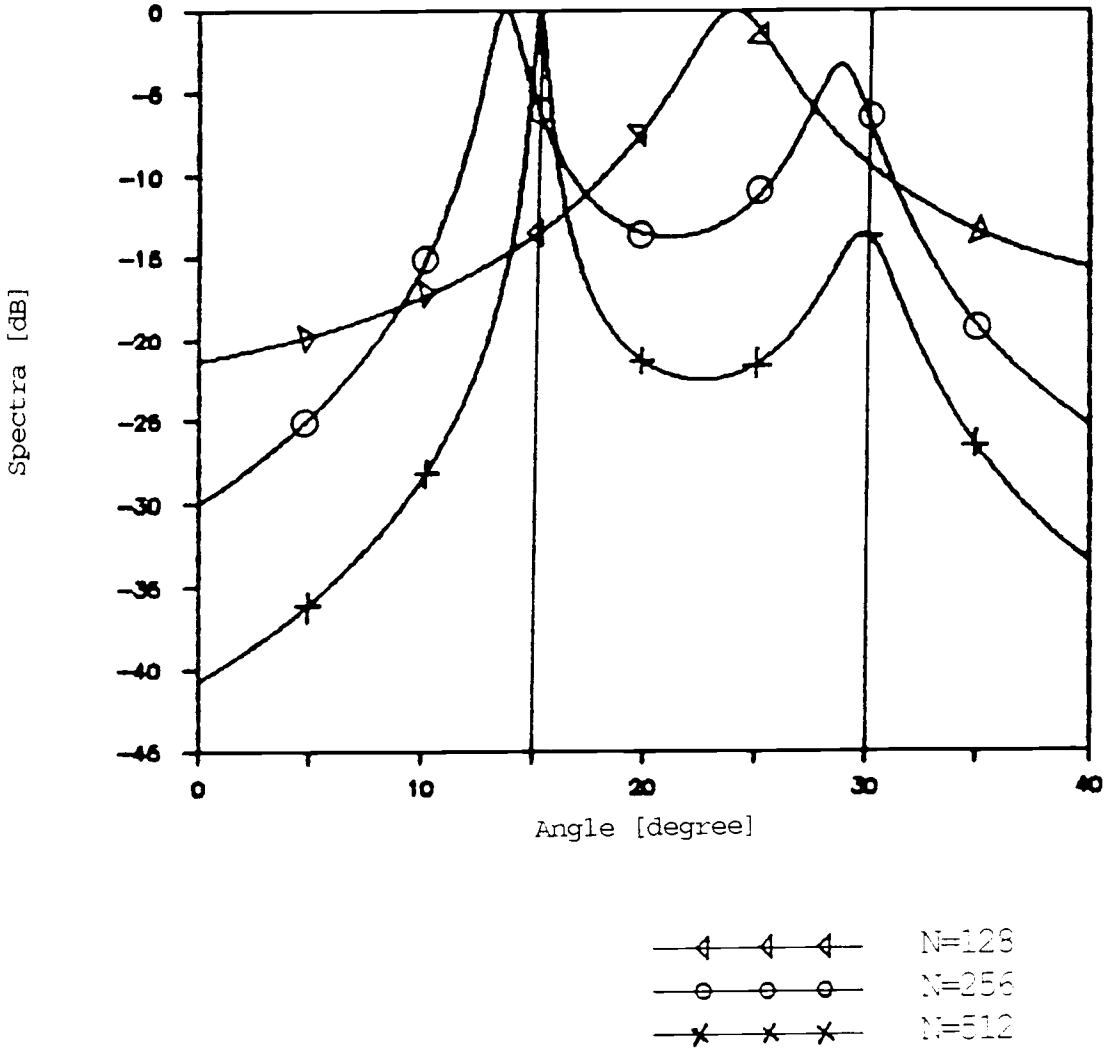

Fig.2-15. MUSIC, for Two Sources, θ_1=15°, θ_2=30°, with 3 Sensors at S/N=7.45 dB in terms of Sample Size.

2.5 Generalized Eigenstructure Algorithm

In this section, a generalized eigenstructure algorithm (GEA) for application to situations where sensor noises are spatially correlated is derived. So long as the positive-valued noise correlation coefficient is known or can be accurately estimated, the matrix **W** can be determined in order to decorrelate correlated noise fields. Algorithm procedures are described as follows:

Let ε_i and $\mathbf{v}_i$, $i=1,2,\cdots,Q$ be the eigenvalues and corresponding eigenvectors of the matrix pair $(\mathbf{R},\mathbf{Q})$, with ε_i in descending order, i.e.,

$$\mathbf{R} = \mathbf{APA}^* + \sigma^2\mathbf{Q}, \tag{2-33}$$

where **P** is the (correlated or uncorrelated) nonsingular $M \times M$ source sample covariance matrix, as in Eq.(2-16) and $\sigma^2\mathbf{Q}$ is the noise covariance matrix in which the correlation coefficient matrix **Q** is known, but the nonnegative multiplicative scalar (or variance of the noise) σ^2 is unknown.

Since the matrix **Q** is positive definite so long as **Q** is non-singular with the positive-valued correlation coefficient, the nonsingular matrix **W** exists such that

$$\mathbf{Q} = \mathbf{WW}^* \tag{2-34}$$

(if each element of **Q** is real, then **W** is real). Then, substituting Eq.(2-34) into Eq.(2-33) yields

$$\mathbf{R} = \mathbf{APA}^* + \sigma^2\mathbf{WW}^*. \tag{2-35}$$

Since $\mathbf{W}$ is nonsingular,

$$(\mathbf{W}^{-1})\mathbf{R}(\mathbf{W}^{*})^{-1} = (\mathbf{W}^{-1})(\mathbf{APA}^{*} + \sigma^{2}\mathbf{WW}^{*})(\mathbf{W}^{*})^{-1} \tag{2-36}$$

or

$$(\mathbf{W}^{-1})\mathbf{R}(\mathbf{W}^{*})^{-1} = (\mathbf{W}^{-1})(\mathbf{APA}^{*})(\mathbf{W}^{*})^{-1} + \sigma^{2}\mathbf{I}. \tag{2-37}$$

Eq.(2-37) then becomes an eigenstructure problem for a Hermitian (for complex correlation coefficients) or symmetric (for real correlation coefficients) single matrix $(\mathbf{W}^{-1})\mathbf{R}(\mathbf{W}^{*})^{-1}$ with the decorrelated noise covariance matrix

$$(\mathbf{W}^{-1})\mathbf{R}(\mathbf{W}^{*})^{-1}\mathbf{z} = \beta\mathbf{z}, \tag{2-38}$$

where the eigenvalues β_i are identical to the originals (ε_i) in $\mathbf{Rv} = \varepsilon\mathbf{Qv}$, and the eigenvectors are related by $\mathbf{z}_i = \mathbf{W}^{*}\mathbf{v}_i$.

Even when the single matrix $\mathbf{Q}^{-1}\mathbf{R}$ can be directly obtained from $\mathbf{Rv} = \varepsilon\mathbf{Qv}$, $\mathbf{Q}^{-1}\mathbf{R}$ cannot be Hermitian (or symmetric).

When $\mathbf{P}$ is nonsingular, the following is true:

i) The minimum eigenvalue of $(\mathbf{W}^{-1})\mathbf{R}(\mathbf{W}^{*})^{-1}$ is σ^2 with multiplicity $Q-M$, or

$$\beta_{M+1} = \beta_{M+2} = \cdots = \beta_{Q} = \sigma^{2}. \tag{2-39}$$

ii) The eigenvectors corresponding to the minimal eigenvalues are orthogonal to the columns of the matrix $(\mathbf{W}^{-1})\mathbf{A}$.

The value of $\mathbf{W}$ may be determined in two ways.

1) The first, for real elements, is to the appearance of Gaussian Elimination to a symmetric matrix. When $\mathbf{Q}$ is

symmetric, and it can be factored into $\mathbf{Q} = \mathbf{LDU}$ without row exchanges to destroy the symmetry, then the upper triangular $\mathbf{U}$ is the transpose of the lower triangular $\mathbf{L}$. A symmetric matrix has a symmetric factorization $\mathbf{Q} = \mathbf{LDL}^T = (\mathbf{L}(\mathbf{D})^{1/2})((\mathbf{D})^{1/2}\mathbf{L}^T)$. Therefore, the first choice for $\mathbf{W}$ is the lower triangular matrix $\mathbf{L}(\mathbf{D})^{1/2}$.

In order to prove the above statement 1), the following well-known theorem is needed.

Theorem 2.2 If $\mathbf{Q} = \mathbf{L}_1\mathbf{D}_1\mathbf{U}_1$ and $\mathbf{Q} = \mathbf{L}_2\mathbf{D}_2\mathbf{U}_2$, where the $\mathbf{L}$ values are lower triangular to the unit diagonal, the $\mathbf{U}$ values are upper triangular to the unit diagonal, and the $\mathbf{D}$ values are diagonal matrices with no zeros on the diagonal, then $\mathbf{L}_1 = \mathbf{L}_2$, $\mathbf{D}_1 = \mathbf{D}_2$, and $\mathbf{U}_1 = \mathbf{U}_2$. The $\mathbf{LDU}$ factorization is uniquely determined by $\mathbf{Q}$.

We now prove the statement in 1). Consider the transpose of $\mathbf{Q} = \mathbf{LDU}$; the transposes come in reverse order to give $\mathbf{Q}^T = \mathbf{U}^T\mathbf{D}^T\mathbf{L}^T$. Since $\mathbf{Q}$ is symmetric it is equal to $\mathbf{Q}^T$, so we now have two factorization of $\mathbf{Q}$ into lower triangular times diagonal times upper triangular. ($\mathbf{L}^T$ is upper triangular with one on the diagonal, as is $\mathbf{U}$). According to Theorem 2.2, such a factorization is unique; therefore $\mathbf{L}^T$ must be identical to $\mathbf{U}$, which completes the proof. ❑

2) The second approach, yielding a $\mathbf{W}$ which differs from the first approach, is to use the fact that all of the eigenvalues of a positive definite matrix are (real) positive. Since the eigenvalues are positive, and the eigenvectors go into an orthogonal $\mathbf{G}$ that diagonalizes $\mathbf{Q}$, $\mathbf{Q} = \mathbf{G}\mathbf{B}\mathbf{G}^T = \mathbf{G}\sqrt{\mathbf{B}}\sqrt{\mathbf{B}}\mathbf{G}^T = (\mathbf{G}\sqrt{\mathbf{B}})(\mathbf{G}\sqrt{\mathbf{B}})^T$. $\mathbf{W}$ becomes the $\mathbf{G}\sqrt{\mathbf{B}}$, where $\mathbf{B}$ is a diagonal matrix, the elements of which are composed of the eigenvalues of $\mathbf{Q}$.

Example 2.3

For $\mathbf{Q} = \begin{bmatrix} 1 & \rho & \rho \\ \rho & 1 & \rho \\ \rho & \rho & 1 \end{bmatrix}$,

where $0 \leq \rho < 1$, the decorrelating matrix $\mathbf{W}$ can be determined as follows:

$$\mathbf{Q} = \begin{bmatrix} 1 & 0 & 0 \\ \rho & 1 & 0 \\ \rho & c & 1 \end{bmatrix} \begin{bmatrix} 1 & 0 & 0 \\ 0 & a & 0 \\ 0 & 0 & d \end{bmatrix} \begin{bmatrix} 1 & \rho & \rho \\ 0 & 1 & b \\ 0 & 0 & 1 \end{bmatrix},$$

where

$a = (1 - \rho^2)$

$b = c = (\rho - \rho^2)/(1 - \rho^2)$

$d = (1 - 3\rho^2 + 2\rho^3)/(1 - \rho^2)$.

Therefore,

$$\mathbf{W} = \begin{bmatrix} 1 & 0 & 0 \\ \rho & 1 & 0 \\ \rho & c & 1 \end{bmatrix} \begin{bmatrix} 1 & 0 & 0 \\ 0 & a^{1/2} & 0 \\ 0 & 0 & d^{1/2} \end{bmatrix} = \begin{bmatrix} 1 & 0 & 0 \\ \rho & a^{1/2} & 0 \\ \rho & h & d^{1/2} \end{bmatrix},$$

where

$$h = (\rho - \rho^2)/(1 - \rho^2)^{1/2} .$$

Example 2.4 This example demonstrates how effectively the GEA may be applied to situations in which sensor noises are spatially correlated, provided that the noise correlation coefficient is known or can be estimated. First, the two incoherent source signals from the directions $\theta_1 = 15°$ and $\theta_2 = 30°$ on three 50 percent, spatially correlated sensors. For S/N = 7.4 dB, the GEA resolves the two peaks at the desired angles, while the SEA shows the two peaks with too much bias at $\theta_1 = 8.7°$ and $\theta_2 = 27.3°$, as shown in Fig. 2-16. The S/N ratio is then decreased to 3 dB, as shown in Fig. 2-17. In this case, both algorithms tend to be biased, but the GEA shows the two peaks at $\theta_1 = 16.8°$ and $\theta_2 = 29.9°$, while the SEA shows two peaks at 6° and 26.6°. However, as the sources approach each other (within 10° of difference), or as the S/N ratio is decreased to around 0 dB (for the two sources at 15° and 30°), the MUSIC based on the GEA arrives at the

limits of its resolution capability, as shown in Figs. 2-18 and 2-19.

However, the following must be considered: When sensor noises are correlated with the correlation coefficient ρ, the array covariance matrix can be expressed as $\mathbf{R} = \mathbf{A}_1\mathbf{P}\mathbf{A}_1^* + 2\sigma^2\mathbf{Q}$. For example, take the 3 x 3 matrix $\mathbf{Q}$ such that

$$2\sigma^2\mathbf{Q} = 2\sigma^2 \begin{bmatrix} 1 & \rho & \rho \\ \rho & 1 & \rho \\ \rho & \rho & 1 \end{bmatrix}.$$

When the SEA is used for correlated noises, this algorithm recognizes only the uncorrelated portion of $2\sigma^2\mathbf{Q}$ by omitting the quantity $2\sigma^2\rho$ in each element of the matrix, i.e., the noise covariance matrix recognized by the SEA becomes

$$2\sigma^2 \begin{bmatrix} 1 & \rho & \rho \\ \rho & 1 & \rho \\ \rho & \rho & 1 \end{bmatrix} - 2\sigma^2 \begin{bmatrix} \rho & \rho & \rho \\ \rho & \rho & \rho \\ \rho & \rho & \rho \end{bmatrix}$$

$$= 2(1 - \rho)\sigma^2 \begin{bmatrix} 1 & 0 & 0 \\ 0 & 1 & 0 \\ 0 & 0 & 1 \end{bmatrix},$$

and the excluded portion of $2\sigma^2$ is added to the matrix $\mathbf{A}_1\mathbf{P}\mathbf{A}_1^*$. As a result, the FOM based on SEA provides a large bias when applied to the correlated noise fields. However, noise variance will be decreased to $2(1-\rho)\sigma^2$ from $2\sigma^2$.

When the SEA is used for the FOM we call it the FOMSEA. In the same manner, the FOMGEA for the FOM based on the GEA, the SOMSEA for the SOM based on the SEA, and the SOMGEA for the SOM based on the GEA, are used, respectively.

Additional comparisons of the FOMSEA, FOMGEA, SOMSEA, and SOMGEA are considered in the statistical approach discussed in Chapter 4.

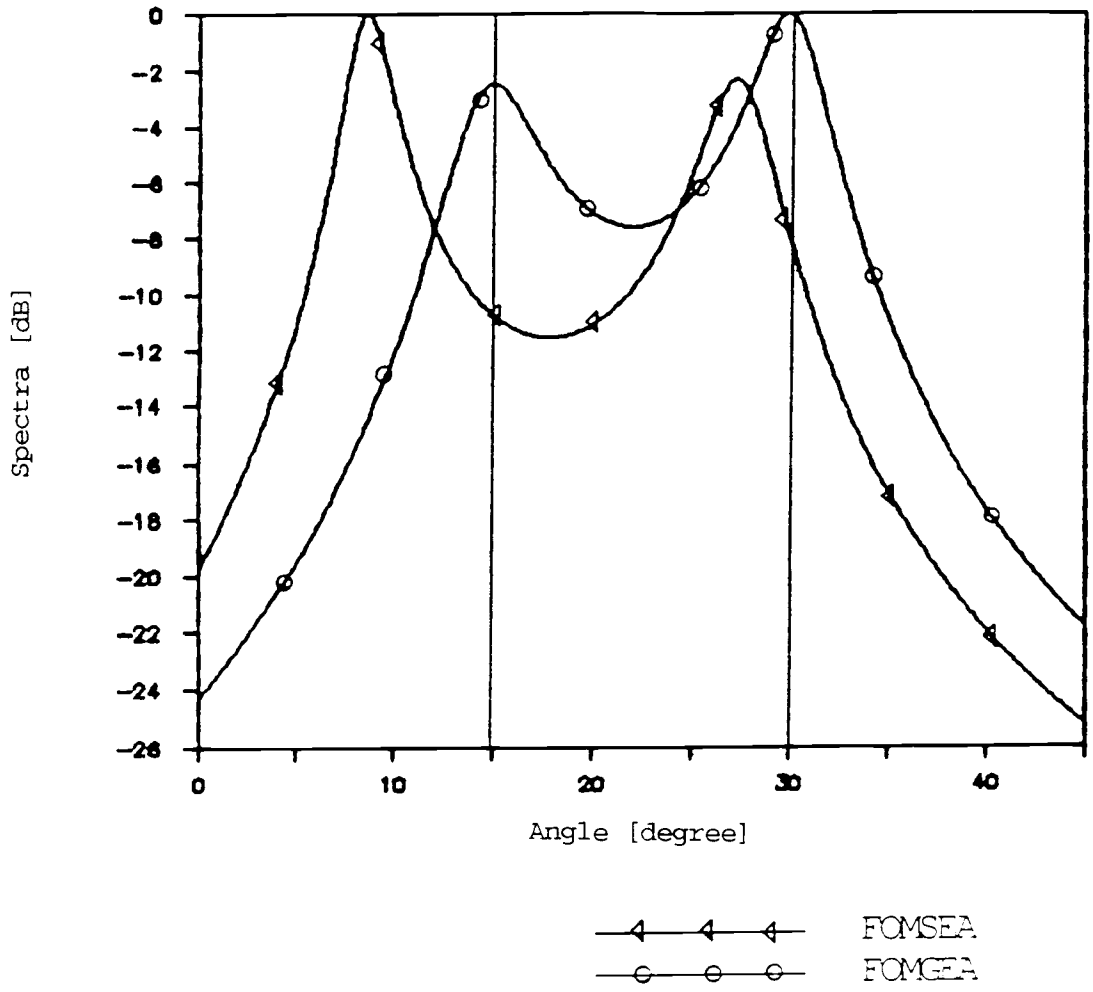

Fig.2-16. MUSIC Based on the Standard and Generalized Eigenstructure algorithms of Two Sources, θ_1=15°, θ_2=30°, with 50% Correlated 3 Sensors at S/N=7.4 dB.

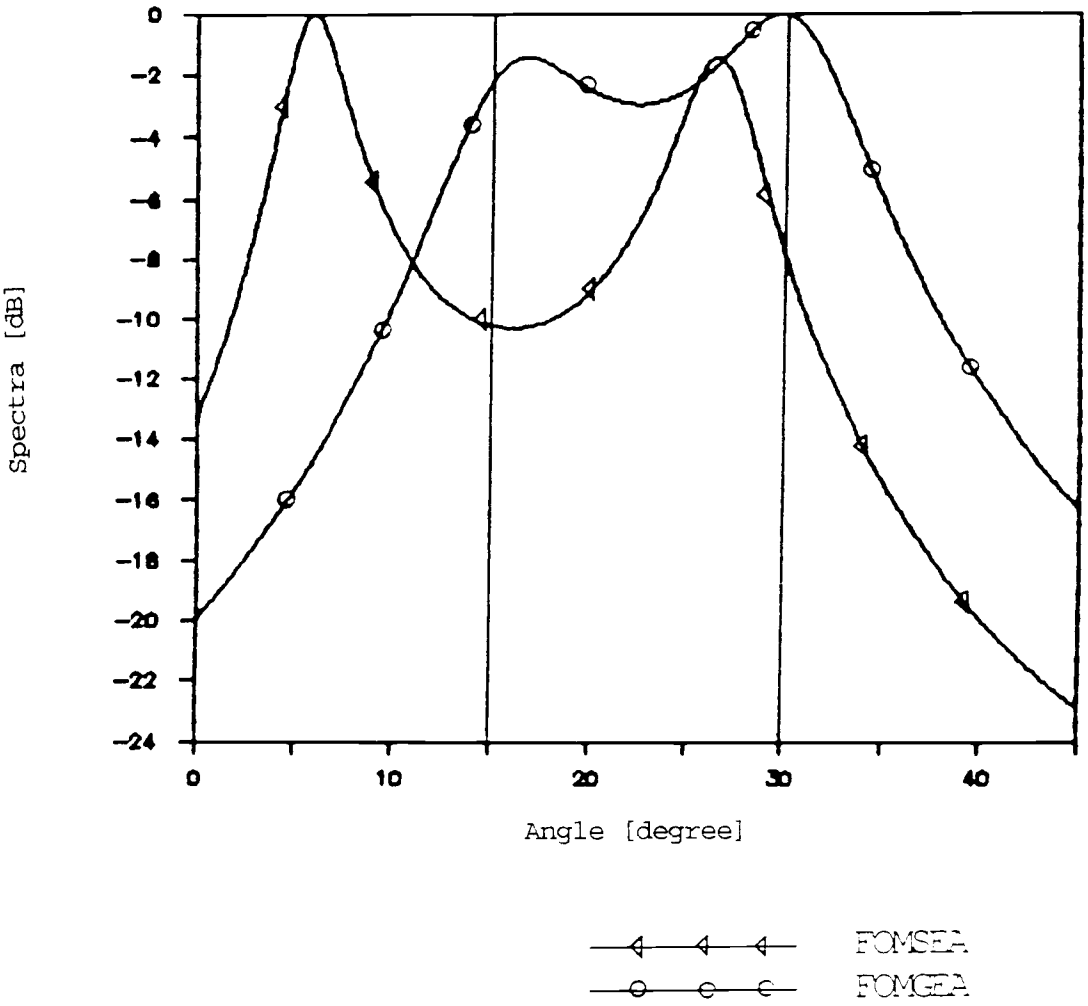

Fig.2-17. MUSIC Based on the Standard and Generalized Eigenstructure algorithms of Two Sources, θ_1=15°, θ_2=30°, with 50% Correlated 3 Sensors at S/N=3.0 dB.

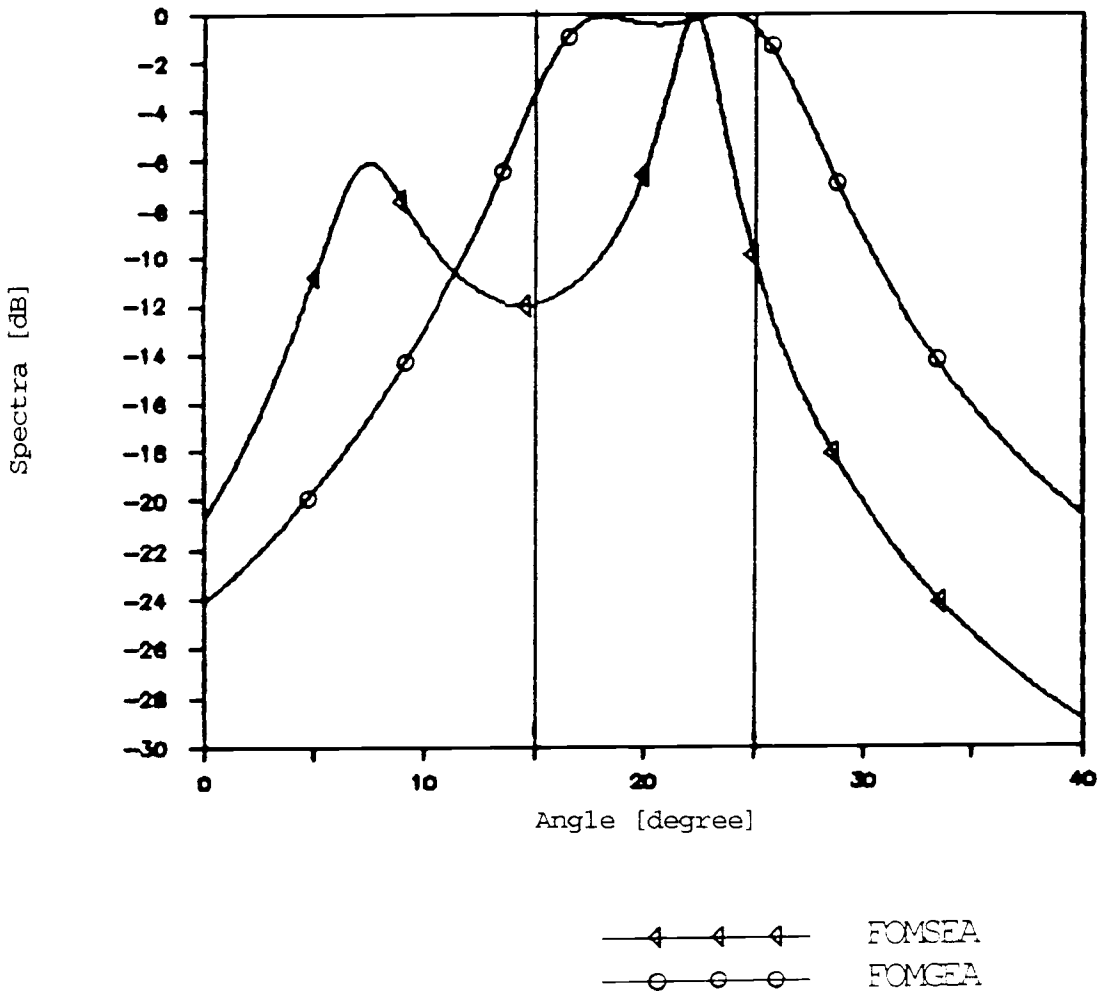

Fig.2-18. MUSIC Based on the Standard and Generalized Eigenstructure algorithms of Two Sources, θ_1=15°, θ_2=25°, with 50% Correlated 3 Sensors at S/N=7.4 dB.

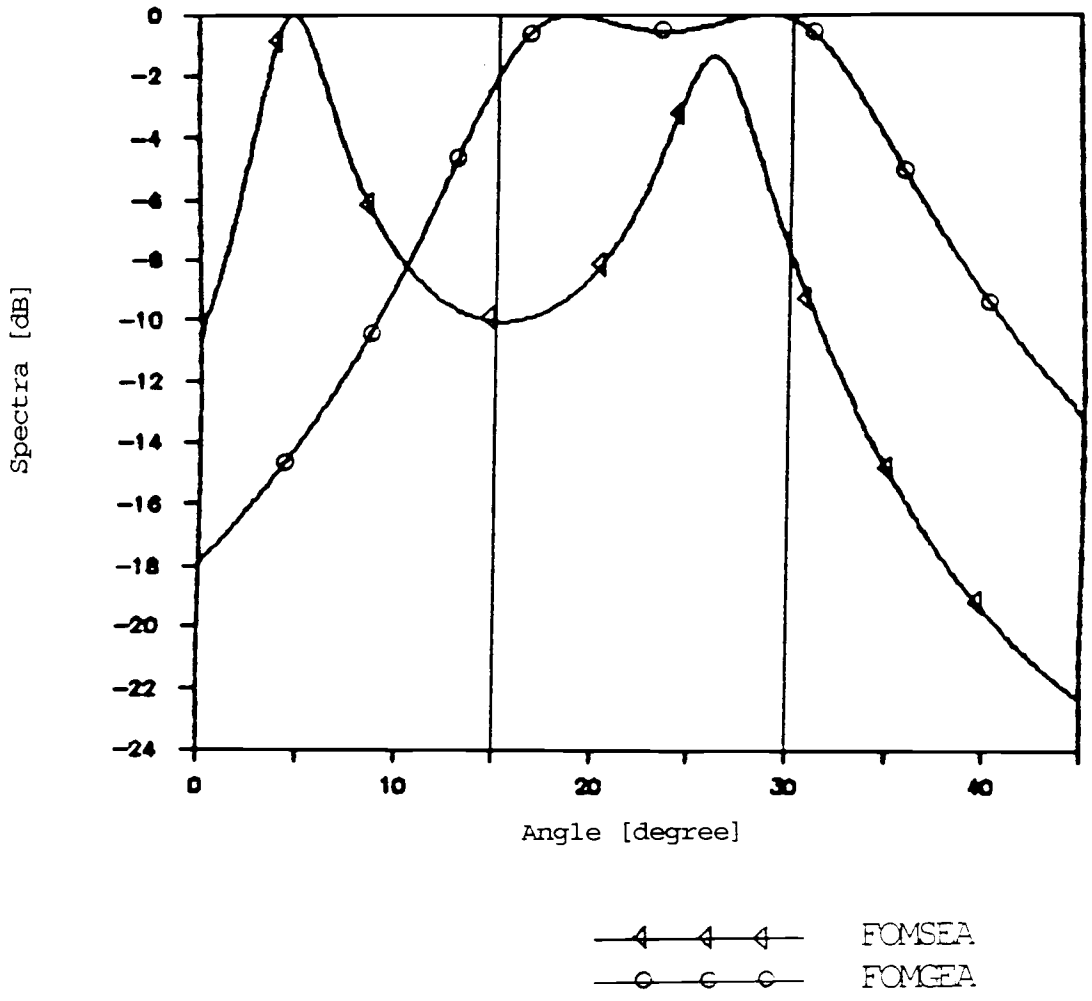

Fig.2-19. MUSIC Based on the Standard and Generalized Eigenstructure algorithms of Two Sources, θ_1=15°, θ_2=30°, with 50% Correlated 3 Sensors at S/N=0.0 dB.

2.6 Information Theoretic Criteria for Determining Number of Source Signals

The eigenstructure algorithm theoretically provides the information on the number of source signals by examining the identical minumum eigenvalues of the array covariance matrix. However, in practice the eigenvalues of the array covariance matrix for a finite sample size result in differences of magnitude. Therefore, the number of source signals must first be determined before using the eigenstructure-based method. In this section, the procedures introduced by Akaike (AIC) [1] and Schwartz and Rissanen (MDL) [34,41] for determining the number of source signals are considered.

Assuming that $\varepsilon_1 > \varepsilon_2 > \cdots > \varepsilon_Q$ are the eigenvalues of the sample-covariance matrix $\mathbf{R}$

$$\hat{\mathbf{R}} = (1/N) \sum_{t=1}^{N} \mathbf{r}(t)\ \mathbf{r}^*(t), \tag{2-40}$$

where $t = 1, 2, \cdots, N$, is the observed data which is i.i.d. and complex Gaussian, and it may be assumed that $M < Q$,

the AIC criterion is then defined by

$$\mathrm{AIC}(k) = -2L(k) + 2\zeta(k)\ , \tag{2-41}$$

where

$$L(k) = -2\log\left[\frac{\prod_{i=k+1}^{Q}\varepsilon_i}{(1/(Q-k))\sum_{i=k+1}^{Q}\varepsilon_i}^{Q-k}\right]^N \qquad (2\text{-}42)$$

is the maximum log-likelihood, and

$$\zeta(k) = k(2Q-k) + 1 \qquad (2\text{-}43)$$

is the number of free adjusted parameters within the model which provide the minimum AIC, i.e., (total number of parameters) - (number of parameters due to the normalization of the eigenvectors) - (number of parameters due to the mutual orthogonalization of the eigenvectors) = $(k+1+2Qk) - (2k) - 2((1/2)k(k-1))$. The number of source signals is then determined by selecting the minimum value of AIC(k), where $k = 0, 1, \cdots, Q-1$.

Note that according to Kashyap [19] the AIC criterion has been found to be statistically inconsistent insofar as the probability of error in choosing the correct number of source signals does not tend to zero as $N \to \infty$. Hence, for the large-sample limit, the AIC criterion tends to overestimate the true rank M.

The other criterion to consider for determination of the number of source signals is the minimum description length (MDL), defined by

$$\mathrm{MDL}(k) = -L(k) + (\log(N/2))\zeta(k), \qquad (2\text{-}44)$$

where $L(k)$ and $\zeta(k)$ are given by Eq. (2-42) and (2-43), respectively. The MDL criterion is known to yield a consistent estimate, i.e., the selection criterion converges to the true rank M in the large-sample limit [13,35,45].

Example 2.5 For this example, simulation results are presented to show the performances of the AIC and MDL in several situations. The source signals considered are plane waves with uniformly distriubuted random phasing on $(0,2\pi)$. First, a situation is considered in which two sources, $\theta_1 = 5°$, $\theta_2 = 10°$, are impinging on an sensor array with seven sensors at S/N = 5 dB, using $N = 128$. As shown in Table 2-1, both the MDL and AIC successfully detect the two closely spaced sources, although the eigenvalues of the sample-covariance matrix are all different, i.e., 15.97, 1.23, 0.37, 0.34, 0.30, 0.26, and 0.24. However, when a third source at 16° is added in the case of two sources with same S/N ratio, i.e., S/N = 5 dB, the AIC minimum value can be correctly obtained for $M = 3$, but the MDL minimum value is incorrectly detected for $M = 2$ (see Table 2-2). To observe the limitations of the detectability of MDL and AIC, the AIC and MDL tests were performed for three sources at 5°, 10°, and 16° in terms of the S/N ratio shown in Table 2-3. It is noteworthy that, according to these experimental results, the AIC criterion is more reliable

than the MDL criterion for determination of the number of source signals when the sources are closely spaced at a very low S/N ratio. For this simulation, with source signals set at $\theta_1 = 5°$, $\theta_2 = 10°$, and $\theta_3 = 16°$, the lowest S/N ratio for the AIC sufficient for precise determination of the number of sources is -2 dB, while the MDL is satisfactory so long as the S/N ratio is above 5 dB.

Table 2-1. The MDL and AIC Criteria for the Two Closely Spaced Sources at 5° and 10°, with S/N=5 dB, N=128.

k	0	1	2	3	4	5	6
MDL	1274.84	177.22	66.76	84.64	98.46	109.29	116.45
AIC	2549.69	317.37	65.07	75.16	82.84	90.24	96.00

Table 2-2. The MDL and AIC Criteria for the Three Closely Spaced Sources at 5°, 10°, and 16°, with S/N=5 dB, N=128.

k	0	1	2	3	4	5	6
MDL	1310.43	588.57	85.03	85.66	98.30	109.33	116.45
AIC	2620.87	1140.07	101.60	77.20	82.51	90.31	96.00

Table 2-3. The Limitations of the MDL and AIC Criteria for the Three Closely Spaced Sources at 5°, 10°, and 16°, with N=128, as the S/N ratio changes.

	k	0	1	2	3	4	5	6
-3[dB]	MDL	449.53	144.99	72.42	85.69	98.50	109.36	116.45
	AIC	899.06	252.90	76.38	77.27	82.90	90.35	96.00
-2[dB]	MDL	534.55	174.33	73.12	85.70	98.47	109.35	116.45
	AIC	1069.11	311.57	77.79	77.28	82.86	90.35	96.00
0[dB]	MDL	728.27	253.53	74.94	85.71	98.42	109.34	116.45
	AIC	1456.54	469.98	81.45	77.30	82.77	90.35	96.00
3[dB]	MDL	1065.36	430.88	79.57	85.70	98.35	109.34	116.45
	AIC	2130.73	824.69	90.69	77.28	82.62	90.33	96.00
5[dB]	MDL	1310.43	588.57	85.03	85.66	98.30	109.33	116.45
	AIC	2620.87	1140.07	101.60	77.20	82.51	90.31	96.00
10[dB]	MDL	2074.62	1196.18	133.39	85.43	98.13	109.29	116.45
	AIC	4149.25	2355.30	198.32	76.74	82.19	90.25	96.00

CHAPTER 3

NONLINEAR SECOND-ORDER DIRECTION FINDING METHODS

In Chapter 2, it was demonstrated that the FOM based on the standard eigenstructure algorithm offers much better resolution limits than the Bartlett, ML, or AR spectral estimates so long as noises are uncorrelated between sensors. Moreover, if the noise correlation coefficient can be accurately estimated, the generalized eigenstructure algorithm can be applied for the determination of source directions. However, in practical terms it is often difficult to accurately estimate the noise correlation coefficients [28].

In this chapter, second-order methods (SOM) based on an eigenstructure algorithm for accomodating cases such as closely-spaced source signals with very low S/N ratios, non-Gaussian noises, or spatially correlated Gaussian noises in absence of noise correlation coefficient information are considered. The key to SOM performance is the use of new data sequences, or second-order signals, by auto-convolution of the original received data on each array sensor, of the array, where each auto-convolved data point provides information on all the other data points in correlation operations with a constant lag. Thus, the S/N ratios for the new data sequences are improved, which is reconsidered using the theoretical derived results in

Chapter 5. In the following section, the second-order signal and noise model are first derived, then the ordinary and revised SOMs are introduced and compared in terms of their resolution capabilities.

3.1 Mathematical Derivations - SOM

The Fourier transform of the received signal vector in Eq.(2-11) has the form of [4]

$$\mathbf{F} = \mathbf{A}_1\mathbf{S} + \mathbf{X} , \tag{3-1}$$

where

$$\mathbf{F} = F[\mathbf{r}], \ \mathbf{S} = F[\mathbf{s}], \text{ and } \mathbf{X} = F[\mathbf{x}].$$

Then, the spectral-density matrix of $\mathbf{L}_{(1)}$ is obtained as

$$\mathbf{L}_{(1)} = \mathbf{A}_1\mathbf{P}_1\mathbf{A}_1^* + \mathbf{D}_{x1} , \tag{3-2}$$

where $\mathbf{L}_{(1)} = E[\mathbf{F}\mathbf{F}^*]$, $\mathbf{P}_1 = E[\mathbf{S}\mathbf{S}^*]$, and $\mathbf{D}_{x1} = E[\mathbf{X}\mathbf{X}^*]$.

The second-order signals are built by (auto) convolution operations on the received signals at the ith sensor as

$$r_{(2)i}(t) = r_i(t) \otimes r_i(t) . \tag{3-3}$$

The corresponding vector for the second-order signals can be expressed in the frequency domain as

$$\mathbf{F}_{(2)}{}^T = [F_1{}^2 \ F_2{}^2 \cdot \cdot \cdot F_Q{}^2] . \tag{3-4}$$

In order to efficiently handle these matrices a new matrix operator Δ, or a "Delta product", performs a component to component multiplication,

$$\mathbf{A} \Delta \mathbf{B} = \mathbf{C} \qquad \leftrightarrow \qquad a_{ij} b_{ij} = c_{ij}, \tag{3-5}$$

where **A**, **B** and **C** are of identical dimensions. The Δ product has the following properties:

1) For p x q matrices:

a) $\mathbf{A} \Delta \mathbf{B} = \mathbf{B} \Delta \mathbf{A}$,

b) $\mathbf{A} \Delta (\mathbf{B} \Delta \mathbf{C}) = (\mathbf{A} \Delta \mathbf{B}) \Delta \mathbf{C}$,

c) $(\mathbf{A} \Delta \mathbf{B})^{*} = \mathbf{A}^{*} \Delta \mathbf{B}^{*}$,

d) $(\mathbf{A} + \mathbf{B}) \Delta \mathbf{C} = (\mathbf{A} \Delta \mathbf{C}) + (\mathbf{B} \Delta \mathbf{C})$,

e) $\mathbf{I} \Delta \mathbf{I} = \mathbf{I}$, and

f) $$(\mathbf{A}+\mathbf{B})^{\Delta M} = \sum_{k=0}^{M} \frac{M!}{k!(M-k)!} \mathbf{A}^{\Delta k} \mathbf{B}^{\Delta (M-k)};$$

2) For p x 1 vector: $(\mathbf{A} \Delta \mathbf{B})(\mathbf{C} \Delta \mathbf{D})^{*} = (\mathbf{A}\mathbf{C}^{*}) \Delta (\mathbf{B}\mathbf{D}^{*})$ $= (\mathbf{A}\mathbf{D}^{*}) \Delta (\mathbf{B}\mathbf{C}^{*})$.

By definition [4], the second-order spectral-density matrix is expressed as

$$\begin{aligned} \mathbf{L}_{(2)} &= E[\mathbf{F}_{(2)} \mathbf{F}_{(2)}^{*}] \\ &= E[(\mathbf{F}\mathbf{F})^{\Delta 2}] \\ &= E\{[\mathbf{A}_1 \mathbf{S} + \mathbf{X})(\mathbf{A}_1 \mathbf{S} + \mathbf{X})^{*}]^{\Delta 2}\} \\ &= E[(\mathbf{A}_1 \mathbf{S}^{*} \mathbf{S} \mathbf{A}_1^{*} + \mathbf{A}_1 \mathbf{S} \mathbf{X}^{*} + \mathbf{X} \mathbf{S}^{*} \mathbf{A}_1^{*} + \mathbf{X}\mathbf{X}^{*})^{\Delta 2}] \; . \end{aligned} \tag{3-6}$$

Note that in Eq. (3-6), each element inside the expectation bracket is the same as an element of $\mathbf{L}_{(1)}$, but is raised to the power of 2. When source signals and noises are uncorrelated, then

$$E[(\mathbf{A}_1\mathbf{S}\mathbf{X}^*)\Delta(\mathbf{X}\mathbf{X}^*)] = \mathbf{0}, \tag{3-7}$$

$$E[(\mathbf{X}\mathbf{S}^*\mathbf{A}_1^*)\Delta(\mathbf{X}\mathbf{X}^*)] = \mathbf{0}, \tag{3-8}$$

$$E[(\mathbf{A}_1\mathbf{S}\mathbf{S}^*\mathbf{A}_1^*)\Delta(\mathbf{A}_1\mathbf{S}\mathbf{X}^*)] = \mathbf{0}, \tag{3-9}$$

and

$$E[(\mathbf{A}_1\mathbf{S}\mathbf{S}^*\mathbf{A}_1^*)\Delta(\mathbf{X}\mathbf{S}^*\mathbf{A}_1^*)] = \mathbf{0}\ . \tag{3-10}$$

For the stationary random process $x_l(t) = a_l(t) + jb_l(t)$, where $a_l(t)$ and $b_l(t)$ are independent, the Fourier transform of $x_l(t)$ is given by

$$X_l = X_{lr} + jX_{li},$$

where $X_{lr} = F[a_l(t)]$ and $X_{li} = F[b_l(t)]$ with zero-means and $\mathrm{Var}[X_{lr}] = \mathrm{Var}[X_{li}] = \sigma_x^2$, *the mean value* of X_l is $E[X_l] = E[X_{lr}] + jE[X_{li}] = 0$ and *the variance* of X_l is $E[X_l X_l^*] = E[|X_l|^2] = E[X_{lr}^2 + X_{li}^2] = \mathrm{Var}[X_{lr}] + \mathrm{Var}[X_{li}] = 2\sigma_x^2$.

Now, when the values of $E[X_l^2]$ and $E[(X_l^*)^2]$ are examined:

i) $E[X_l^2] = E[(X_{lr}+jX_{li})^2]$

$= E[X_{lr}^2 - X_{li}^2 + j2X_{lr}X_{li}] = E[X_{lr}^2] - E[X_{li}^2]$

$+ j2E[X_{lr}]E[X_{li}] = 0$.

ii) $E[(X_l^*)^2] = E[X_{lr}^2] - E[X_{li}^2] - j2E[X_{lr}]E[X_{li}] = 0$.

Thus, for a complex Gaussian random variable,

$$E[X_l^2(X_m^*)^2] = E[X_l^2]E[(X_m^*)^2] = 0 \quad \text{if } l \neq m\ .$$

On the other hand, if $l=m$, then

$$E[X_l^2(X_l^*)^2] = 3\sigma_x^4 + 3\sigma_x^4 + 2\sigma_x^4 = 8\sigma_x^4$$

since $E[X_{lr}^4]=E[X_{li}^4]= 3\mathrm{Var}^2[X_{lr}]= 3\sigma_x^4$. Using these results, it is possible to obtain

$$E[(\mathbf{A}_1\mathbf{S}\mathbf{X}^*)\Delta(\mathbf{A}_1\mathbf{S}\mathbf{X}^*)] = E[(\mathbf{A}_1\mathbf{S}\mathbf{X}^*)^{\Delta 2}] = \mathbf{0}$$

and

$$E[(\mathbf{X}\mathbf{S}^*\mathbf{A}_1^*)\Delta(\mathbf{X}\mathbf{S}^*\mathbf{A}_1^*)] = E[(\mathbf{X}\mathbf{S}^*\mathbf{A}_1^*)^{\Delta 2}] = \mathbf{0}.$$

Example 3.1 For $Q = 3$ and $M = 2$:

$$E[(\mathbf{A}_1\mathbf{S}\mathbf{X}^*)\Delta(\mathbf{A}_1\mathbf{S}\mathbf{X}^*)] = E\left(\left(\begin{bmatrix} a_{11} & a_{12} \\ a_{21} & a_{22} \\ a_{31} & a_{32} \end{bmatrix}\begin{bmatrix} s_1 \\ s_2 \end{bmatrix}\begin{bmatrix} x_1^* & x_2^* & x_3^* \end{bmatrix}\right)^{\Delta 2},$$

$$E[(\mathbf{A}_1\mathbf{S}\mathbf{X}^*)^{\Delta 2}]_{11}$$

$$= E[(a_{11}s_1x_1^* + a_{12}s_2x_1^*)^2]$$

$$= a_{11}^2\,E[s_1^2]E[(x_1^*)^2] + a_{12}^2\,E[s_2^2]E[(x_1^*)^2]$$

$$+ 2a_{11}a_{12}\,E[s_1]E[s_2]E[(x_1^*)^2] = 0,$$

and

$$E[(\mathbf{A}_1\mathbf{S}\mathbf{X}^*)^{\Delta 2}]_{12} = E[(a_{11}s_1x_2^* + a_{12}s_2x_2^*)^2]$$

$$= a_{11}^2\,E[s_1^2]E[(x_2^*)^2] + a_{12}^2\,E[s_2^2]E[(x_2^*)^2]$$

$$+ 2a_{11}a_{12}\,E[s_1]E[s_2]E[(x_2^*)^2] = 0.$$

In the same manner, $E[(\mathbf{A}_1\mathbf{S}\mathbf{X}^*)^{\Delta 2}]_{ij} = 0$ for $i,j = 1,2,3$.

The remaining terms of Eq.(3-6) become

$$\mathbf{L}_{(2)} = E[(\mathbf{A}_1\mathbf{S}\mathbf{S}^*\mathbf{A}_1^*)^{\Delta 2}] + 2E[(\mathbf{A}_1\mathbf{S}\mathbf{S}^*\mathbf{A}_1^*)\Delta(\mathbf{X}\mathbf{X}^*)]$$

$$+ 2E[(\mathbf{A}_1\mathbf{S}\mathbf{X}^*)\Delta(\mathbf{X}\mathbf{S}^*\mathbf{A}_1^*)] + \mathbf{D}_{x2}\,, \qquad (3\text{-}11)$$

where $\mathbf{D}_{x2} = E[(\mathbf{X}\mathbf{X}^*)^{\Delta 2}]$.

Now, to solve for $E[(\mathbf{A}_1\mathbf{S}\mathbf{S}^*\mathbf{A}_1^*)^{\Delta 2}]$ in the case of independent sources,

$$E[(\mathbf{A}_1\mathbf{S}\mathbf{S}^*\mathbf{A}_1^*)^{\Delta 2}]_{ij} = E\{[(\sum_{k1} a_{ik1}s_{k1})(\sum_{k2} s_{k2}a_{jk2}^*)]^2\}$$

$$= E[\sum_{k1}\sum_{k2}\sum_{k3}\sum_{k4} a_{ik1}a_{ik3}s_{k1}s_{k3}s_{k2}s_{k4}a_{jk2}^*a_{jk4}^*]:$$

i) When $k_1=k_3 (=,\neq) k_2=k_4$,

$$E[(\mathbf{A}_1\mathbf{S}\mathbf{S}^*\mathbf{A}_1^*)^{\Delta 2}]_{ij} = E[\sum_{k1}\sum_{k2} a_{ik1}^2 s_{k1}^2 s_{k2}^2 (a_{jk2}^*)^2]$$

$$= \sum_{k1}\sum_{k2} a_{ik1}^2\, E[s_{k1}^2 s_{k2}^2]\,(a_{jk2}^*)^2$$

$$= [\mathbf{A}_2\mathbf{P}_2\mathbf{A}_2^*]_{ij} \;;$$

where $\mathbf{A}_2 = \mathbf{A}_1^{\Delta 2}$, $\mathbf{P}_2 = E[(\mathbf{S}\mathbf{S}^*)^{\Delta 2}]$;

ii) When $k_1=k_2\neq k_3=k_4$,

$$E[(\mathbf{A}_1\mathbf{S}\mathbf{S}^*\mathbf{A}_1^*)^{\Delta 2}]_{ij} = E[\sum_{k1}\sum_{k3}(a_{ik1}s_{k1}^2 a_{jk1}^*)(a_{ik3}s_{k3}^2 a_{jk3}^*)]$$

$$= E[\sum_{k1}(a_{ik1}s_{k1}^2 a_{jk1}^*)]E[\sum_{k3}(a_{ik3}s_{k3}^2 a_{jk3}^*)]$$

$$= E(\mathbf{A}_1\mathbf{P}_1\mathbf{A}_1^*)(\mathbf{A}_1\mathbf{P}_1\mathbf{A}_1^*)]_{ij} - \sum a_{ik3}^2\, E^{\,2}[s_{k3}^2]\,(a_{jk3}^*)^2$$

$$= [(\mathbf{A}_1\mathbf{P}_1\mathbf{A}_1^*)(\mathbf{A}_1\mathbf{P}_1\mathbf{A}_1^*) - \mathbf{A}_2\mathbf{P}_1^{\Delta 2}\mathbf{A}_2^*]_{ij};$$

iii) When $k_1=k_4\neq k_3=k_2$,

$$E[(\mathbf{A}_1\mathbf{S}\mathbf{S}^*\mathbf{A}_1^*)^{\Delta 2}]_{ij} = [(\mathbf{A}_1\mathbf{P}_1\mathbf{A}_1^*)(\mathbf{A}_1\mathbf{P}_1\mathbf{A}_1^*) - \mathbf{A}_2\mathbf{P}_1^{\Delta 2}\mathbf{A}_2^*]_{ij},$$

in the same manner as ii); and

iv) In all the other cases,

$$E[s_{k1}s_{k2}s_{k3}s_{k4}] = 0.$$

Therefore, the sum of i) through iv) gives

$$E[(\mathbf{A}_1\mathbf{S}\mathbf{S}^*\mathbf{A}_1^*)^{\Delta 2}]$$

$$= \mathbf{A}_2\mathbf{P}_2\mathbf{A}_2^* + 2\,[(\mathbf{A}_1\mathbf{P}_1\mathbf{A}_1^*)^{\Delta 2} - \mathbf{A}_2\mathbf{P}_1^{\Delta 2}\mathbf{A}_2^*]. \qquad (3\text{-}12)$$

Using the characteristics of the "Delta product",

$$E[(\mathbf{A}_1\mathbf{S}\mathbf{X}^*)\Delta(\mathbf{X}\mathbf{S}^*\mathbf{A}_1^*)]$$

$$= E[(\mathbf{A}_1\mathbf{S}\mathbf{S}^*\mathbf{A}_1^*)\Delta(\mathbf{X}\mathbf{X}^*)] = (\mathbf{A}_1 E[\mathbf{S}\mathbf{S}^*]\mathbf{A}_1^*)\Delta E[\mathbf{X}\mathbf{X}^*]$$

$$= (\mathbf{A}_1\mathbf{P}_1\mathbf{A}_1^*)\Delta\mathbf{D}_{x1} \qquad (3\text{-}13)$$

can be derived. For pure sinusoidal sources, with or without uniformly distributed random phasing, we have the relationship

$$\mathbf{P}_2 = \mathbf{P}_1^{\Delta 2}. \qquad (3\text{-}14)$$

Substituting Eqs.(3-12)-(3-14), into (3-11) yields

$$\mathbf{L}_{(2)} = \mathbf{A}_2\mathbf{P}_2\mathbf{A}_2^* + 2[(\mathbf{A}_1\mathbf{P}_1\mathbf{A}_1^*) - \mathbf{A}_2\mathbf{P}_2\mathbf{A}_2^*)]$$

$$+ 2(\mathbf{A}_1\mathbf{P}_1\mathbf{A}_1^*)\Delta\mathbf{D}_{x1} + 2(\mathbf{A}_1\mathbf{P}_1\mathbf{A}_1^*)\Delta\mathbf{D}_{x1} + \mathbf{D}_{x2}. \qquad (3\text{-}15)$$

Then, from Eq.(3-2),

$$\mathbf{A}_1\mathbf{P}_1\mathbf{A}_1^* = \mathbf{L}_{(1)} - \mathbf{D}_{x1}. \qquad (3\text{-}16)$$

3.2 Ordinary and Revised Second-Order Methods

Combining Eq.(3-15) with Eq.(3-16) results in:

$$\mathbf{L}_{(2)} = \mathbf{A}_2\mathbf{P}_2\mathbf{A}_2^* + 2[(\mathbf{L}_{(1)} - \mathbf{D}_{x1})^{\Delta 2} - \mathbf{A}_2\mathbf{P}_2\mathbf{A}_2^*]$$

$$+ 4(\mathbf{L}_{(1)} - \mathbf{D}_{x1})\Delta\mathbf{D}_{x1} + \mathbf{D}_{x2}$$

$$= -\mathbf{A}_2\mathbf{P}_2\mathbf{A}_2^* - 2\mathbf{D}_{x1}^{\Delta 2} + \mathbf{D}_{x2} + 2\mathbf{L}_{(1)}^{\Delta 2}. \qquad (3\text{-}17)$$

If $\mathbf{L}_{(2)} = \mathbf{L}_{(1)}^{\Delta 2}$ [18], then

$$\mathbf{L}_{(2)} = \mathbf{A}_2\mathbf{P}_2\mathbf{A}_2^* + (2\mathbf{D}_{x1}^{\Delta 2} - \mathbf{D}_{x2}) \quad . \tag{3-18}$$

This is the ordinary second-order spectral density matrix derived in Bugnon and Mohler [4] and Bugnon, Mohler, and Rhee [5].

Now, the first-order and second-order spectral density matrix in Eq.(3-17) can be used by defining the revised second-order spectral density matrix as

$$\mathbf{L}_{(2)R} = 2\mathbf{L}_{(1)}^{\Delta 2} - \mathbf{L}_{(2)} . \tag{3-19}$$

Then,

$$\mathbf{L}_{(2)R} = \mathbf{A}_2\mathbf{P}_2\mathbf{A}_2^* + \mathbf{D}_x \tag{3-20}$$

where

$$\mathbf{D}_x = 2\mathbf{D}_{x1}^{\Delta 2} - \mathbf{D}_{x2} \quad . \tag{3-21}$$

The right-hand side of Eq.(3-20) takes exactly the same form as the right-hand side of Eq.(3-18). However, the revised second-order spectral density matrix provides more accurate information on second-order data sequences than the ordinary second-order spectral density matrix since $\mathbf{L}_{(2)}$ cannot be exactly equal to $\mathbf{L}_{(1)}^{\Delta 2}$.

Now, the same orthogonality test can be performed for both Eqs.(3-18) and (3-20) as for the MUSIC by squaring each element of the searching vector in Eq.(2-25). This doubles the effective aperture of the sensor array and in theory resolution becomes twice that of the FOM.

Fig. 3-1 depicts the procedure of performing the revised SOM. The following example provides a comparison of

the performances of the relative resolution capabilities between the MUSIC, the ordinary SOM, and the revised SOM.

Example 3.2 In this example, the computer simulation results for the resolution of two plane waves in uncorrelated Gaussian sensor noises, with N = 256, are given. First, from Fig. 3-2, two sources at $\theta_1 = 8^\circ$ and 13° were estimated using the MUSIC, the ordinary SOM, and the revised SOM, where S/N = -3 dB. This indicates that the ordinary and revised SOMs could successfully resolve the two peaks (the ordinary SOM: 8.0° and 13.7°; the revised SOM: 8.05° and 13.65°), while the MUSIC could not. Figs. 3-3 and 3-4 show the resolution capabilities of all three proposed methods for the two sources at 8° and 12° and 8° and 11°, respectively, at S/N = -3 dB. The ordinary SOM fails to resolve the two peaks of 3° separation, S/N = -3 dB, and the revised SOM still shows two peaks at 7.45° and 11.75° (Fig. 3-4). When the S/N ratio is increased from -3 dB to -2 dB, the two sources at 8° and 11° can be resolved, using both the ordinary and revised SOMs, as shown in Fig. 3-5. However, as shown in Fig. 3-6, all three methods at S/N = -3 dB cannot resolve the two peaks at 8° and 10°.

This example demonstrates that in comparision to the ordinary SOM, the revised SOM has the relatively improved resolution limit. More specific results and additional

discussion of the ordinary and revised SOMs may be found in Chapter 4.

This section is concluded by mentioning a very useful simulation tip for the SOM. The Fourier transform of the auto-convolution of the data sequence $\{r_n\}$, which is non-zero for only $0 \leq n \leq N-1$,

$$y_n = \sum_{k=0}^{N-1} r_k r_{n-k} \tag{3-22}$$

is given by the square of the Fourier transform of $\{r_n\}$,

$$Y(\omega) = R(\omega) R(\omega) \quad . \tag{3-23}$$

Since the length of the convolution of the two sequences, each of length N, is in general $2N$, the discrete Fourier transform (DFT) in the left member of the analog of Eq.(3-23) must be of length $2N$ when the DFTs in the right member of the analog of Eq.(3-23) are of length N. Therefore, if the sequence $\{r_n\}$ of length N is first zero-padded out to the length $2N$, then $\{y_n\}$, as given in Eq.(3-22), will still have the length $2N$ (for its non-zero portion) and a DFT of length $2N$ can be used for both members in the analog of Eq.(3-23). In fact, in this case the analog of Eq.(3-23) for the DFT is simply the frequency-sampled version of Eq.(3-22).

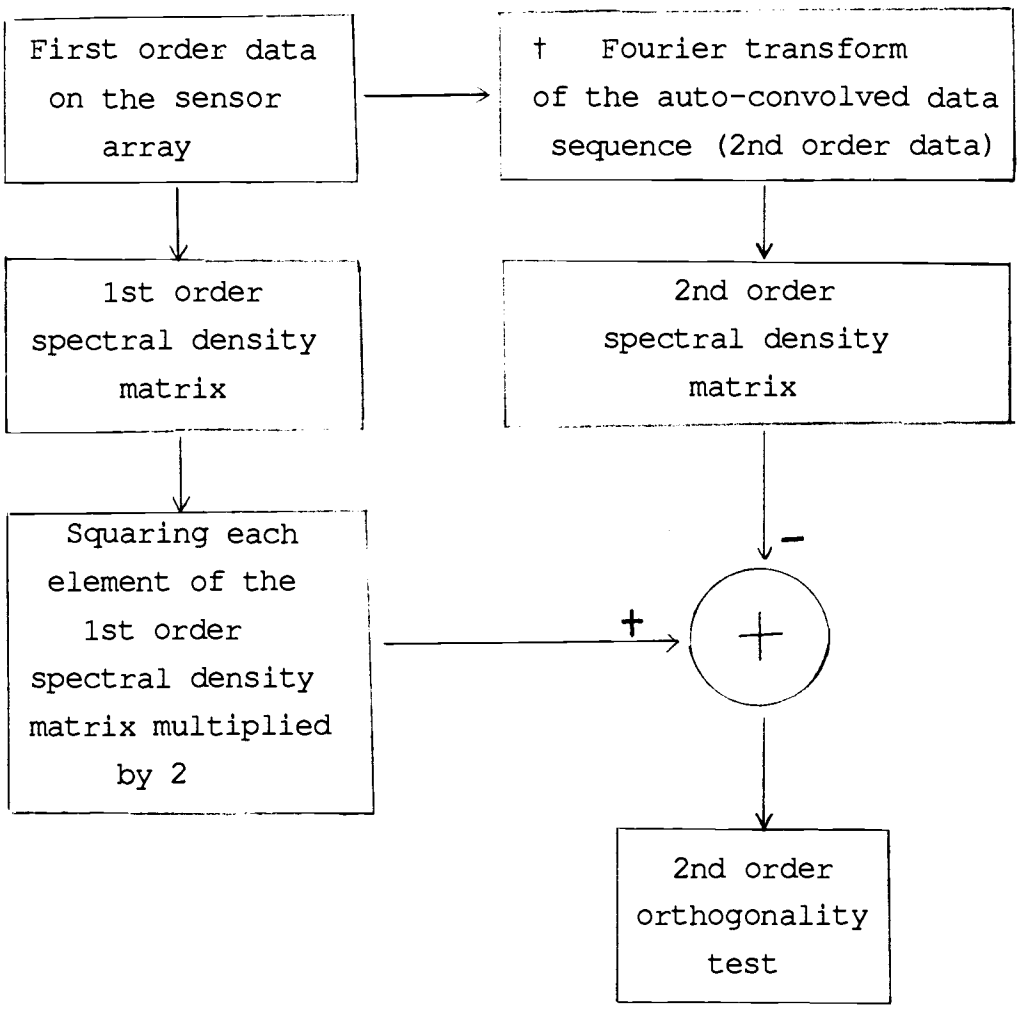

† Refer to the simulation tip in page 66 .

Fig.3-1. The procedure of the revised SOM.

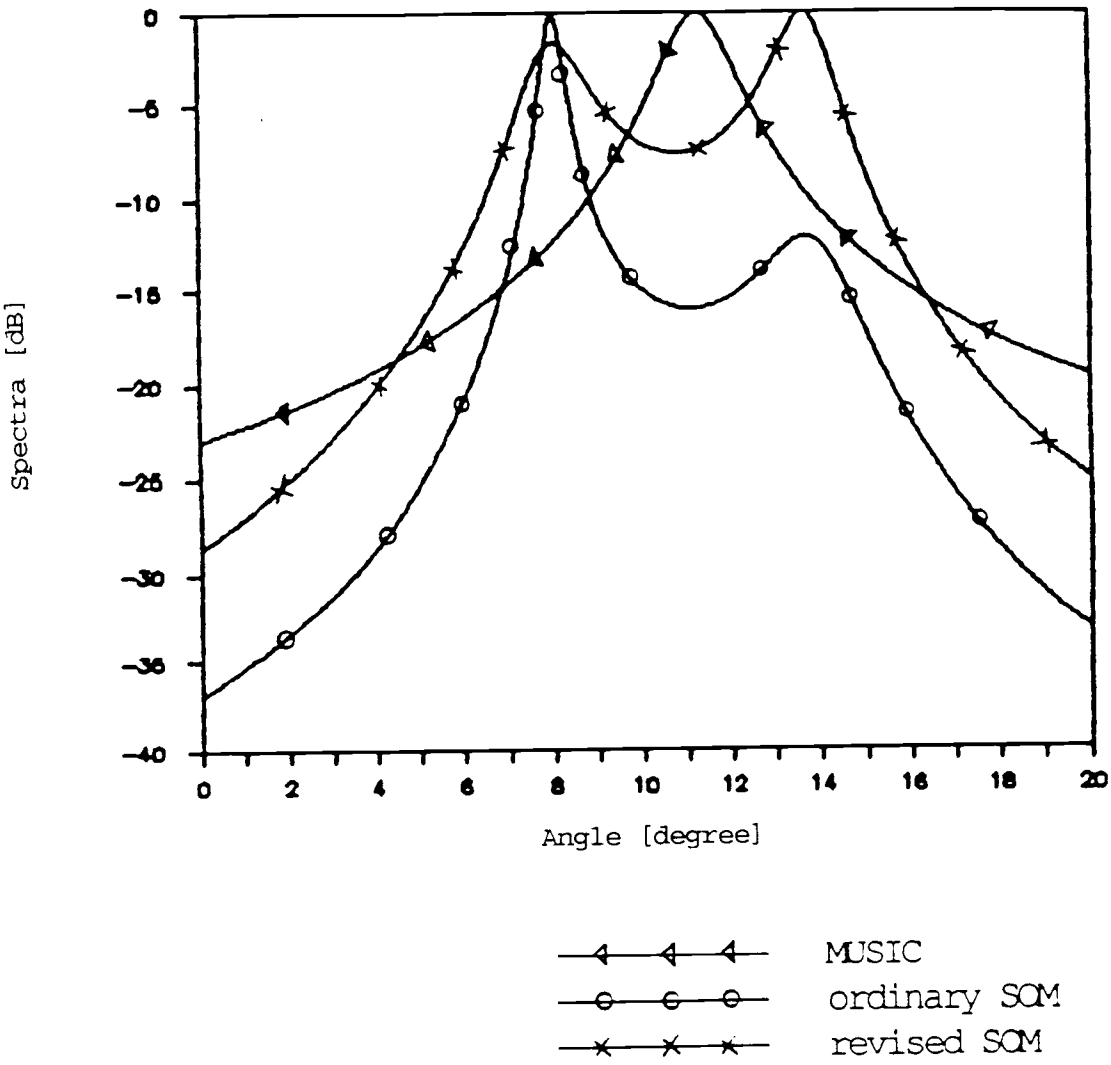

Fig.3-2. MUSIC, Ordinary SOM, and Revised SOM Spectra of Two Sources, θ_1=8° and θ_2=13°, with 3 Sensors at S/N=-3.0 dB, N=256.

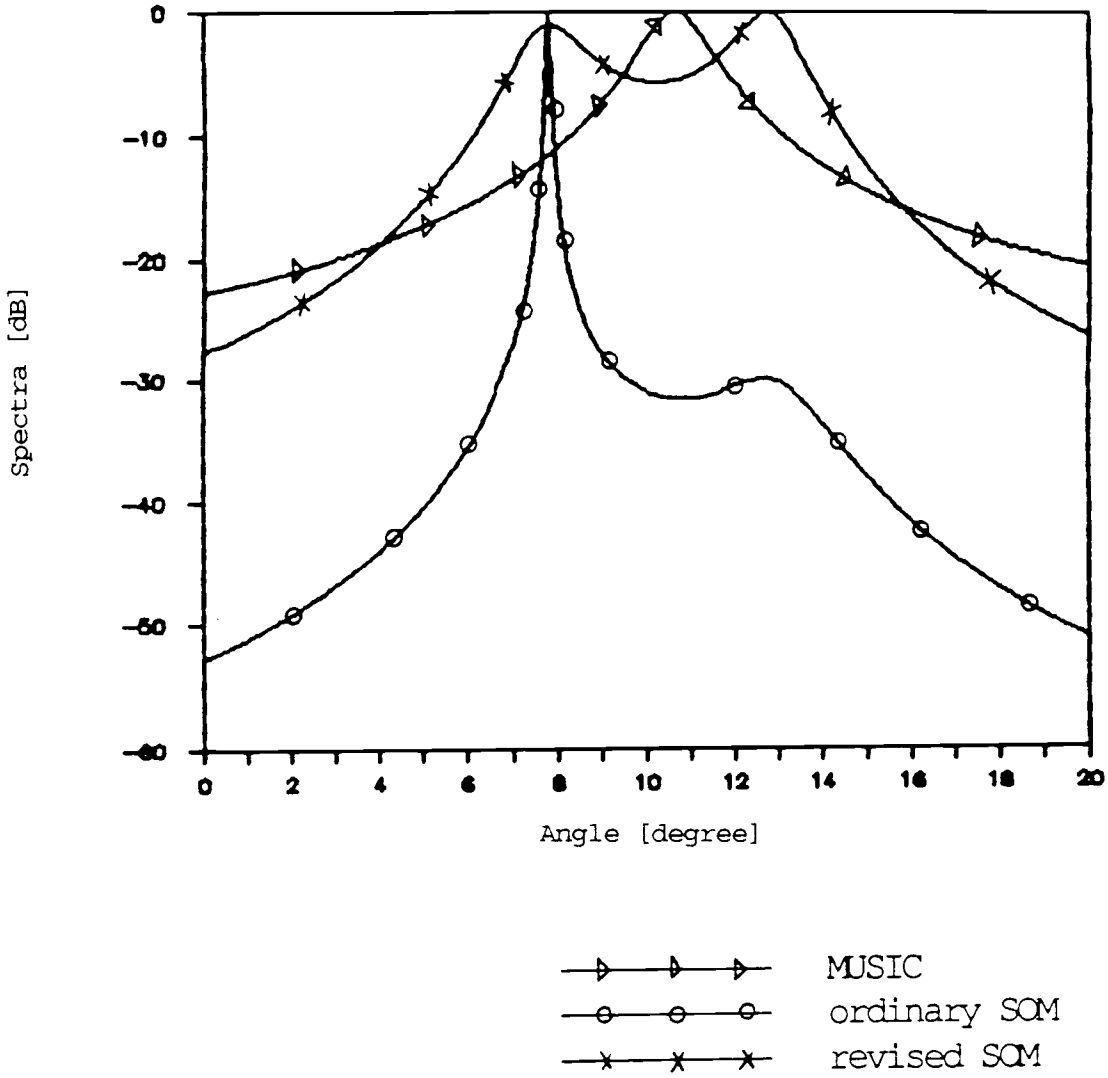

Fig.3-3. MUSIC, Ordinary SQM, and Revised SQM Spectra of Two Sources, θ_1=8° and θ_2=12°, with 3 Sensors at S/N=-3.0 dB, N=256.

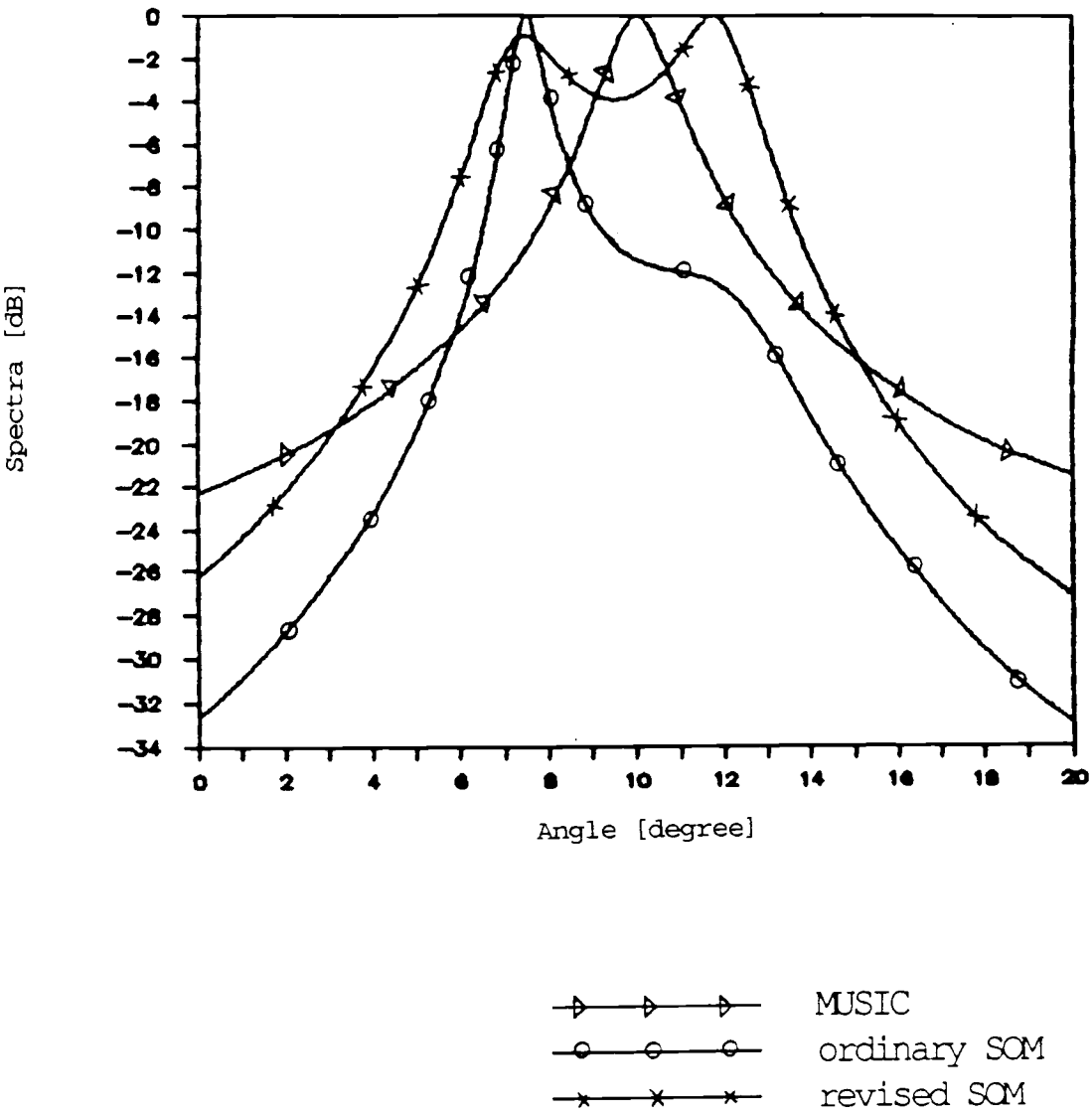

Fig.3-4. MUSIC, Ordinary SOM, and Revised SOM Spectra of Two Sources, θ_1=8° and θ_2=11°, with 3 Sensors at S/N=-3.0 dB, N=256.

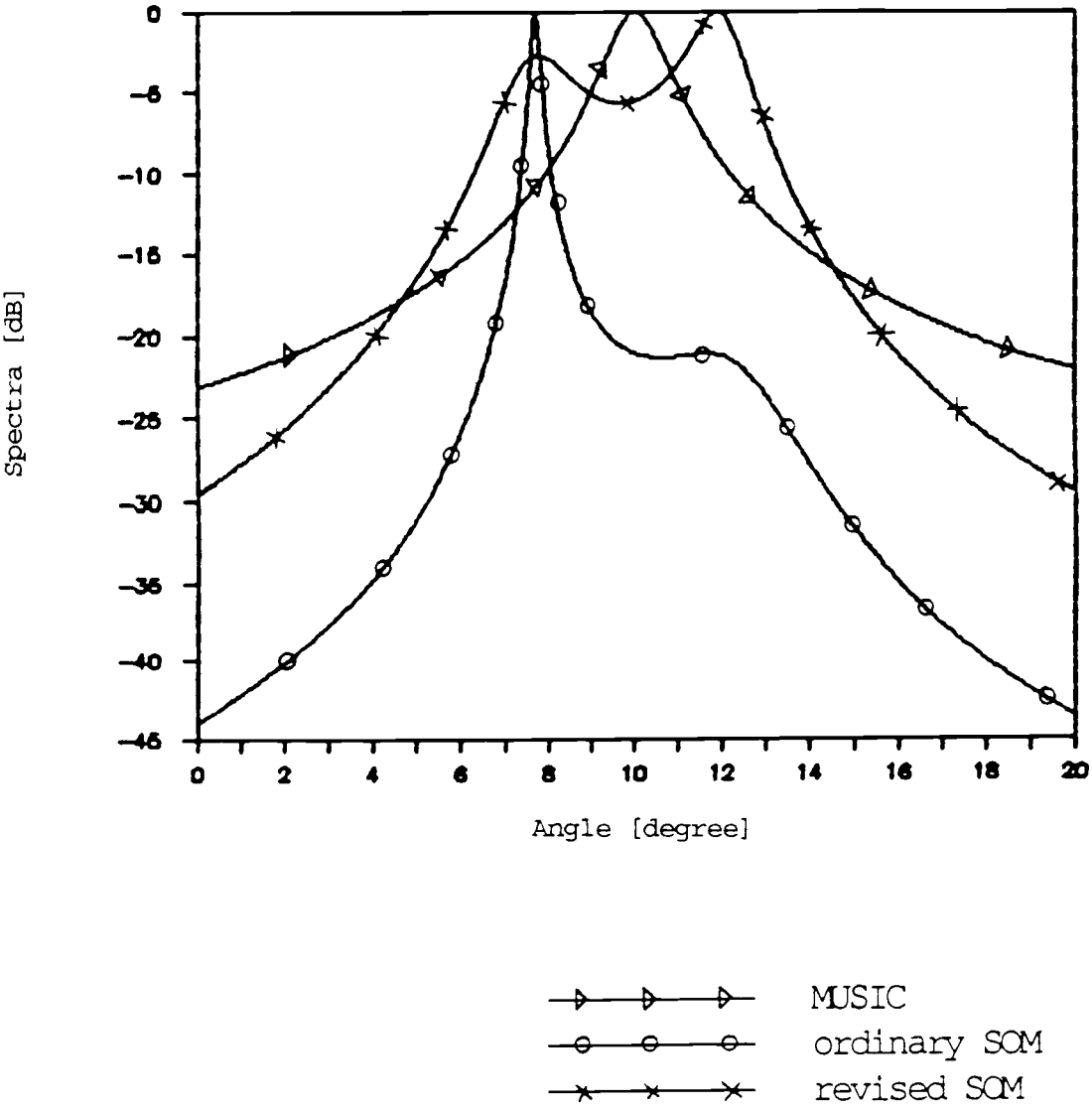

Fig.3-5. MUSIC, Ordinary SQM, and Revised SQM Spectra of Two Sources, θ_1=8° and θ_2=11°, with 3 Sensors at S/N=-2.0 dB, N=256.

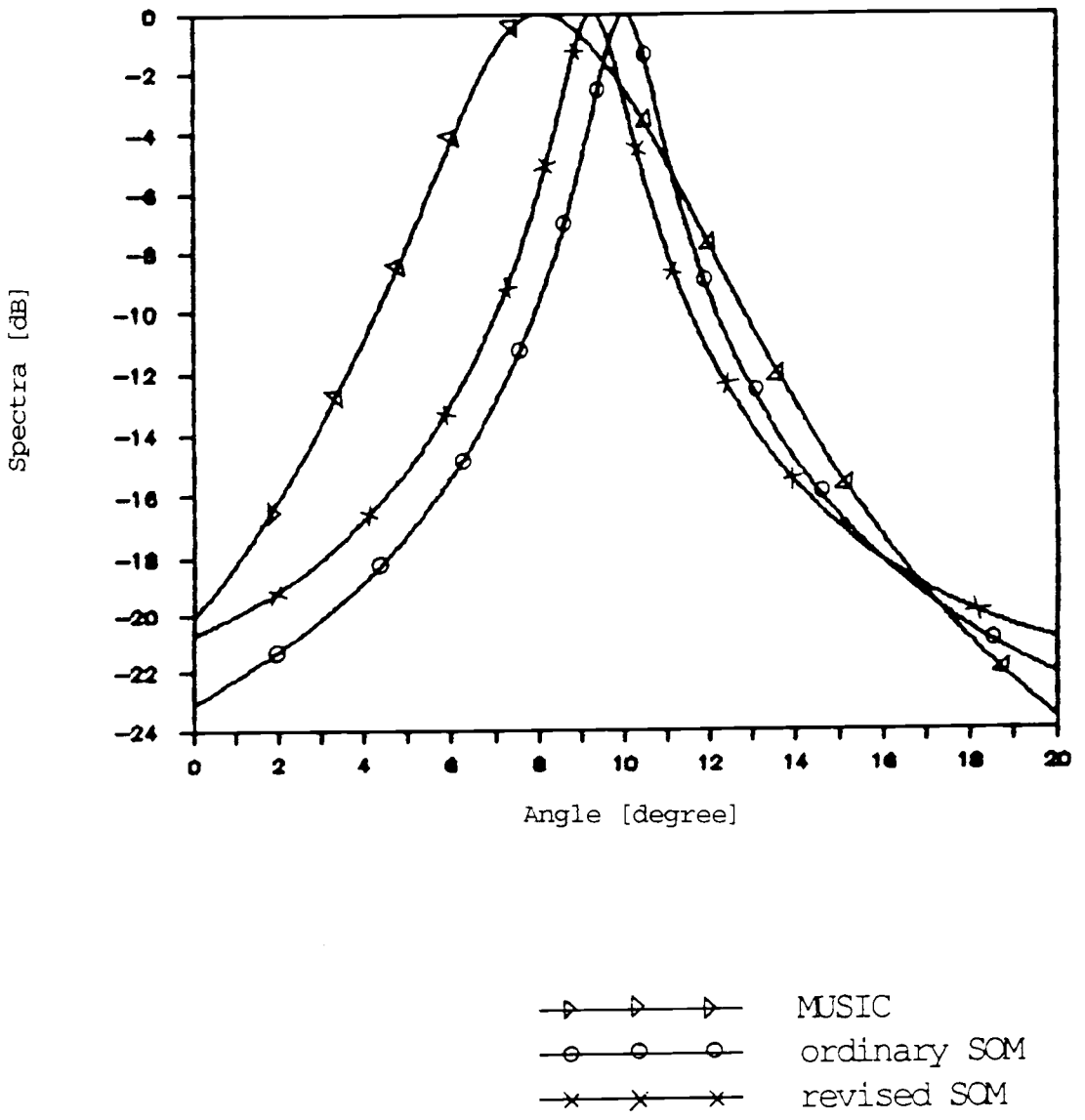

Fig.3-6. MUSIC, Ordinary SOM, and Revised SOM Spectra of Two Sources, θ_1=8° and θ_2=10°, with 3 Sensors at S/N=-3.0 dB, N=256.

3.3 Application: Combining SOMs with Spatial Smoothing Method

Recently, several eigenstructure-based methods yielding high resolution direction-finding estimates, so long as the source signals are uncorrelated or correlated, have been developed [2,29,32,39,44]. However, in practice, those methods do not resolve multiple sources which are coherent. In this section, a spatial smoothing scheme for the decorrelation of coherent sources is described [33,42], then applied as a spatial scheme to the FOMSEA and (ordinary) SOMSEA in order to compare FOM and SOM perfomance when combined with spatial smoothing techniques.

Consider a uniform linear array with Y identical sensors $\{1,2,\cdots,Y\}$ divided into L overlapping subarrays of size Q as shown in Fig. 3-7. Assume that the M ($M<Q$) source signals $s_1(t), s_2(t), \cdots, s_M(t)$ are coherent, i.e., $s_k(t) = \alpha_k s_1(t)$, $k = 1,2,\cdots,M$, with α_k designating a complex scalar of phase-delayed and amplitude-scaled replicas of one of the source signals. Applying complex (analytic) signal representation to the expression of the received signals from the directions $\{\theta_1, \theta_2, \cdots, \theta_M\}$ at the ith sensor, we have

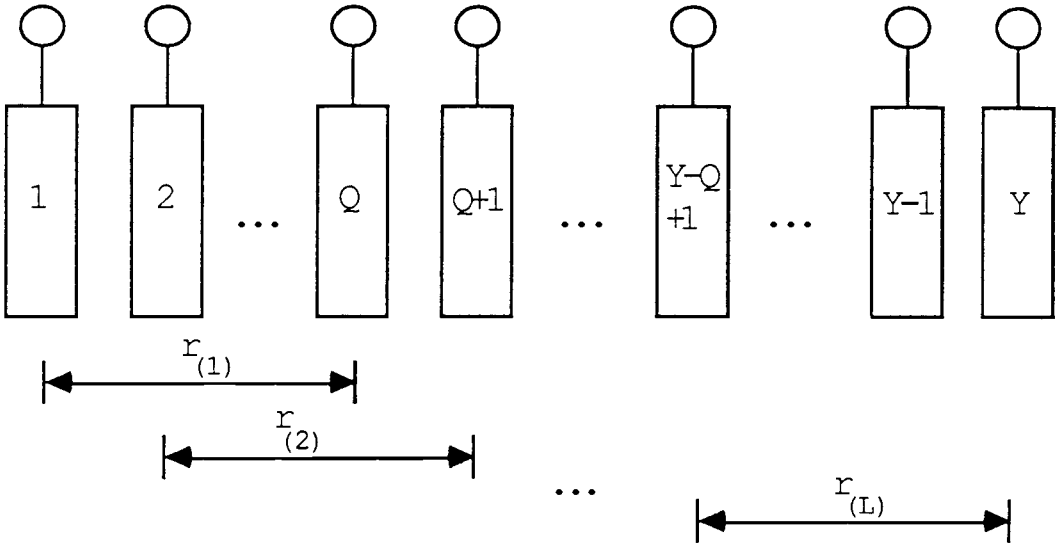

Fig. 3-7. Confuguartion of Subarrays for Spatial Smoothing.

$$r_i(t) = \sum_{k=1}^{M} s_k(t)\exp[-j\omega_{ik}] + x_i(t) \tag{3-24}$$

where $\omega_{ik} = \omega_o(i-1)(D/c)\sin\theta_k$, (3-25)

$x_i(t)$ is the additive noise at the ith sensor.

Rewriting Eq.(3-24) in vector form yields

$$\mathbf{r}^T(t) = [r_1(t),\ r_2(t),\ \cdots,\ r_Y(t)]$$

$$= \mathbf{A}_Y\mathbf{s}(t) + \mathbf{x}(t) \tag{3-26}$$

where

$$\mathbf{s}^T(t) = [s_1(t),\ s_2(t),\ \cdots,\ s_M(t)], \tag{3-27}$$

$$\mathbf{x}^T(t) = [x_1(t),\ x_2(t),\ \cdots,\ x_Y(t)], \text{ and} \tag{3-28}$$

$$\mathbf{A}_Y = [\mathbf{a}_Y(\theta_1),\ \mathbf{a}_Y(\theta_2),\ \cdots,\ \mathbf{a}_Y(\theta_M)], \tag{3-29}$$

with $\mathbf{a}_Y(\theta_k)$ representing the directional-vector

(associated with the arrival angle θ_k) expressed as

$$\mathbf{a}_Y^T(\theta_k) = [1, \exp(-j\omega_{2k}), \exp(-j\omega_{3k}), \cdots, \exp(-j\omega_{Yk})]. \quad (3\text{-}30)$$

Then, let $\mathbf{r}_{(l)}(\cdot)$ represent the vector of the received signals of the lth subarray for $l = 1,2,\cdots,L$, where $L = Y-Q+1$. Following the notation of Eq.(3-26),

$$\mathbf{r}_{(l)}(t) = [r_l(t), r_{l+1}(t), \cdots, r_{l+Q-1}(t)]^T$$
$$= \mathbf{A}_Q\mathbf{G}^{(l-1)}\mathbf{s}(t) + \mathbf{x}_{(l)}(t), \quad 1 \le l \le L, \quad (3\text{-}31)$$

where

$$\mathbf{x}_{(l)}(t) = [x_l(t), x_{l+1}(t), \cdots, x_{l+Q-1}(t)]^T, \text{ and} \quad (3\text{-}32)$$

$\mathbf{G}^{(l-1)}$ = $(l-1)$th power of the $M \times M$ diagonal matrix,

or

$$\mathbf{G} = \text{diag}[\chi_1, \chi_2, \cdots, \chi_M] \quad (3\text{-}33)$$

with

$$\chi_k = \exp[-j\omega_o(D/c)\sin\theta_k], \quad k = 1,2,\cdots,M. \quad (3\text{-}34)$$

Thus, the spatial covariance matrix of the lth subarray is

$$\mathbf{R}_{(l)} = E[\mathbf{r}_{(l)}(t)\mathbf{r}_{(l)}^*(t)]$$
$$= \mathbf{A}_Q\mathbf{G}^{(l-1)}\mathbf{P}(\mathbf{G}^{(l-1)})^*\mathbf{A}_Q^* + \sigma^2\mathbf{Q}_{(l)}, \quad (3\text{-}35)$$

where

$\mathbf{P}$ is the source sample covariance matrix defined in Eq.(2-16) and $\sigma^2\mathbf{Q}_{(l)} = E[\mathbf{X}_{(l)}(t)\mathbf{X}_{(l)}^*(t)]$ with common variance σ^2.

If the noises are uncorrelated and identical between sensors

with constant variance σ^2, Eq.(3-35) can be written as

$$\mathbf{R}_{(l)} = \mathbf{A}_Q \mathbf{G}^{(l-1)} \mathbf{P} (\mathbf{G}^{(l-1)})^* \mathbf{A}_Q^* + \sigma^2 \mathbf{I}_Q, \tag{3-36}$$

where $\mathbf{I}_Q$ denotes the Q x Q identity matrix.

Defining the spatial smoothing output covariance matrix as

$$\mathbf{R} = (1/L) \sum_{l=1}^{L} \mathbf{R}_{(l)} \tag{3-37}$$

and substituting Eq.(3-36) into Eq.(3-37) gives

$$\mathbf{R} = \mathbf{A}_Q \mathbf{P}_s \mathbf{A}_Q^* + \sigma^2 \mathbf{I}_Q \ , \tag{3-38}$$

where $\mathbf{P}_s$ denotes the spatial smoothing source covariance matrix:

$$\mathbf{P}_s = (1/L) \sum_{l=1}^{L} \mathbf{G}^{(l-1)} \mathbf{P} (\mathbf{G}^{(l-1)})^* \ . \tag{3-39}$$

On the other hand, the spatial smoothing source covariance matrix $\mathbf{P}_s$ can be expressed as

$$\mathbf{P}_s = (1/L) [\mathbf{I} \ \mathbf{G} \cdots \mathbf{G}^{(L-1)}] \begin{bmatrix} \mathbf{P} & & & 0 \\ & \mathbf{P} & & \\ & & \ddots & \\ 0 & & & \mathbf{P} \end{bmatrix} \begin{bmatrix} \mathbf{I} \\ \mathbf{G}^* \\ \vdots \\ (\mathbf{G}^{(L-1)})^* \end{bmatrix} \tag{3-40}$$

or

$$\mathbf{P}_s = (1/L) \mathbf{C} \mathbf{C}^*, \tag{3-41}$$

where $\mathbf{C}$ is the M x L matrix such that

$$\mathbf{C} = [\mathbf{E} \quad \mathbf{GE} \; \mathbf{G}^{(2)}\mathbf{E} \cdot \cdot \cdot \mathbf{G}^{(L-1)}\mathbf{E}] \tag{3-42}$$

with

$$\mathbf{EE}^{*} = \mathbf{P} \tag{3-43}$$

(i.e., $\mathbf{E}$ denotes the Hermitian square root of $\mathbf{P}$).

To show that the $\mathbf{P}_s$ is a nonsingular matrix, we let $(1/N)\sum|s_1(t)|^2 = 1$, without loss of generality. Then, from Eq.(3-43) in the case of coherence of the source signals, the vector E can be derived as follows:

$$\mathbf{E} = \begin{pmatrix} \alpha_1 \\ \alpha_2 \\ \cdot \\ \cdot \\ \alpha_M \end{pmatrix} . \tag{3-44}$$

Substituting Eqs.(3-33) and (3-44) into Eq.(3-42) yields

$$\mathbf{C} = \begin{pmatrix} \alpha_1 & \alpha_1\chi_1 & \alpha_1\chi_1^2 & \cdot \cdot \cdot & \alpha_1\chi_1^{L-1} \\ \alpha_2 & \alpha_2\chi_2 & \alpha_2\chi_2^2 & \cdot \cdot \cdot & \alpha_2\chi_2^{L-1} \\ \cdot & \cdot & \cdot & \cdot \cdot \cdot & \cdot \\ \cdot & \cdot & \cdot & \cdot \cdot \cdot & \cdot \\ \alpha_M & \alpha_M\chi_M & \alpha_M\chi_M^2 & \cdot \cdot \cdot & \alpha_M\chi_M^{L-1} \end{pmatrix} = \mathbf{MU} \tag{3-45}$$

where

$$\mathbf{M} = \begin{bmatrix} \alpha_1 & & & 0 \\ & \alpha_2 & & \\ & & \cdot & \\ & 0 & & \cdot \\ & & & \alpha_M \end{bmatrix} \tag{3-46}$$

and

$$\mathbf{U} = \begin{bmatrix} 1 & \chi_1 & \chi_1^2 & \cdot & \cdot & \cdot & \chi_1^{L-1} \\ 1 & \chi_2 & \chi_2^2 & \cdot & \cdot & \cdot & \chi_2^{L-1} \\ \cdot & \cdot & \cdot & & \cdot & & \cdot \\ \cdot & \cdot & \cdot & & & \cdot & \cdot \\ \cdot & \cdot & \cdot & & & \cdot & \cdot \\ 1 & \chi_M & \chi_M^2 & \cdot & \cdot & \cdot & \chi_M^{L-1} \end{bmatrix} . \tag{3-47}$$

Since the square matrix **M** is of full rank, i.e., $\rho(\mathbf{M}) = M$ and **U** is the $M \times L$ Vandermonde matrix, which is known to be nonsingular with $\rho(\mathbf{U}) = \min(M, L)$, the rank of **C** in Eq. (3-45) is $\rho(\mathbf{C}) = \min(M, L)$. Also, it is clear that the rank of $\mathbf{P_s}$ in Eq. (3-41) is equal to the rank of **C**. Thus, if $L \geq M$, the spatial smoothing source covariance matrix $\mathbf{P_s}$ is nonsingular, or $\rho(\mathbf{P_s}) = M$, and the eigenstructure algorithm can be successfully applied to the spatial smoothing output covariance matrix **R** (in Eq. (3-38)), which takes exactly the same form as the covariance matrix of the uncorrelated source signals, regardless of the coherence of the source signals.

Consequently, the spatial smoothing technique can be applied to the FOM and SOM to resolve the coherent multiple sources. Fig. 3-8 shows the procedure for the (ordinary) SOM combined with the spatial smoothing. The following example demonstrates that when compared to the FOM, the SOM is superior for the even coherent sources in conjunction with the spatial smoothing scheme.

Example 3.3 Two completely coherent sources with $\alpha_1 = (0.5, 0.7)$ and $\alpha_2 = (-0.3, 0.9)$ from the directions of 5° and 12°, respectively, are resolved using the MUSIC, the ordinary SOM, and the revised SOM combined with the spatial smoothing technique. Seven sensors, divided into five overlapping subarrays of size three are considered.

Resolution capabilities are tested as S/N ratio is changed from 3 dB to -3 dB, as shown in Figs. 3-9 - 3-11. For the MUSIC, 7° of separation is too close to resolve the two peaks of the fully coherent sources for all examined ranges of the S/N ratios. However, both of the SOMs show two peaks with very similar shapes, due to the averaging effect of the subarray data. From Figs. 3-9 - 3-11, it is readily seen that the bias for both SOMs increase as the S/N ratio is decreased. Nevertheless, this example indicates that in comparison to the FOM, the SOM is a very effective methods for the resolution of coherent sources when combined with the spatial smoothing technique.

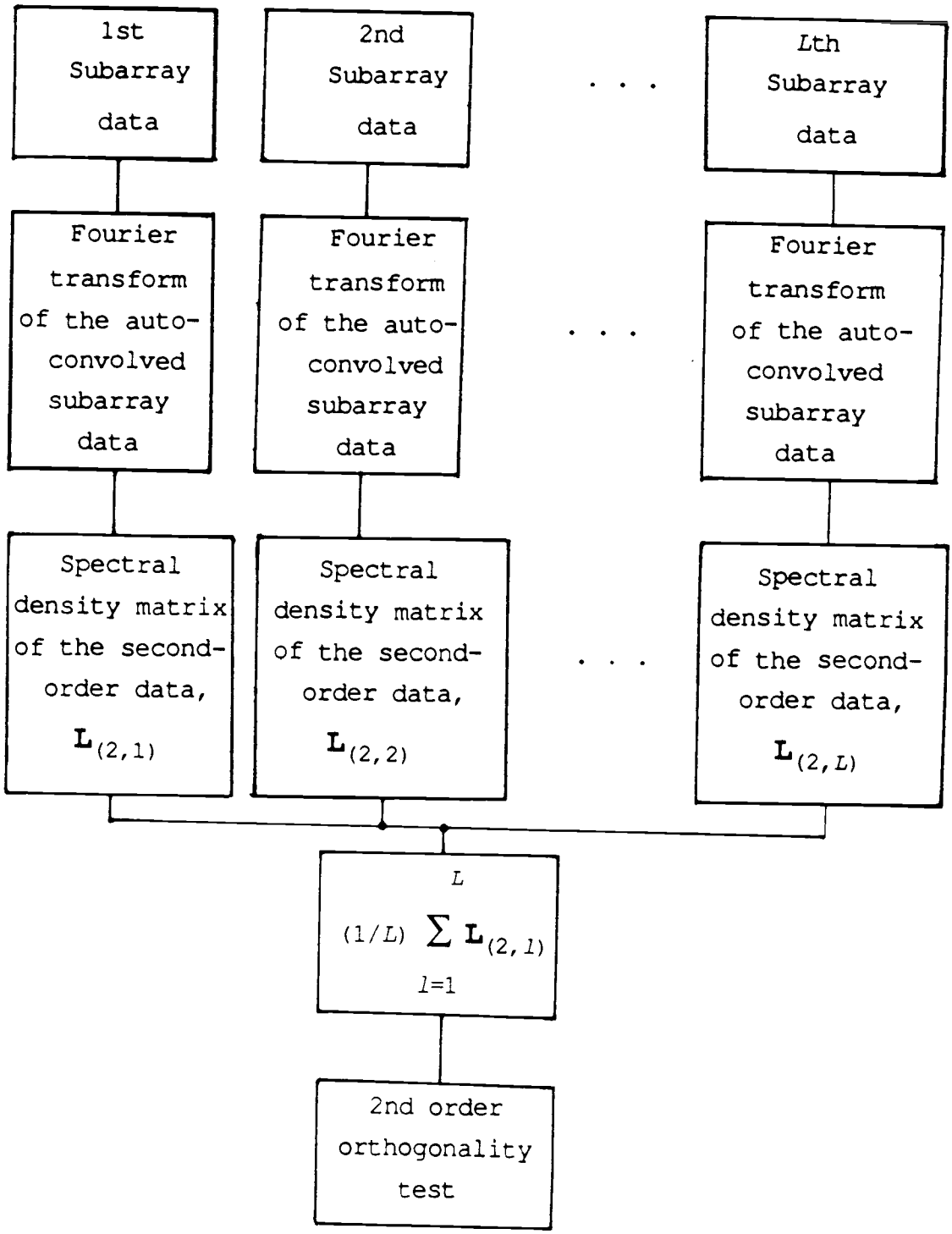

Fig.3-8. The Procedure of the SOM Combined with the Spatial Smoothing.

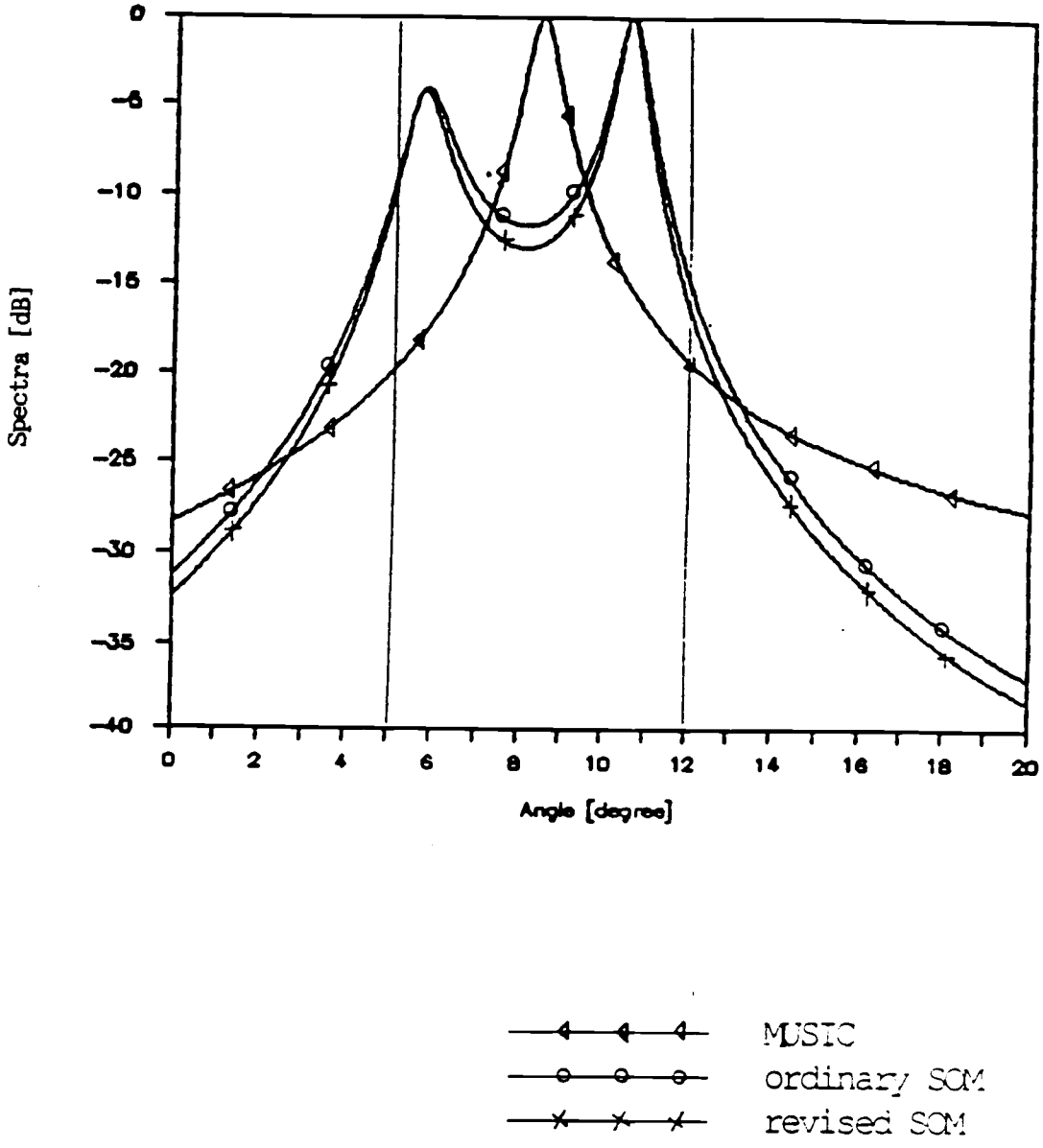

Fig.3-9. MUSIC, Ordinary SOM, and Revised SOM, all combined with Spatial Smoothing for Two Fully Coherent Sources, θ_1=5° and θ_2=12°, with 3 Sensors at S/N=3 dB, N=256.

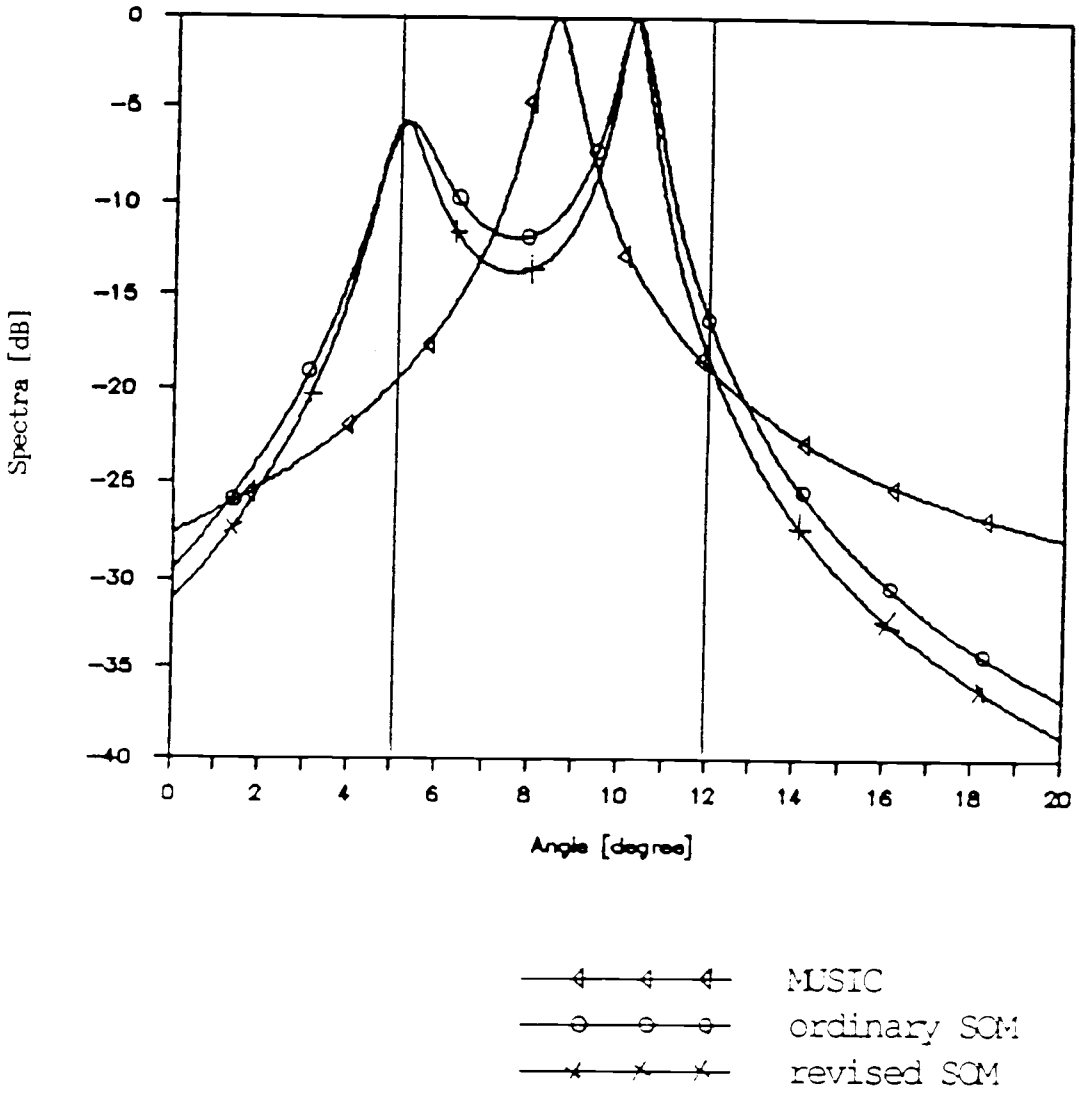

Fig.3-10. MUSIC, Ordinary SOM, and Revised SOM, all combined with Spatial Smoothing for Two Fully Coherent Sources, θ_1=5° and θ_2=12°, with 3 Sensors at S/N=0 dB, N=256.

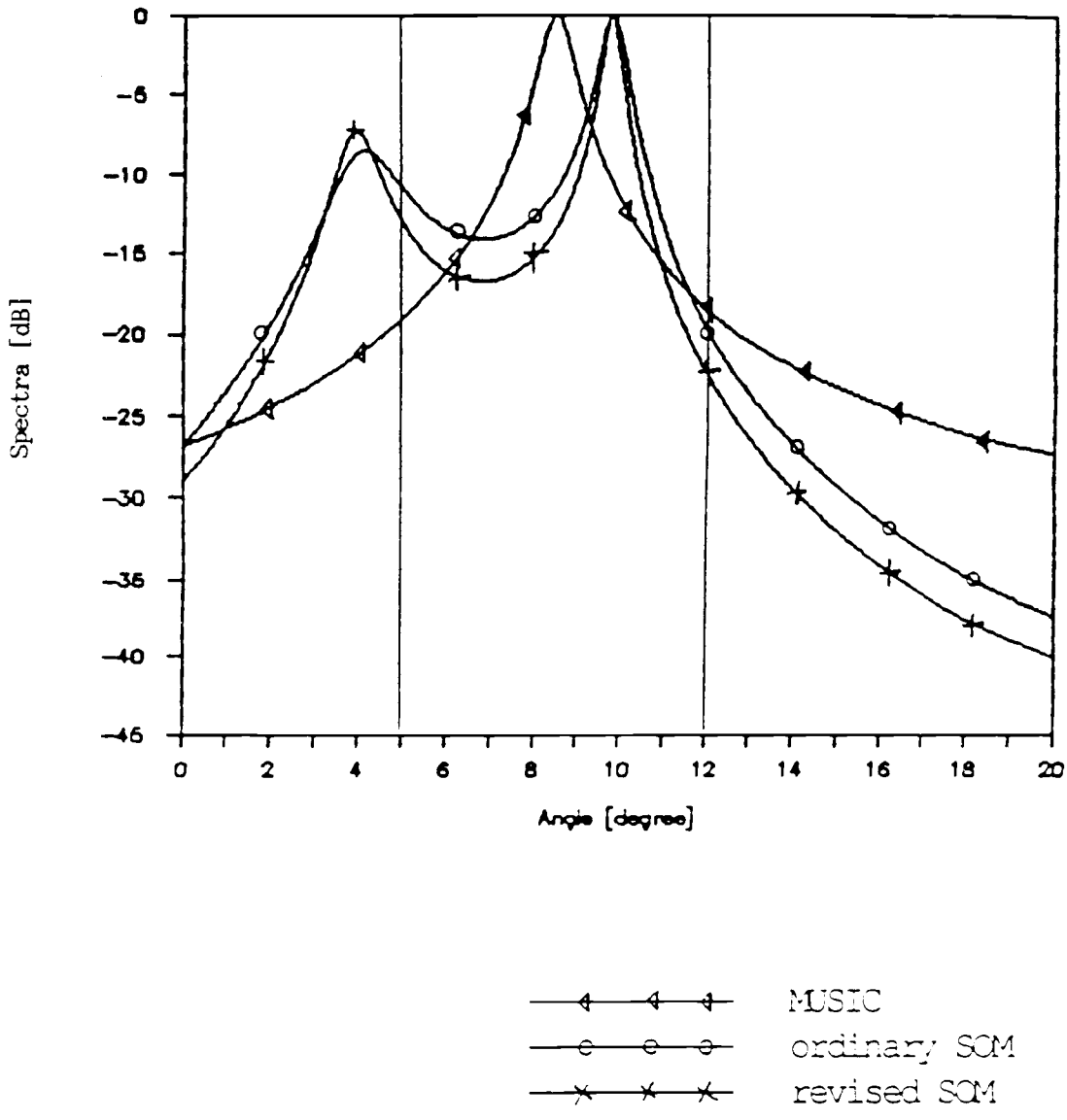

Fig.3-11. MUSIC, Ordinary SCM, and Revised SCM, all combined with Spatial Smoothing for Two Fully Coherent Sources, θ_1=5° and θ_2=12°, with 3 Sensors at S/N=-3 dB, N=256.

CHAPTER 4
COMPARISONS AND DISCUSSIONS WITH EXAMPLES USING COMPUTER SIMULATIONS

In this chapter, FOM, ordinary SOM, and revised SOM are compared and discussed, using such concrete examples as single source detection when sensor noises are spatially uncorrelated or are correlated with low S/N ratio and the resolution limits of the uncorrelated or coherent closely-spaced multiple sources with non-Gaussian as well as Gaussian noises. To assure the reliability of the results, the statistical approach is generally preferred. Prior to the comparisons and discussion, the generation of spatially correlated noises between sensors for computer simulation is first considered.

4.1 Generation of Spatially Correlated Random Noises

In this section, the process of obtaining correlated random variables from statistically independent random variables by a linear transformation is discussed. The method considered is used specially for the simulation of correlated random noise in this study. An optional method of obtaining more generally correlated random variables from statistically independent random variables, the Cholesky method or the square root method, is discussed in Appendix B.

4.1.1 Real Random Noises

Consider $\mathbf{V} = [V_1, V_2, \cdots, V_Q]^T$, a $Q \times 1$ real Gaussian random vector with $\mu_v = [0, 0, \cdots, 0]^T$ and the $\mathrm{Cov}(\mathbf{V}) = \sigma^2 \mathbf{I}_Q$, where $\mathbf{I}_Q$ is a $Q \times Q$ identity matrix, as obtained from a Gaussian Random Number Generator, (from $N \sim (0, 1)$, we can have $N \sim (\mu, \sigma^2)$ by transformation $F(N) = \sigma G(N) + \mu$), a $Q \times 1$ real Gaussian random vector $\mathbf{W}$ with $\mu_w = [\mu_1, \mu_2, \cdots, \mu_Q]^T$ and the

$$\mathrm{Cov}(\mathbf{W}) = \sigma^2 \begin{bmatrix} 1 & \rho & \cdot & \cdot & \rho \\ \rho & 1 & & \cdot & \rho \\ \cdot & \cdot & \cdot & & \cdot \\ \rho & & \cdot & 1 & \rho \\ \rho & & \cdot & \rho & 1 \end{bmatrix},$$

where $0 \leq \rho < 1$ and ρ is a real constant, can be obtained from the linear transformation

$$\mathbf{W} = (\rho)^{1/2} \mathbf{A}\, Vo + (1-\rho)^{1/2} \mathbf{I}_Q \mathbf{V} + \mu_w , \qquad (4\text{-}1)$$

where $\mathbf{A} = [1, 1, \cdots, 1]^T$ and Vo is a Gaussian random variable, independent of $V_1, V_2, \cdots, V_Q$ with a zero-mean and variance σ^2.

This method is not limited to Gaussian random variables, but can be used for any variables with the given mean vector and covariance matrix.

4.1.2 Complex Random Noises

Consider $\mathbf{V} = [V_1, V_2, \cdots, V_Q, V_{Q+1}, \cdots, V_{2Q}]^T$ a $2Q \times 1$ real Gaussian random vector with $\mu_v = [0, 0, \cdots, 0]^T$ and the $\mathrm{Cov}(\mathbf{V}) = \sigma^2 \mathbf{I}_{2Q}$, where $\mathbf{I}_{2Q}$ is $2Q \times 2Q$ identity matrix, as obtained a Gaussian Random Number Generator, then a $Q \times 1$ complex Gaussian random vector $\mathbf{Z}$ with $\mu_z = [\mu_1, \mu_2, \cdots, \mu_Q]$ and the

$$\mathrm{Cov}(\mathbf{Z}) = 2\sigma^2 \begin{bmatrix} 1 & |\rho| & \cdot & \cdot & \cdot & |\rho| \\ |\rho| & 1 & \cdot & & \cdot & |\rho| \\ \cdot & \cdot & & \cdot & & \cdot \\ \cdot & & \cdot & & 1 & |\rho| \\ |\rho| & \cdot & \cdot & \cdot & |\rho| & 1 \end{bmatrix},$$

where $0 \leq |\rho| < 1$ and ρ is a real or complex constant, can be obtained from the linear transformation

$$\mathbf{Z} = [(|\rho|)^{1/2}\mathbf{A}V_o + (1 - |\rho|)^{1/2}\mathbf{I}_Q\mathbf{V_A}] + j[(|\rho|)^{1/2}\mathbf{A}Vo + (1 - |\rho|)^{1/2}\mathbf{I}_Q\mathbf{V_B}] + \mu_z , \qquad (4\text{-}2)$$

where $\mathbf{A} = [1, 1, \cdot\ \cdot\ \cdot, 1]^T$ and V_o is a Gaussian random variable which is independent of $V_1, V_2, \cdots, V_Q, V_{Q+1}, \cdots, V_{2Q}$ with zero-mean and variance σ^2, $\mathbf{V_A} = [V_1, V_2, \ldots, V_Q]^T$, and $\mathbf{V_B} = [V_{Q+1}, V_{Q+2}, \cdots, V_{2Q}]^T$.

As in the case of real random noises, this method is applicable to any random variables with the given mean vector and covariance matrix, and not just to Gaussian random variables.

Example 4.1 Let $\mathbf{V}$ be a 6 x 1 real Gaussian random vector with $\mu_v = [0,0,\cdots,0]^T$ and the $\mathrm{Cov}(\mathbf{V}) = \mathbf{I}_6$. It follows that a 3 x 1 complex Gaussian vector $\mathbf{Z}$ with $\mu_z = [0,0,0]^T$ and the

$$\mathrm{Cov}(\mathbf{Z}) = 2 \begin{bmatrix} 1 & |\rho| & |\rho| \\ |\rho| & 1 & |\rho| \\ |\rho| & |\rho| & 1 \end{bmatrix}$$

can be obtained as follows.

Given the statistically independent real random variables, V_o, V_1, V_2, ..., V_6 with zero means and unit variances, we let

$$Z_1 = W_1 + jY_1,$$

$$Z_2 = W_2 + jY_2, \text{ and}$$

$$Z_3 = W_3 + jY_3,$$

where
$$W_1 = (|\rho|)^{1/2} V_o + (1 - |\rho|)^{1/2} V_1,$$

$$W_2 = (|\rho|)^{1/2} V_o + (1 - |\rho|)^{1/2} V_2,$$

$$W_3 = (|\rho|)^{1/2} V_o + (1 - |\rho|)^{1/2} V_3,$$

$$Y_1 = (|\rho|)^{1/2} V_o + (1 - |\rho|)^{1/2} V_4,$$

$$Y_2 = (|\rho|)^{1/2} V_o + (1 - |\rho|)^{1/2} V_5, \text{ and}$$

$$Y_3 = (|\rho|)^{1/2} V_o + (1 - |\rho|)^{1/2} V_6.$$

Then,

$$\mathrm{Var}[Z_1] = E[|Z_1|^2]$$

$$= E[W_1^2 + Y_1^2]$$

$$= E[|\rho| V_0^2 + (1 - |\rho|) V_1^2 + |\rho| V_0^2 + (1-|\rho|) V_4^2]$$

$$= 2 ,$$

$$\mathrm{Var}[Z_2] = \mathrm{Var}[Z_3] = 2 ,$$

and similarly,

$$\mathrm{Cov}[Z_1, Z_2] = E[Z_1 Z_2^*]$$

$$= E[(W_1 + jY_1)(W_2 - jY_2)]$$

$$= E[W_1 W_2 + Y_1 Y_2 + j(Y_1 W_2 - Y_2 W_1)]$$

$$= 2 |\rho| .$$

In the same manner, the

$$\mathrm{Cov}[Z_1, Z_3] = \mathrm{Cov}[Z_2, Z_3] = \mathrm{Cov}[Z_2, Z_1]$$

$$= \mathrm{Cov}[Z_3, Z_1] = \mathrm{Cov}[Z_3, Z_2]$$

$$= 2 |\rho|$$

can be obtained.

4-2. On Single Source (at low S/N ratio) with Uncorrelated and Correlated Sensor Noises

In this section, a statistical approach is applied for performance comparison of several direction finding algorithms. The results given are for the case of a single source, arriving at a uniform linear array consisting of three identical sensors with an interelement distance of one-half of the wavelength. Since a large number of independent variables are available and it is difficult to claim that any particular set is representative, it is not useful to consider results of

single situations, except as examples of expected performance. The plots obtained provide statistical results based on direction errors measured from different angles around the sensor array.

Fig. 4-1 shows the results of a performance comparison of a FOM (MUSIC) and a SOM the performances of as a function of signal-to-noise (S/N) ratio for a single source, stepped between 0° and 180° at a step sizes of 0.02° (for each step, N = 256 samples of data are used and errors are in multiples of 0.02°) when the sensor noises are uncorrelated with each other. Though the standard deviations of signal directions are decreased for both methods as the S/N ratio is increased, it is apparent that the SOM provides better result than the FOM throughout the change of S/N ratios. In particular, the SOM estimates signal direction with approximately one-half of the error of the FOM for S/N ratio levels below 0 dB (refer to Table 4-1).

Fig. 4-2 (N=256) compares the effects using various methods, including the FOMSEA, FOMGEA, SOMSEA, and SOMGEA (refer to page 45 for those abbreviations), for a single source stepped between 0° and 180° at step size of 0.02° when the noises are 40% correlated between sensors. As previously noted, the generalized algorithm offers better results for the estimation of directions of closely spaced source signals with additive noises that are correlated

between the sensors. In Fig. 4-2, the values plotted are the standard deviations of direction errors obtained from 91 signal directions for each of the S/N ratios, as in Fig. 4-1. For both the SOMSEA and SOMGEA, the standard deviations of errors in the direction of source signal measurement are very similar, with less than 1.5° a S/N ratio levels higher than 0 dB. However, the SOMGEA provides definitely superior results in comparison to either the SOMSEA, FOMSEA, or FOMGEA as the S/N ratio levels are decreased below 0 dB (refer to Table 4-2).

Finally, Fig. 4-3 shows SOMSEA performance for uncorrelated sensor noises in terms of a number of data samples, i.e., N = 128, 256, and 512. These results demonstrate that the provision of additional data points offers an obviously better performance in direction finding problem of source signals (refer to Table 4-3).

4.3 On Closely-Spaced Multiple (Uncorrelated/Correlated) Sources with Uncorrelated/Correlated Gaussian Sensor Noises

In section 3.2, it has established that the ordinary and revised SOMs provide resolution capabilities which are supirior to those of the FOM (MUSIC). In this section, the MUSIC and (ordinary) SOM are compared with respect to the reliability of resolved peaks for multiple sources at high S/N ratios, since the MUSIC tends to be unable to resolve closely-spaced sources as the S/N ratios are

decreased. Two peaks of plane waves at $\theta_1 = 5^\circ$ and $\theta_2 = 12^\circ$ are estimated for a sensor array with three spatially uncorrelated sensors at S/N = 10.97 dB (N=256), using 30 runs with independent noise records for each run. As shown in Table 4-4, for all catagories, including mean error, rms error, and std. of an error, the SOM provides results which are superior to those of the MUSIC. In Figs. 4-4 and 4-5, six sample runs are shown for the MUSIC and the SOM, respectively. It is apparent that the results shown in these figures indicate the reliability of the SOM in comparison to the MUSIC near the true direction angles.

Also, in section 3.2, the relative resolution capabilities between the ordinary and revised SOMs were noted when different angles were compared, to the advantage of the revised SOM. In this section, two plane waves at $\theta_1 = 8^\circ$ and $\theta_2 = 13^\circ$ with three sensors at S/N = -3 dB (N=256) are considered for 30 runs with independent noise records for each run. The sensor noises are spatially uncorrelated white Gaussian. In this case, the ordinary SOM failed to resolve the two peaks 16.67 percent of the time (5 of 30 runs), while the revised SOM failed only 3.33 percent of the time (1 of 30 runs) (Table 4-5). Note that under the given conditions, the two peaks for the MUSIC could not be resolved throughout entire runs.

Using the runs which could resolve the two peaks, the ordinary and revised SOMs were compared in terms of mean error, rms error, and std. of error (Table 4-5). For both $\theta_1 = 8°$ and $\theta_2 = 13°$, the revised SOM indicated smaller mean error and std. of error, but the ordinary SOM showed a smaller rms error for $\theta_1 = 8°$, while the revised SOM had a smaller rms error for $\theta_2 = 13°$. Therefore, these limited observations indicate that the revised SOM offers better resolution probability than the ordinary SOM, however it is difficult to reach a conclusion when the reliability of the resolved peaks for the ordinary and revised SOMs are compared.

Finally, two plane waves at $\theta_1 = 5°$ and $\theta_2 = 9°$, with three sensors which are 30 % correlated each other, were resolved at S/N = 2 dB (N=256), using the MUSIC, ordinary and revised SOMs. Once again, the MUSIC failed to resolve the two peaks throughout the 30 runs, while both the ordinary and revised SOMs provided 100 percent resolvability during these runs. As shown in Table 4-6, for this relatively high S/N ratio it is difficult to determine which is more reliable, since the ordinary SOM provided a slightly better std. of errors for both 5° and 9°, while the revised SOM provided better results for rms. errors at both 5° and 9°.

Overall, it may be stated that the ordinary and revised SOMs can be effectively applied to the resolution of multiple sources, even in such situations as very closely-spaced sources at low S/N ratios, spatially correlated sensor noises. Moreover, the revised SOM provides a resolution probability which is superior to that of the ordinary SOM when the S/N ratios are relatively low.

4.4 On Sources with Uniformly Distributed Random Noises

In this section it is demonstrated that the ordinary and revised SOMs have resolution capabilities even when the additive sensor noises are uniformly distributed. Uniformly distributed random noises on $(-\pi,\pi)$ were used as sensor noises. We have two complex sinusoidal waves from the directions $\theta_1 = 5^\circ$ and $\theta_2 = 13^\circ$, with three sensors at S/N = 8 dB (N=256) for 30 independent runs. The MUSIC failed to resolve the two peaks for all runs, but the ordinary and revised SOMs successfully resolved two peaks. As shown in Table 4-7, for the high S/N ratios, it was difficult to compare resolution capabilities since the revised SOM was better in terms of rms. errors at 5° and 13°, while the ordinary SOM was better with respect to std. of errors at 5° and 13°. However, the resolution capabilities of these SOMs can be checked by using lower S/N ratios.

Therefore, the SOMs can be successfully applied to resolve multiple source signals even for uniformly distributed random noises since they are capable of rejecting the noise variances.

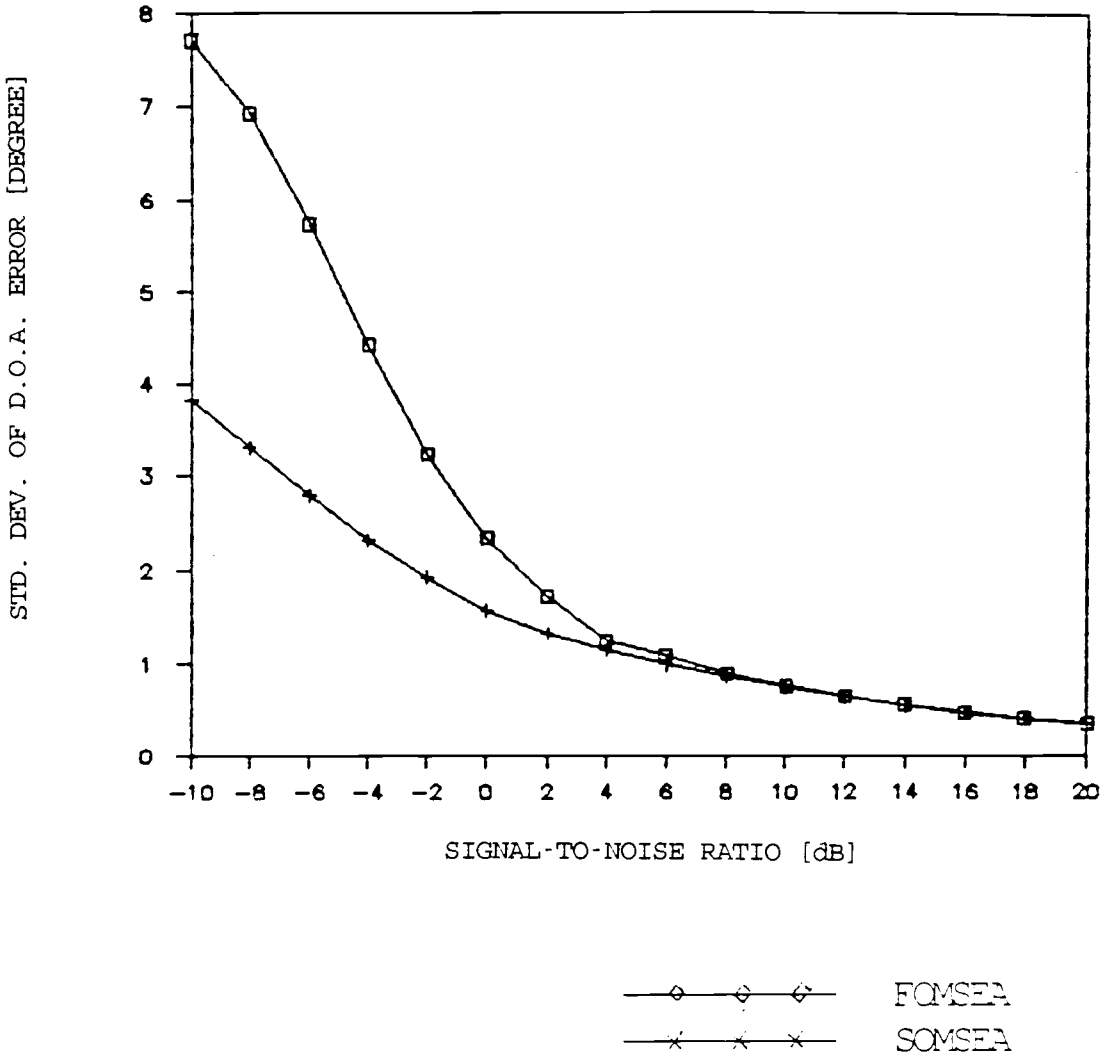

Fig.4-1. Standard Deviation of the Direction Error in terms of S/N ratio of the FOMSEA and SOMSEA with 3 Uncorrelated Sensors.

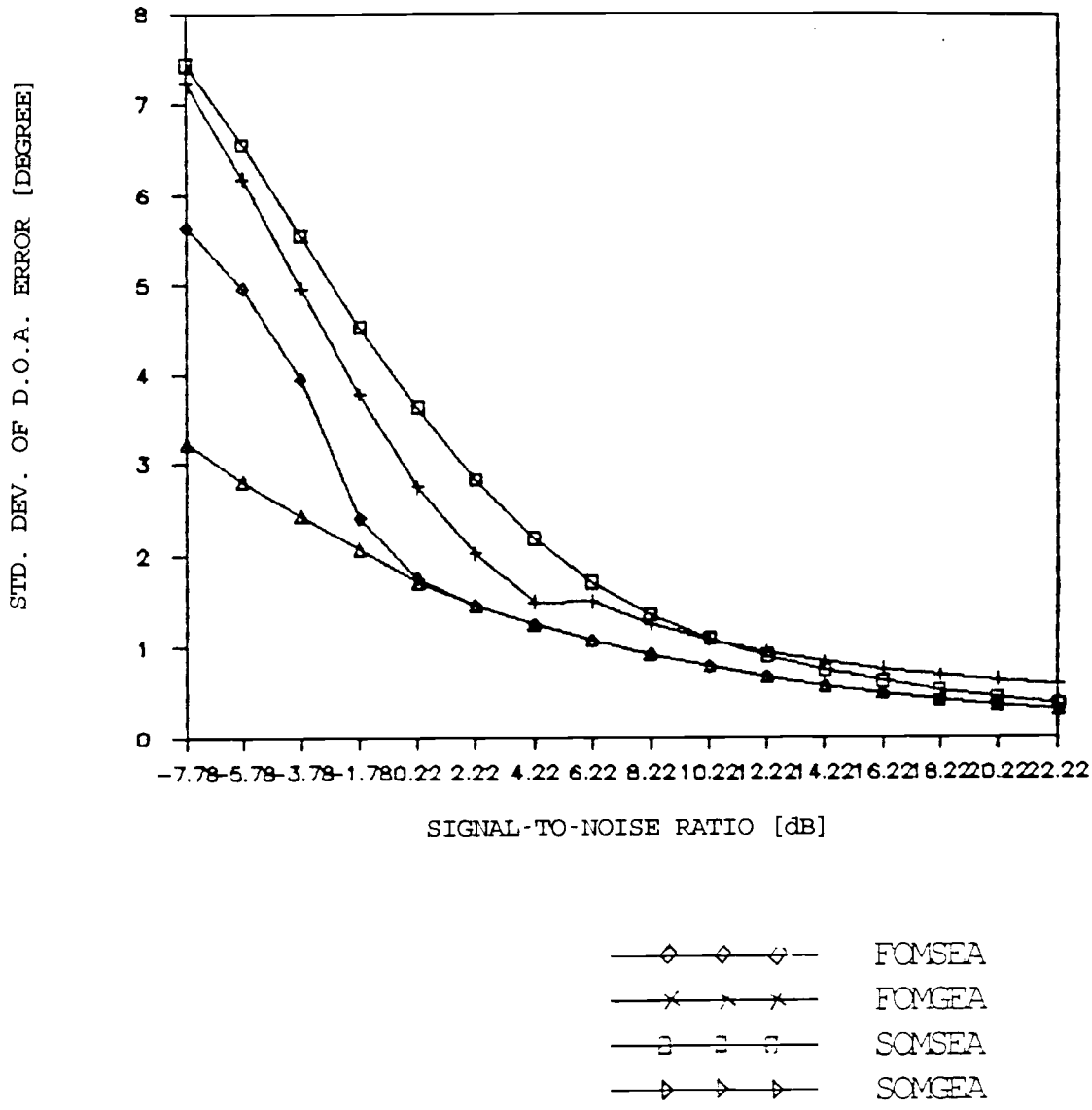

Fig.4-2. Standard Deviation of the Direction Error in terms of S/N ratio of the FOMSEA, FOMGEA, SOMSEA, and SOMSEA with 40% Correlated Sensor Noises.

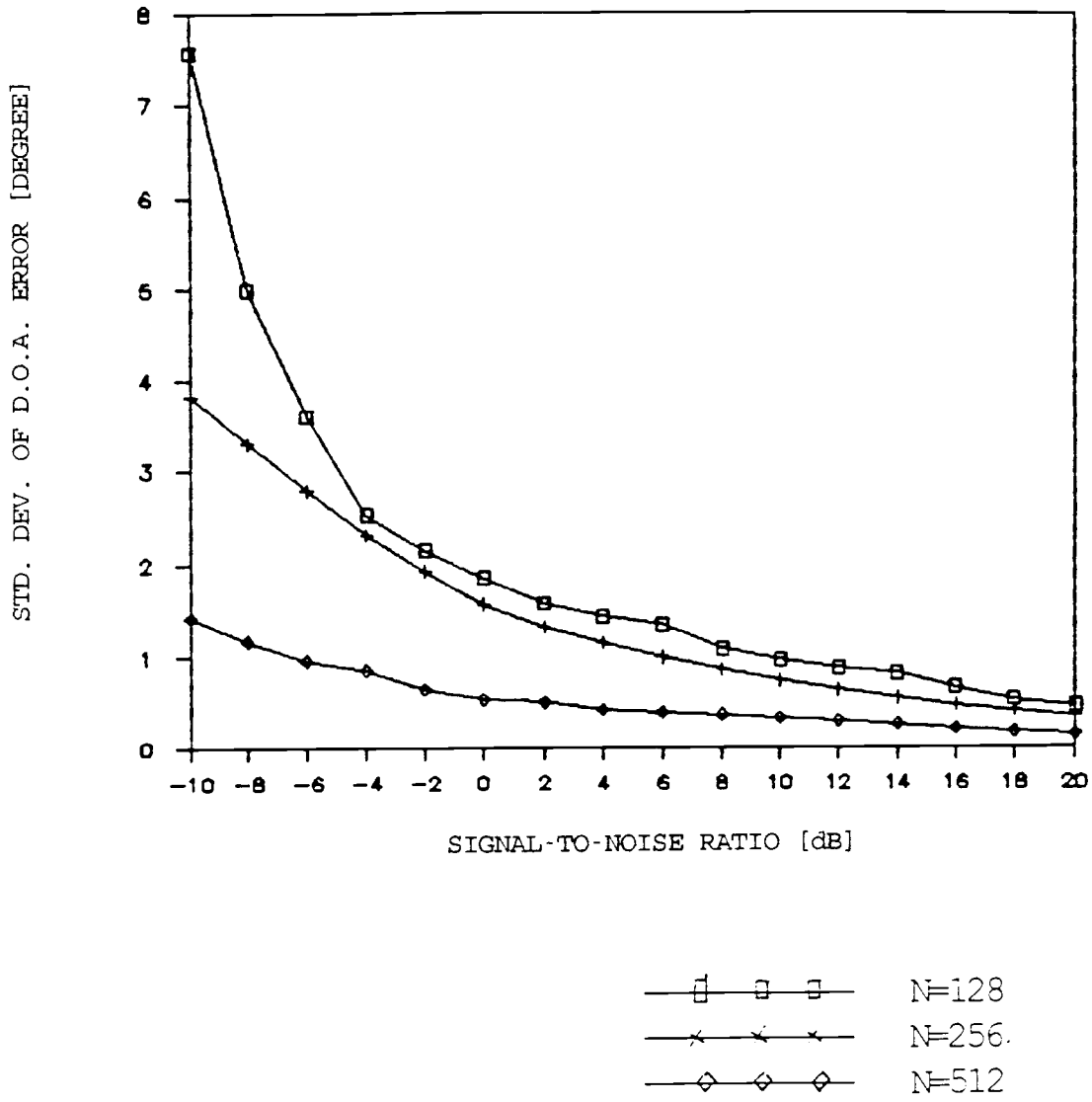

Fig.4-3. Standard Deviation of the Direction Error in terms of S/N ratio of the SOMSEA for Different Sample Sizes with 3 Uncorrelated Sensors.

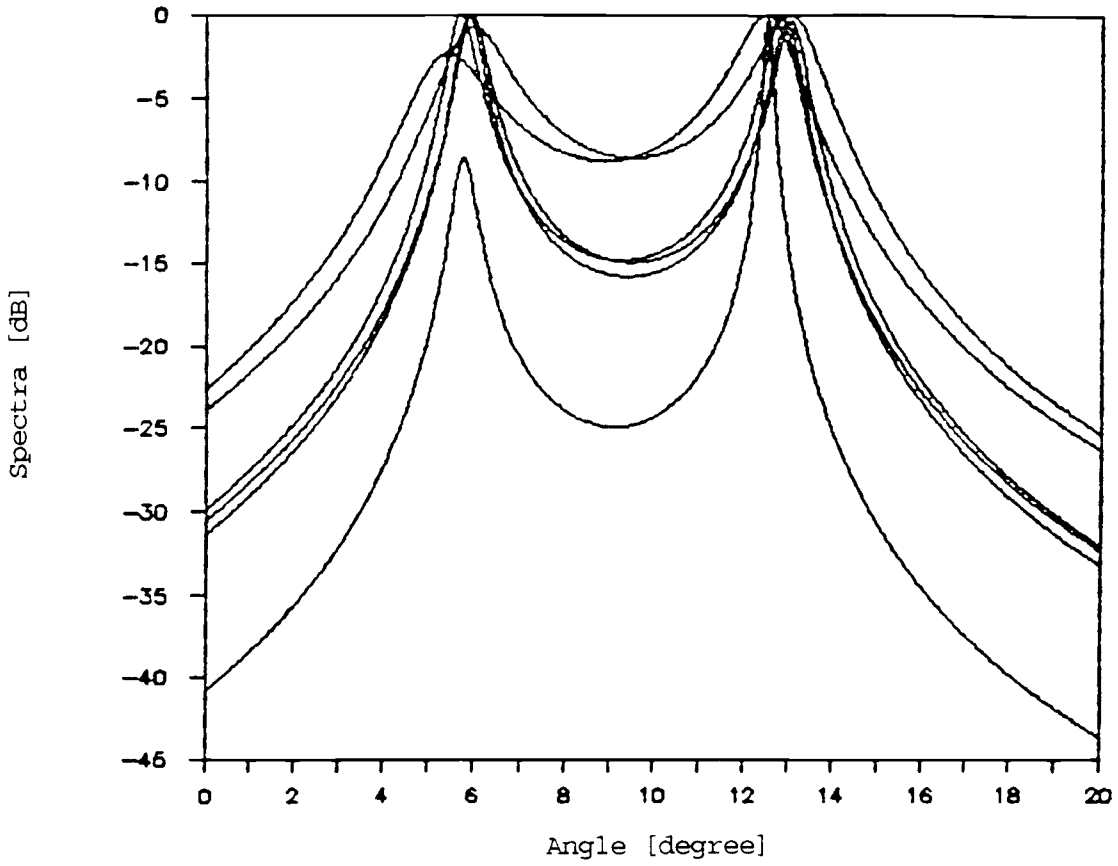

Fig.4-4. Six Sample Runs for the FOM for Two Sources, θ_1=5°, θ_2=12°, at S/N=10.97 dB, N=256.

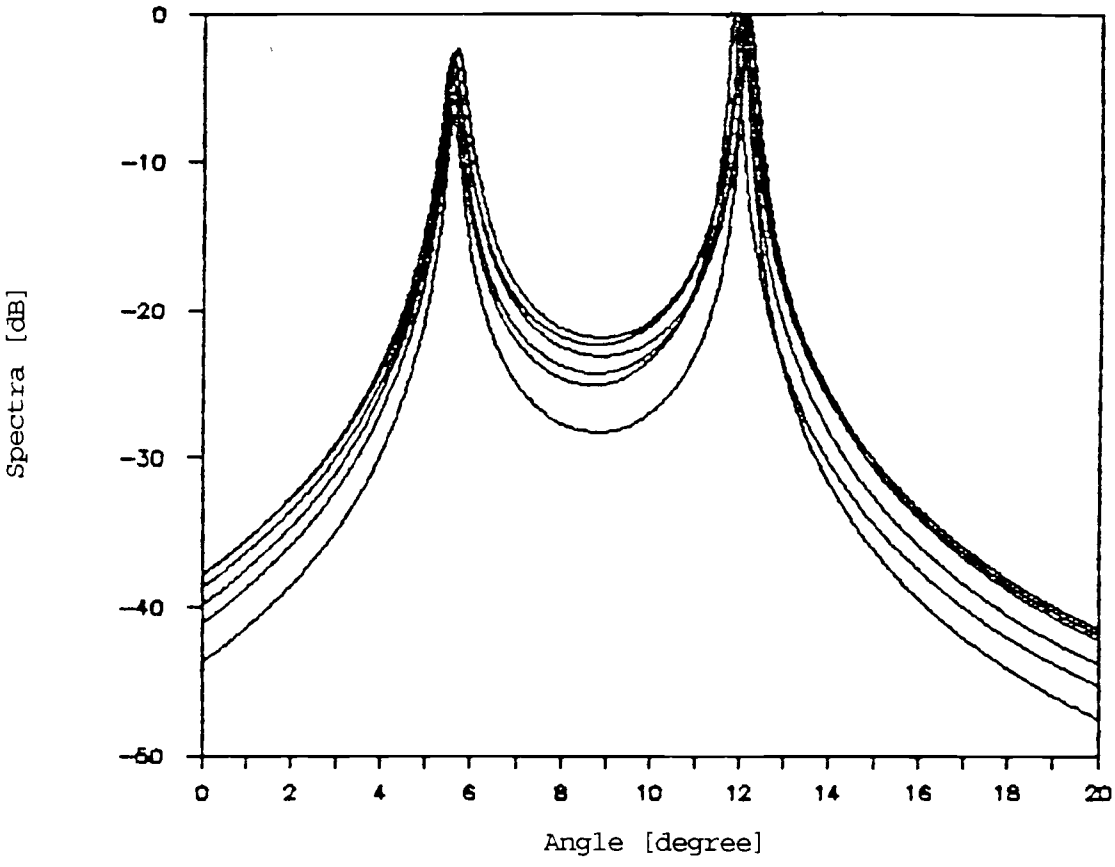

Fig.4-5. Six Sample Runs for the SOM for Two Sources, θ_1=5°, θ_2=12°, at S/N=10.97 dB, N=256.

Table 4-1. Mean, Rms., and Std. of the Direction Error in terms of S/N ratio When Sensor Noises are Uncorrelated Each Other.

	FIRST ORDER METHOD (FOMSEA)			SECOND ORDER METHOD (SOMSEA)		
S/N RATIO	MEAN ERROR	R.M.S. ERROR	S.T.D. ERROR	MEAN ERROR	R.M.S. ERROR	S.T.D. ERROR
-10.0	0.095	7.700	7.742	0.109	3.794	3.814
-8.0	0.095	6.933	6.971	0.109	3.287	3.303
-6.0	0.093	5.737	5.768	0.109	2.786	2.799
-4.0	0.088	4.419	4.443	0.097	2.316	2.327
-2.0	0.082	3.237	3.254	0.086	1.914	1.923
0.0	0.075	2.343	2.354	0.076	1.558	1.565
2.0	0.068	1.717	1.725	0.068	1.318	1.324
4.0	0.062	1.252	1.258	0.061	1.140	1.144
6.0	0.055	1.082	1.087	0.055	0.987	0.991
8.0	0.050	0.891	0.894	0.050	0.852	0.856
10.0	0.044	0.752	0.755	0.045	0.735	0.738
12.0	0.040	0.640	0.642	0.040	0.631	0.633
14.0	0.035	0.549	0.551	0.037	0.541	0.543
16.0	0.031	0.471	0.473	0.033	0.463	0.464
18.0	0.028	0.404	0.406	0.029	0.395	0.396
20.0	0.025	0.348	0.349	0.026	0.337	0.338

Table 4-2. Mean, Rms., and Std. of the Direction Error in terms of S/N ratio When Sensor Noises are 40% Correlated Each Other.

	FOMSEA		FOMGEA		SOMSEA		SOMGEA	
S/N RATIO	MEAN ERROR	S.T.D. ERROR	MEAN ERROR	S.T.D. ERROR	MEAN ERROR	S.T.D. ERROR	MEAN ERROR	S.T.D. ERROR
-7.78	0.093	7.437	0.094	7.243	0.097	5.629	0.110	3.230
-5.78	0.090	6.561	0.091	6.177	0.096	4.956	0.104	2.806
-3.78	0.086	5.537	0.086	4.954	0.091	3.937	0.095	2.436
-1.78	0.080	4.525	0.080	3.774	0.086	2.407	0.088	2.066
0.22	0.073	3.628	0.074	2.753	0.079	1.750	0.080	1.708
2.22	0.066	2.834	0.067	2.024	0.072	1.457	0.073	1.453
4.22	0.060	2.181	0.060	1.494	0.066	1.247	0.066	1.247
6.22	0.054	1.702	0.054	1.499	0.059	1.067	0.059	1.070
8.22	0.048	1.354	0.049	1.255	0.053	0.914	0.053	0.915
10.22	0.043	1.092	0.043	1.077	0.048	0.784	0.048	0.785
12.22	0.038	0.894	0.039	0.938	0.043	0.669	0.043	0.669
14.22	0.034	0.740	0.035	0.832	0.038	0.569	0.038	0.570
16.22	0.031	0.618	0.031	0.748	0.034	0.488	0.034	0.488
18.22	0.027	0.518	0.028	0.680	0.031	0.419	0.031	0.420
20.22	0.024	0.435	0.024	0.624	0.027	0.357	0.027	0.357
22.22	0.022	0.366	0.022	0.576	0.024	0.306	0.024	0.307

Table 4-3. Mean, Rms., and Std. of the Direction Error of the SOMSEA with N=128, 256, 512, respectively, When Sensor Noises are Uncorrelated Each Other.

	SECOND ORDER METHOD (SOMSEA)								
	N=128			N=256			N=512		
S/N RATIO	MEAN ERROR	R.M.S. ERROR	S.T.D ERROR	MEAN ERROR	R.M.S. ERROR	S.T.D ERROR	MEAN ERROR	R.M.S. ERROR	S.T.D ERROR
-10.0	-0.000	7.524	7.566	0.109	3.794	3.814	0.000	1.422	1.430
-8.0	-0.000	4.955	4.982	0.109	3.287	3.303	-0.000	1.155	1.161
-6.0	0.000	3.580	3.600	0.109	2.786	2.799	0.000	0.950	0.956
-4.0	0.000	2.525	2.539	0.097	2.316	2.327	-0.000	0.846	0.851
-2.0	-0.000	2.137	2.149	0.086	1.914	1.923	0.000	0.636	0.639
0.0	0.000	1.841	1.851	0.076	1.558	1.565	0.000	0.525	0.528
2.0	0.000	1.569	1.577	0.068	1.318	1.324	0.000	0.497	0.500
4.0	-0.000	1.429	1.437	0.061	1.140	1.144	-0.000	0.412	0.414
6.0	0.000	1.341	1.349	0.055	0.987	0.991	-0.000	0.383	0.385
8.0	-0.000	1.075	1.080	0.050	0.852	0.856	-0.004	0.355	0.357
10.0	0.000	0.955	0.960	0.045	0.735	0.738	-0.008	0.322	0.323
12.0	0.000	0.871	0.876	0.040	0.631	0.633	-0.010	0.286	0.288
14.0	0.000	0.807	0.811	0.037	0.541	0.543	0.012	0.251	0.252
16.0	0.000	0.654	0.658	0.033	0.463	0.464	-0.009	0.203	0.204
18.0	0.000	0.521	0.524	0.029	0.395	0.396	0.009	0.170	0.170
20.0	-0.000	0.443	0.445	0.026	0.337	0.338	-0.007	0.140	0.141

Table 4-4. Mean, Rms., and Std. of the Direction Error of the FOM and SOM for Two Sources, θ_1=5°, θ_2=12°, with 3 Uncorrelated Sensors at S/N=10.97 dB, N=256, Using 30 Runs.

	θ_1 = 5°		θ_2 = 12°	
	FOMSEA	SOMSEA	FOMSEA	SOMSEA
MEAN ERROR [degree]	0.86	0.61	0.83	-0.02
R.M.S. ERROR [degree]	0.89	0.61	0.90	0.10
S.T.D. ERROR [degree]	0.21	0.07	0.35	0.10

Table 4-5. Resolvable Probability, Mean, Rms., and Std. of the Direction Error of the FOM and SOM for Two Sources, $\theta_1=8^\circ, \theta_2=13^\circ$, with 3 Uncorrelated Sensors at S/N=-3 dB, N=256, Using 30 Runs.

	$\theta_1 = 8^\circ$		$\theta_2 = 13^\circ$			
	ordinary SOM	revised SOM	ordinary SOM	revised SOM	ordinary SOM	revised SOM
RESOLVABLE PROBABILITY [%]					83.33	96.67
MEAN ERROR [degree]	0.11	-0.06	1.32	1.07		
R.M.S. ERROR [degree]	0.43	0.45	1.63	1.40		
S.T.D. ERROR [degree]	0.43	0.11	0.98	0.92		

Table 4-6. Mean, Rms., and Std. of the Direction Error of the Ordinary and Revised SOMs for Two Sources, $\theta_1=5^\circ, \theta_2=9^\circ$, with 30% Correlated 3 Sensors at S/N=2 dB, N=256, Using 30 Runs.

	$\theta_1 = 5^\circ$		$\theta_2 = 9^\circ$	
	ordianry SOM	revised SOM	ordinary SOM	revised SOM
MEAN ERROR [degree]	0.32	0.21	1.01	1.00
R.M.S. ERROR [degree]	0.39	0.31	1.11	1.10
S.T.D. ERROR [degree]	0.22	0.23	0.46	0.47

Table 4-7. Mean, Rms., and Std. of the Direction Error of the Ordinary and Revised SOMs for Two Sources, $\theta_1=5^\circ, \theta_2=13^\circ$, with Uniformly Distributed 3 Uncorrelated Sensors at S/N=8 dB, N=256, Using 30 Runs.

	$\theta_1 = 5^\circ$		$\theta_2 = 13^\circ$	
	ordianry SOM	revised SOM	ordinary SOM	revised SOM
MEAN ERROR [degree]	1.14	1.11	0.43	0.37
R.M.S. ERROR [degree]	1.14	1.12	0.61	0.60
S.T.D. ERROR [degree]	0.08	0.11	0.43	0.48

CHAPTER 5

THEORETICAL COMPARISON OF THE FIRST- AND SECOND-ORDER MEHTODS

In this chapter, the performances of the FOM and SOM based on the theoretically derived threshold S/N ratio and computer simulation results, obtained by several runs, for the resolution of very closely spaced sources, are compared and discussed.

5.1 Signal-to-Noise Ratio

The FOM and SOM S/N ratio are derived from the deterministic source $s(t) = A\exp(j\omega t)$, $t=1,2,\cdots,N$, with zero-sample mean and complex stationary random noise $x(t)$ with zero-mean and variance $2\sigma_x^2$. When the source and noise are uncorrelated with each other, the FOM S/N ratio can be obtained as

$$[S/N]_f = A^2/(2\sigma_x^2). \tag{5-1}$$

A received signal with additive noise, i.e., $r(t) = s(t) + x(t)$, can be auto-convolved to obtain the second-order signal, i.e.,

$$\begin{aligned} r_s(t) &= r(t) \otimes r(t) \\ &= \{s(t) + x(t)\} \otimes \{s(t) + x(t)\} \\ &= s_s(t) + x_s(t) + 2\{s(t) \otimes x(t)\}, \end{aligned}$$

where $s_s(t) = s(t) \otimes s(t)$ and $x_s(t) = x(t) \otimes x(t)$.

For $s(t)$ and $x(t)$ to be independent, $E_s[r_s(t)]$, where $E_s[\cdot]$ denotes the sample mean through $t = 2,3,\cdots,2N$, must be equal to zero. Therefore, the variance of $r_s(t)$ can be obtained as

$$\begin{aligned}\mathrm{Var}_s[r_s(t)] &= E_S[r_s(t)\,r_s^*(t)] \\ &= E_s[s_s(t)\,s_s^*(t)] + E_s[x_s x_s^*(t)] + E_s[s_s(t)\,x_s^*(t)] \\ &+ E_s[x_s(t)\,x_s^*(t)] + 2E_s[s_s(t)\{s(t) \otimes x(t)\}^*] \\ &+ 2E_s[\{s(t) \otimes x(t)\}x_s^*(t)] + 2E_s[\{s(t) \otimes x(t)\}s_s^*(t)] \\ &+ 2E_s[x_s(t)\{s(t) \otimes x(t)\}^*] \\ &+ 4E_s[\{s(t) \otimes x(t)\}\{s(t) \otimes x(t)\}^*].\end{aligned}$$

Given that each odd moment of the zero-mean process is zero and the independence of $s(t)$ and $x(t)$, the remaining terms of the obove equation become

$$\begin{aligned}E_s[r_s(t)\,r_s^*(t)] &= E_s[s_s(t)\,s_s^*(t)] + E_s[x_s(t)\,x_s^*(t)] \\ &+ 4E_s[\{s(t) \otimes x(t)\}\{s(t) \otimes x(t)\}^*].\end{aligned}$$

Thus, the value of $E_s[\{s(t)\otimes x(t)\}\{s(t)\otimes x(t)\}^*]$ is approximated in the finite discrete case by

$$\begin{aligned}&E_s[\{s(t) \otimes x(t)\}\{s(t) \otimes x(t)\}^*] \\ &\approx E_s[\sum_{k=1}^{N}\sum_{l=1}^{N} s(k)\,x(t-k)\,s^*(l)\,x^*(t-l)]. \qquad (5\text{-}2)\end{aligned}$$

Note that $x(t)$ takes the form

$$x(t) = a(t) + jb(t),\ t=1,2,\cdots,N,$$

where $a(t)$ and $b(t)$ are independent and real-valued random variables.

If $a(t)$ and $b(t)$ have the same distributions with zero-mean and variance σ_x^2, then

$$E[x(t)] = E[a(t) + jb(t)] = 0,$$

and $E[x(t)x^*(t)] = E[a^2(t) + b^2(t)] = 2\sigma_x^2$.

Eq.(5-2) can be rewritten as follows:

i) <u>When $k=1$</u> ,

$$E_s[\{s(t) \otimes x(t)\}\{s(t) \otimes x(t)\}^*]$$

$$\approx E_s[(\sum_{k=1}^{N} s(k)s^*(k))(x(t-k)x^*(t-k))]$$

$$\approx (\sum_{k=1}^{N} (s(k)s^*(k))E_s(x(t-k)x^*(t-k))]$$

$$\approx (NA^2)((N/(2N-1))(2\sigma_x^2))$$

$$\approx (N^2A^2/(2N-1))(2\sigma_x^2); \qquad (5-3)$$

ii) <u>Otherwise</u> ,

$$E_s[\{s(t) \otimes x(t)\}\{s(t) \otimes x(t)\}^*] = 0,$$

since all the terms of the above equation consist of odd moments of $s(t)$ and $x(t)$.

The values of $E_s[s_s(t)s_s^*(t)]$ and $E_s[x_s(t)x_s^*(t)]$, are then obtained, one-by-one. The second-order source signal $s_s(t)$ can be obtained by taking the auto-convolution of the first-order source signal as

$$s_s(t) = s(t) \otimes s(t)$$

$$= \sum_{k=1}^{N} s(k)s(t-k), \qquad (5-4)$$

Since

$$s_S(t) = \begin{cases} A^2\exp(j\omega) & \text{when } t=1, \\ 2A^2\exp(j2\omega) & \text{when } t=2, \\ \quad\cdot \\ \quad\cdot \\ \quad\cdot \\ (N-1)A^2\exp(j(N-1)\omega) & \text{when } t=N-1, \\ NA^2\exp(jN\omega) & \text{when } t=N, \\ \qquad \text{(max. in magnitude)} & \\ (N-1)A^2\exp(j(N+1)\omega) & \text{when } t=N+1, \\ (N-2)A^2\exp(j(N+2)\omega) & \text{when t=}N+2, \\ \quad\cdot \\ \quad\cdot \\ \quad\cdot \\ A^2\exp(j(2N-1)\omega) & \text{when } t=2N-1, \\ 0 & \text{otherwise ,} \end{cases}$$

$$\begin{aligned} & E_s[s_s(t)\,s_s^*(t)] \\ &\approx (1/(2N-1)) \sum_{i=1}^{2N-1} s_s(i)\,s_s^*(i) \\ &= (A^4/(2N-1))\,(2(\sum_{i=1}^{N} i^2) - A^2) \\ &= (A^4/(2N-1))\,\{(2N(N+1)(2N+1)/6) - N^2\} \\ &= \{A^4(2N^3+N)\}/\{3(2N-1)\}\ . \end{aligned} \tag{5-5}$$

The variance of the second-order noise $x_s(t)$ can be expressed as

$$E_s[x_s(t)\,x_s^*(t)]$$

$$\approx E_s[\sum_{k=1}^{N}\sum_{l=1}^{N} x(k)\,x(t-k)\,x^*(l)\,x^*(t-l)]$$

$$\approx (1/(2N-1))\sum_{i=1}^{2N-1} x_s(i)\,x_s^*(i)\ , \qquad (5\text{-}6)$$

where

$$x_s(t) = \sum_{k=1}^{N} x(k)\,x(t-k)\ .$$

Then Eq. (5-6) can be successfully analyzed by considering the following cases:

i) <u>When $k \neq l$ and $t=k+l$</u> ,

rewrite Eq. (5-6) as

$$E_s[x_s(t)\,x_s^*(t)]$$

$$= E_s[\sum_{k=1}^{N}\sum_{l=1,\,l\neq k}^{N} x(k)\,x^*(l)\,x(l)\,x^*(k)]$$

$$= (1/(2N-1))\,[\sum_{k=1}^{N}\sum_{l=1,\,l\neq k}^{N} x(k)\,x^*(k)\,x(l)\,x^*(l)] \qquad (5\text{-}7)$$

$$= (1/(2N-1))\,\{\sum_{k=1}^{N} x(k)\,x^*(k)\}\ \{\sum_{l=1,\,l\neq k}^{N} x(l)\,x^*(l)\}, \qquad (5\text{-}8)$$

and for large N,

$$E[x(t)\,x^*(t)] = 2\sigma_x^2 = (1/N)\sum_{l=1}^{N} x(l)\,x^*(l)\,. \qquad (5\text{-}9)$$

Thus, Eq.(5-8)

$$= (1/(2N-1))\{N^2(4\sigma_x^4) - \sum_{l=1}^{N} x^2(l)(x^*(l))^2\}$$

$$= (1/(2N-1))\{N^2(4\sigma_x^4) - N(2(K+1)\sigma_x^4)\}, \qquad (5\text{-}10)$$

where

$$K = \{E[a^4(t)]/E^2[a^2(t)]\}. \qquad (5\text{-}11)$$

Note that for $x(t) = a(t) + jb(t)$, $t=1,2,\cdots,N$, where $a(t)$ and $b(t)$ are independent and real-valued random processes,

$$E[x^2(t)] = E[(a(t) + jb(t))^2]$$
$$= E[a^2(t) - b^2(t) + j2a(t)b(t)] = 0, \qquad (5\text{-}12)$$

since $a(t)$ and $b(t)$ are independent and have the same distributions with a zero-mean and a variance σ_x^2. In the same manner,

$$E[(x^*(t))^2] = 0 . \qquad (5\text{-}13)$$

Furthermore,

$$E[x^2(t)(x^*(t))^2]$$
$$= E[(a(t)+jb(t))^2(a(t)-jb(t))^2]$$
$$= E[a^4(t)] + E[b^4(t)] + 2E[a^2(t)]E[b^2(t)]$$
$$= KE^2[a^2(t)] + KE^2[b^2(t)] + 2E[a^2(t)]E[b^2(t)]$$
$$= 2K\sigma_x^4 + 2\sigma_x^4$$
$$= 2(K+1)\sigma_x^4 . \qquad (5\text{-}14)$$

ii) <u>When $k \neq l$ and $t \neq k+l$</u> ,

since Eq.(5-6) is composed of all odd moments and each odd moment of a symmetrically distributed zero-mean process is zero, the result is

$$E_s[x_s(t)\,x_s^*(t)] = 0 \ . \tag{5-15}$$

iii) When $k=1$,

Eq.(5-8) can be rewritten as

$$E_s[x_s(t)\,x_s^*(t)]$$

$$= E_s[\sum_{k=1}^{N} x(k)\,x^*(k)\,x(t-k)\,x^*(t-k)] \tag{5-16}$$

$$= \sum_{k=1}^{N} [x(k)\,x^*(k)]\ E_s[x(t-k)\,x^*(t-k)] \tag{5-17}$$

$$= (N^2/(2N-1))\,(4\sigma_x^4), \tag{5-18}$$

where $k+1 \le t \le N+k$.

Now, adding Eqs.(5-10), (5-15), and (5-18) yields

$$E_s[x_s(t)\,x_s^*(t)]$$

$$= (4N-K-1)\,((2N\sigma_x^4)/(2N-1)) . \tag{5-19}$$

The value in Eq.(5-3) causes an error in the SOM S/N ratio, when the S/N for the SOM is defined as

$$[S/N]_s = E_s[s_s(t)\,s_s^*(t)] \ / \ E_s[x_s(t)\,x_s^*(t)] . \tag{5-20}$$

However, the value in Eq.(5-3) can be neglected if $A^2 \ll$

$2\sigma_x^2$, since, under this condition,

$$E_s[\{s(t) \otimes x(t)\}\{s(t) \otimes x(t)\}^*] \ll E_s[x_s(t)x_s^*(t)]. \quad (5\text{-}21)$$

From Eqs.(5-5) and (5-19), the SOM S/N ratio can then be expressed as

$$[S/N]_s = \{A^4(2N^2+1)\}/\{6\sigma_x^4(4N-K-1)\}, \quad (5\text{-}22)$$

or, using the expression of $[S/N]_f$ in Eq.(5-1),

$$[S/N]_s = ([S/N]_f)^2\{2(2N^2+1)\}/\{3(4N-K-1)\}. \quad (5\text{-}23)$$

Example 5.1 If $a(t)$ and $b(t)$ are Gaussian (i.e., K=3), then $[S/N]_s \approx (N/3)([S/N]_f)^2$. Eq.(5-23) shows that $\{[S/N]_s/[S/N]_f\} \geq 1$ so long as

$$[S/N]_f \geq \{3(4N-K-1)\}/\{2(2N^2+1)\}, \quad (5\text{-}24)$$

which indicates that the SOM provides better resolution than the FOM so long as the inequality in Eq.(5-24) is maintained.

In section 5.3, it is shown that the SOM is relatively more accurate than the FOM for small S/N ratios.

5.2 Threshold Signal-to-Noise Ratio

In this section, the theoretical threshold S/N ratio criteria for the resolution of two closely spaced equipowered sources in the FOM and SOM is established.

The underlying concept for obtaining the resolution threshold at the S/N ratio is that the resolution of two closely spaced sources can be achieved when the biases of both $D_c(\omega_1)$ and $D_c(\omega_2)$ have values which are less than that of $D_c(\omega_m)$, where ω_m is the mid-direction angle between ω_1 and ω_2. The procedure is as follows: 1) Obtain expressions for $E[D_c(\omega_k)]$, k=1,2, i.e., the mean value of the FOM and SOM spectra at the desired $\omega_k = 2\pi f_o(D/c)\sin\theta_k$, k=1,2; 2) Take the mid-direction angle ω_m between ω_1 and ω_2, i.e., $\omega_m = (\omega_1 + \omega_2)/2$ to obtain the expression for $E[D_c(\omega_m)]$; and 3) formulate the resolution threshold in the sense of the S/N ratio for two closely spaced sources by equating $E[D_c(\omega_k)]$, k=1,2, and $E[D_c(\omega_m)]$, i.e.,

$$E[D_c(\omega_1)] = E[D_c(\omega_2)] = E[D_c(\omega_m)], \tag{5-25}$$

with small standard deviations for $D_c(\omega_1)$ and $D_c(\omega_2)$ in comparison to their means. The resolution of two closely spaced sources can be accomplished so long as $D_c(\omega_1)$ and $D_c(\omega_2)$ are both less than $D_c(\omega_m)$. When the equality in Eq.(5-25) is true, the S/N ratio at a given small angular separation, with the resolution probability between 0.333 and 0.50, becomes the desired threshold S/N ratio for the

angular separation, which is defined as $2\omega_d = 2\pi f_o (D/c)(\sin\theta_1 - \sin\theta_2)$. Throughout this study, the sensor spacing D takes the value of one-half the wavelength, unless otherwise specified, implying that $2\omega_d = \pi(\sin\theta_1 - \sin\theta_2)$. For the equality in Eq. (5-25), the resolution probability has its range from 0.333, in which all the variations of $D_c(\omega_1)$, $D_c(\omega_2)$, and $D_c(\omega_m)$ are totally uncorrelated, to 0.5, when $D_c(\omega_1)$ and $D_c(\omega_2)$ vary in fully correlated manner.

The FOM and SOM threshold S/N ratio expressions can then be derived. For the MUSIC (FOM), using the signal subpace, the inverse spectrum can be expressed as [20]

$$D_c(\omega) = 1 - \mathbf{a}^*(\omega) \left[\sum_{i=1}^{M} \mathbf{V_i}\mathbf{V_i}^*\right] \mathbf{a}(\omega)$$

where $\mathbf{a}^T(\omega) = Q^{-1/2}[1, e^{-j\omega}, \ldots, e^{-j(Q-1)\omega}]$, Q is the number of sensors, M is the number of sources, $Q > M$, and $\omega = 2\pi f_o (D/c)\sin\theta$.

Or, using the noise subspace, the inverse spectrum is expressed as

$$D_c(\omega) = \mathbf{a}^*(\omega) \left[\sum_{i=M+1}^{Q} \mathbf{V_i}\mathbf{V_i}^*\right] \mathbf{a}(\omega) \quad .$$

Therefore, $\mathbf{a}(\omega_i) \perp \mathbf{V_i} \Rightarrow D_c(\omega_i) = 0$, for $i=M+1, \ldots, Q$.

The expression for the $E[D_c(\omega)]$ is obtained by Kaveh and Barabell [20],

$E[D_c(\omega)] \approx$

$$D_c(\omega) - \mathbf{a}^*(\omega) \Big[\sum_{i=1}^{M}\sum_{\substack{j=1 \\ j\neq i}}^{Q} (\varepsilon_i\varepsilon_j/N(\varepsilon_i-\varepsilon_j)^2)\,(\mathbf{V}_j\mathbf{V}_j^*-\mathbf{V}_i\mathbf{V}_i^*)\Big]\mathbf{a}(\omega). \quad (5\text{-}26)$$

For M=2,

$$E[D_c(\omega_k)]=N^{-1}(Q-2)\,(2\sigma_x^2)\,\mathbf{a}^*(\omega_k)\,[\varepsilon_1\mathbf{V}_1\mathbf{V}_1^*/(\varepsilon_1-2\sigma_x^2)^2 + \varepsilon_2\mathbf{V}_2\mathbf{V}_2^*/(\varepsilon_2-2\sigma_x^2)^2]\mathbf{a}(\omega_k),\ k=1,2, \quad (5\text{-}27)$$

where ε_1, ε_1, $\mathbf{V}_1$, and $\mathbf{V}_2$ are eigenvalues and the corresponding eigenvectors of the estimated array covariance matrix, and $2\sigma_x^2$ is the noise variance. Define centered direction vectors by $\mathbf{U}_i = e^{-j[(Q-1)/2]\omega_i}\mathbf{a}(\omega_i)$, i=1,2, for two uncorrelated signals. Let $d = \mathbf{a}^*(\omega_1)\mathbf{a}(\omega_2)$, then by [42]

$\varepsilon_i = A^2Q(1 \pm |d|)$ and $\mathbf{V}_i = (\mathbf{U}_1+\mathbf{U}_2)/[2(1+|d|)]^{1/2}$, i=1,2,

where $d = e^{-j(Q-1)\omega_d}[1 - (Q^2\omega_d^2/6) + (Q^4\omega_d^4/120)]$, for $(Q\omega_d)^2 \ll 1$ (i.e., very closely spaced sources), with $2\omega_d = 2\pi f_o(D/c)[\sin\theta_1-\sin\theta_2]$, $\varepsilon_1' = \varepsilon_1 - 2\sigma_x^2$, $\varepsilon_2' = \varepsilon_2 - 2\sigma_x^2$. Let $\Delta_1^2 = Q^2\omega_d^2/3$, then $\varepsilon_1' = 2A^2Q[1 - (\Delta_1^2/4) + (3\Delta_1^4/80)]$, and $\varepsilon_2' = 2A^2Q[(\Delta_1^2/4) - (3\Delta_1^4/80)]$.

Also,

$$\mathbf{V}_1 = (\mathbf{U}_1+\mathbf{U}_2)/[2(1+|d|)]^{1/2}$$

$$\Rightarrow \quad |\mathbf{a}^*(\omega_i)\mathbf{V}_1|^2 = \varepsilon_1'/(2A^2Q)$$

$$\approx 1 - (\Delta_1^2/4) + (3\Delta_1^4/80)$$

$$\approx 1, \tag{5-28}$$

$$\mathbf{V}_2 = (\mathbf{U}_1-\mathbf{U}_2)/[2(1-|d|)]^{1/2}$$

$$\Rightarrow \quad |\mathbf{a}^*(\omega_i)\mathbf{V}_2|^2 = \varepsilon_2'/(2A^2Q)$$

$$\approx (\Delta_1^2/4) - (3\Delta_1^2/80)$$

$$\approx \Delta_1^2/4\ , \tag{5-29}$$

and

$$|\mathbf{a}^*(\omega_m)\mathbf{V}_1|^2 \approx 1 - (\Delta_1^2/8) \tag{5-30}$$

$$|\mathbf{a}^*(\omega_m)\mathbf{V}_2|^2 \approx 0\ . \tag{5-31}$$

Thus,

$$E[D_c(\omega_k)] \approx N^{-1}(Q-2)[(1/\zeta_1) + 1/(\Delta_1^2\zeta_1^2)], \tag{5-32}$$

for large N, k=1,2, where $\zeta_1 = A^2Q/(2\sigma_x^2)$ (called array S/N ratio (ASNR)).

For the mid-arrival direction angle ω_m, $E[D_c(\omega_m)]$ can be obtained by substituting Eqs.(5-30) and (5-31) into Eq.(5-26) and simplifying, i.e.,

$$E[D_c(\omega_m)] = b_1 + N^{-1}[(b_2/\zeta_1) + (b_3/\zeta_1)], \tag{5-33}$$

where $\omega_m = (\omega_1 + \omega_2)/2$,

$$b_1 = D_c(\omega_m) \approx \Delta_1^4/80,$$

$$b_2 \approx (1/2)(Q-2)(1 + \Delta_1^2/4), \text{ and}$$

$$b_3 \approx (1/4)(Q-2)(1 + \Delta_1^2/4) .$$

Equating Eq.(5-32) and (5-33), i.e.,

$$N^{-1}(Q-2)[(1/\zeta_1) + (1/(\zeta_1^2\Delta_1^2))]$$

$$= b_1 + N^{-1}[(b_2/\zeta_1) + (b_3/\zeta_1^2)],$$

yields,

$$\zeta_1^2 + (b_2-Q+2)\zeta_1/(b_1N) + [b_3 - (Q-2)\Delta_1^{-2}]/(b_1N) = 0. \quad (5-34)$$

Solving Eq.(5-34) for ζ_1 gives

$$\zeta_1 = (2b_1N)^{-1}(Q-2-b_2)\{1 + [1 + 4b_1N((Q-2)\Delta_1^{-2} - b_3)/(Q-2-b_2)^2]^{1/2}\}.$$

Thus, we have

$$\zeta_1 \approx 20N^{-1}(Q-2)\Delta_1^{-4}\{1 + [1 + N\Delta_1^2/(5(Q-2))]^{1/2}\}, \quad (5-35)$$

since $(Q-2-b_2)/2b_1N \approx 20(Q-2)/N\Delta_1^4$, and

$$4b_1N[(Q-20)\Delta_1^{-2}-b_3]/(Q-2-b_2)^2 \approx N\Delta_1^2/(5(Q-2)).$$

Now, the threshold ASNR for the SOM can be conceptually obtained using the S/N ratio relationship derived in Section 5.1. For Gaussian noises, i.e., K=3, from Eq.(5-23),

$$[S/N]_s \approx (N/3)([S/N]_f)^2, \text{ for large } N. \quad (5-36)$$

Therefore, the threshold ASNR for the FOM should be

$$\zeta_1 = (N/3Q)\zeta_2^2 , \quad (5-37)$$

where ζ_2 denotes the SOM threshold ASNR.

Equating Eq.(5-35) and (5-37) yields

$$\zeta_2^2 = (2b_1N^2)^{-1}[3Q(Q-2-b_2)]\{1 + [1 + 4b_1N(Q-2-b_3\Delta_1^2)/\Delta_1^2(Q-2-b_2)^2]^{1/2}\},$$

or

$$\zeta_2 = N^{-1}[60Q(Q-2)]^{1/2}\Delta_1^{-2}\{1 + [1 + N\Delta_1^2/5(Q-2)]^{1/2}\}^{1/2}. \quad (5-38)$$

Eq.(5-38) indicates the approximated expressions for the SOM threshold ASNR, while Eq.(5-35) indicates the FOM threshold ASNR. Based upon these equations, Figs. 5-1 - 5-4 show the difference between the FOM and SOM threshold ASNR becomes larger as fewer sensors are used. Thus, when only a limited number of sensors is available, the SOM is capable of resolving closely spaced sources more effectively than the FOM. Also, variations in the ASNR have been examined for different numbers of data points in Fig. 5-5. It shows that the ASNR becomes gradually worse as the number of data points are reduced. In Table 5-1, simulation results are provided for the ASNRs and the resolution probabilities for the FOM and SOM, for which the ASNR is chosen for 0.333 to 0.5 resolution probability region, as explained in page 118. For each result in Table 5-1, 60 independent simulations have been conducted. The simulation results indicate close agreement with the theoretical calculations carried out for this investigation.

5.3 Envelopes of the Validity of the SOM

The regions, in which the SOM offers better resolution of both equipowered and non-equipowered source signal directions than the FOM does, are established with a fixed noise power two in this section.

5.3.1 Equipowered Case

When multiple source signals (M=2) have same power, the resolution superiority between the FOM and SOM has been determined, using three sensors, with respect to the bias from true direction angles, throughout 30 different runs at certain angular separation and S/N ratio. Fig. 5-6 shows that the angular separation region, in which the SOM guarantees better resolutions compared to the FOM, becomes wider as the S/N ratio becomes less, so long as two source directions are resolved. Also, from Fig. 5-6, it is easily seen that the resolution superiority of the SOM is confined to the smaller region containing very closely spaced source signals when the S/N ratio becomes relatively larger.

5.3.2 Non-Equipowered Case

The non-equipowered multiple source directions are examined in the case that one source power is fixed to P_1=100 and the other weaker source power p_2 is changing (Fig. 5-7). In this case, S/N ratio refers to the ratio

of weaker source power and noise power. Fig. 5-7 has very similar form as Fig. 5-6. However, the accuracy region of the SOM over the FOM in Figs. 5-7 is narrower than that of the FOM in Fig. 5-6 throughout the S/N ratios because the ratio of the two source power of the SOM is squared to the ratio of the FOM, which makes the resolution of the SOM become worse than that of the FOM.

5.4 Comparisons between SOM and ESPRIT

Relatively new scheme for the direction finding problem called the Estimation of Signal Parameters via Rotational Invariance Techniques (ESPRIT) [27,28] is briefly discussed and compared with the SOM in certain scenarios. The ESPRIT utilizes an underlying rotational invariance among signal subspaces by constructing the auto- and cross-covariance matrices. This method can be applied to a uniformly distributed sensor array or a pairwise matched arbitrary array with codirectional sensor doublets when noise are uncorrelated between sensors with same variance. In this study, for consistency, a uniformly distributed sensor array will be used. Using the notation of subarrays with size Q in Eq.(3-32), we have

$$\mathbf{r}(t) = \mathbf{r}_{(1)}(t) = \mathbf{A}\mathbf{s}(t) + \mathbf{x}_{(1)}(t) \tag{5-39}$$

and

$$\mathbf{q}(t) = \mathbf{r}_{(2)}(t) = \mathbf{A}\mathbf{G}\mathbf{s}(t) + \mathbf{x}_{(2)}(t), \tag{5-40}$$

where **A** is Q x Q Vandermonde matrix as in Eq.(2-15) and **G** is given by Eqs.(3-33) and (3-34). Therefore, the auto- and cross-covariance matrices are expressed as

$$\mathbf{R}_{rr} = \mathbf{APA}^{*} + \sigma^{2}\mathbf{I} \tag{5-41}$$

and

$$\mathbf{R}_{rq} = \mathbf{APG}^{*}\mathbf{A}^{*} + \sigma^{2}\mathbf{B} \ , \tag{5-42}$$

where **B** denotes an Q x Q matrix with ones along the first lower diagonal off the major diagonal and zeros elsewhere. Once σ2 can be obtained from Eq.(5-41) using the standard eigenstructure algorithm mentioned in section 2.4, we have

$$\mathbf{C}_{rr} - \lambda\mathbf{C}_{rq} = \mathbf{AP}(\mathbf{I}_{M} - \lambda\mathbf{G}^{*})\mathbf{A}^{*}, \tag{5-43}$$

where

$$\mathbf{C}_{rr} = \mathbf{R}_{rr} - \sigma^{2}\mathbf{I} = \mathbf{APA}^{*} \quad \text{and} \quad \mathbf{C}_{rq} = \mathbf{R}_{rq} - \sigma^{2}\mathbf{B} = \mathbf{APG}^{*}\mathbf{A}^{*}.$$

Therefore, the singular values of the above matrix pencil $(\mathbf{C}_{rr},\mathbf{C}_{rq})$ in Eq.(5-43) are the roots of

$$|\mathbf{I}_{M} - \lambda\mathbf{G}^{*}| = \mathbf{0} \tag{5-44}$$

because both **A** and **P** are of rank M.

Using Eq.(3-34) gives

$$\lambda_{i} = \chi_{k} = \exp[-j\omega_{o}(D/c)\sin\theta_{k}], \quad k = 1,2,\cdots,M. \tag{5-45}$$

The ESPRIT does not need a search technique to estimate the direction angles and in that respect computation and storage costs are considerably reduced. However, the ESPRIT may have inferior results due to the effect of subtraction the estimated noise variance from the estimated auto- and cross-covariance matrices.

The following example provides the brief comparisons between the ESPRIT and proposed SOM for resolving the direction angles of very closely spaced multiple source signals. Two uncorrelated and very closely-spaced sources are to be resolved using the SOM and ESPRIT, at different S/N ratios. While three sensors are used for the SOM, four sensors which are divided into two overlapping subarrays of size three are used. As shown in Table 5-2, broadly, the SOM has the superiority in resolution over the ESPRIT in all the cases examined. However, the ESPRIT is known to have some implementational advantages such as speed and storage, in comparison to the other proposed methods.

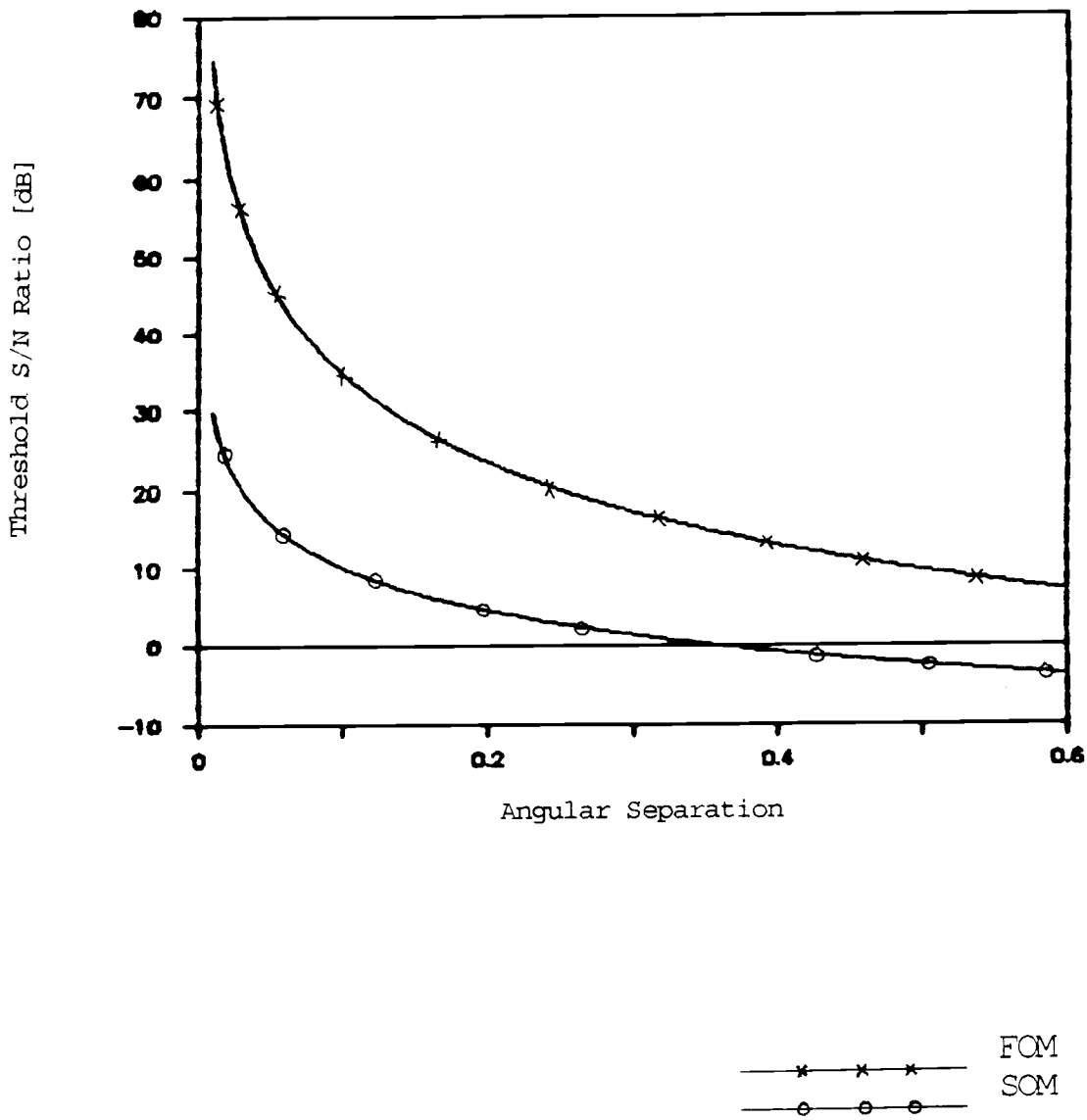

Fig.5-1. Array Threshold S/N Ratio for the FOM and SOM when Q=3 and N=256.

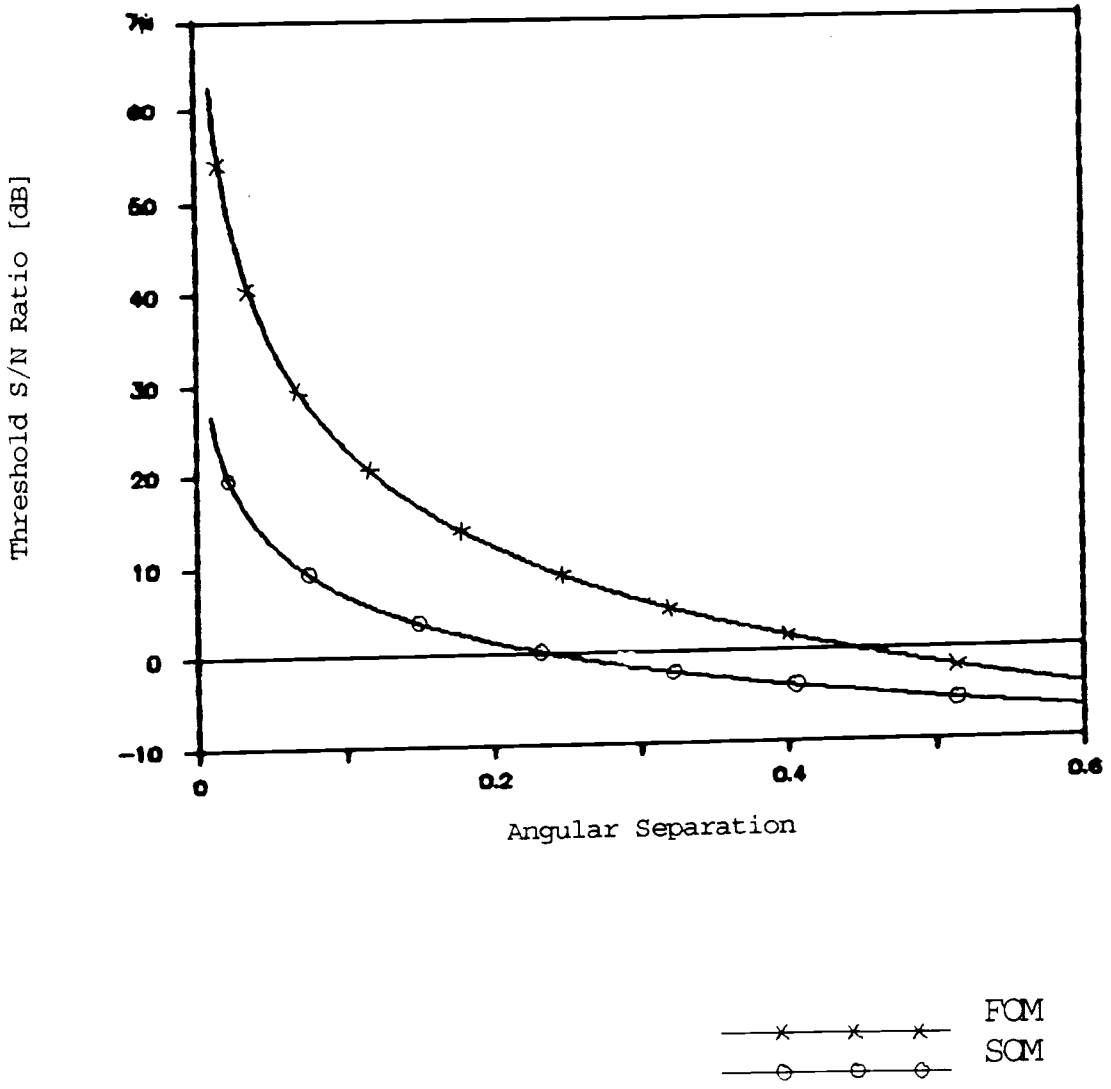

Fig.5-2. Array Threshold S/N Ratio for the FCM and SCM when Q=10 and N=256.

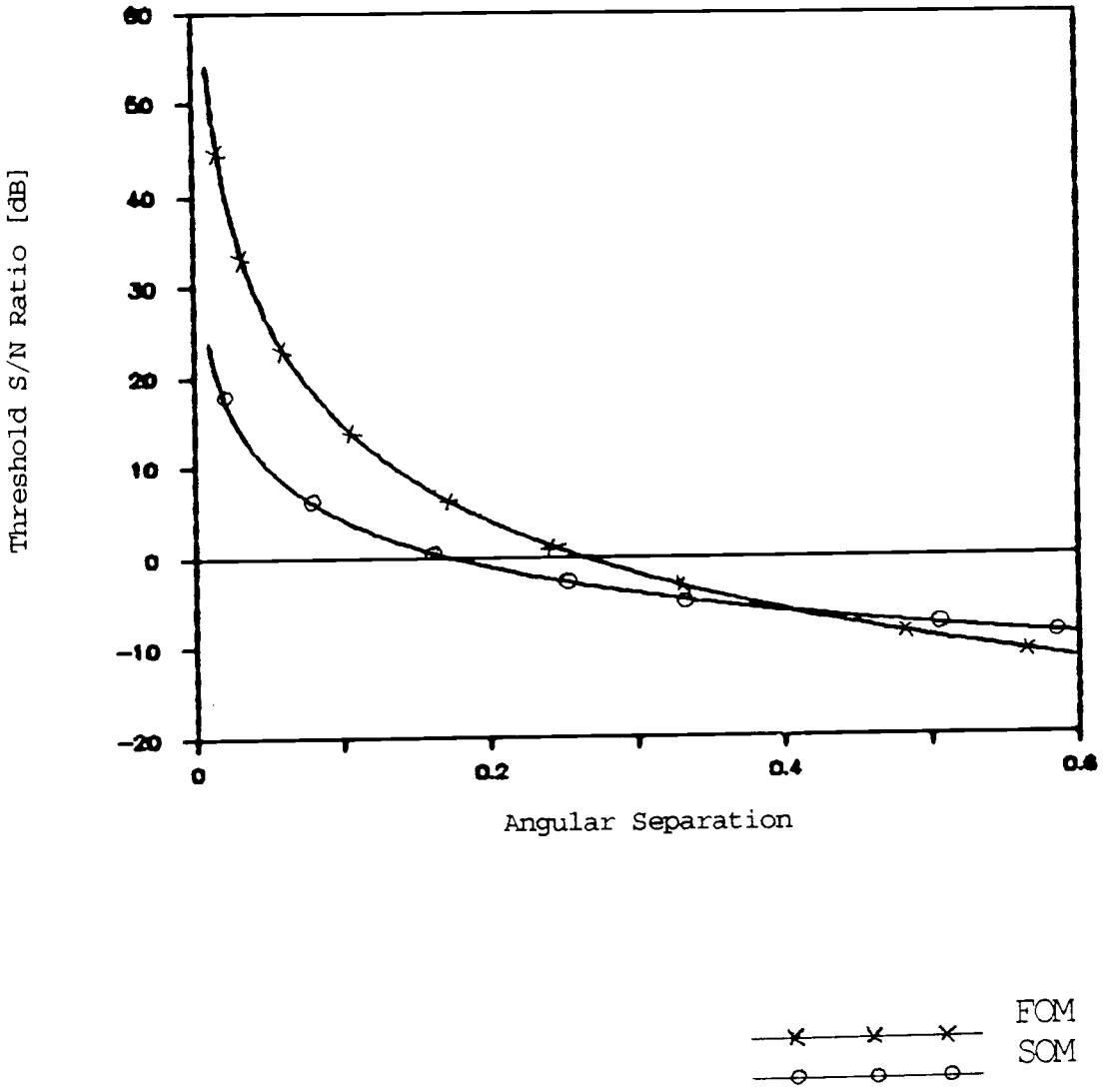

Fig.5-3. Array Threshold S/N Ratio for the FOM and SOM when Q=20 and N=256.

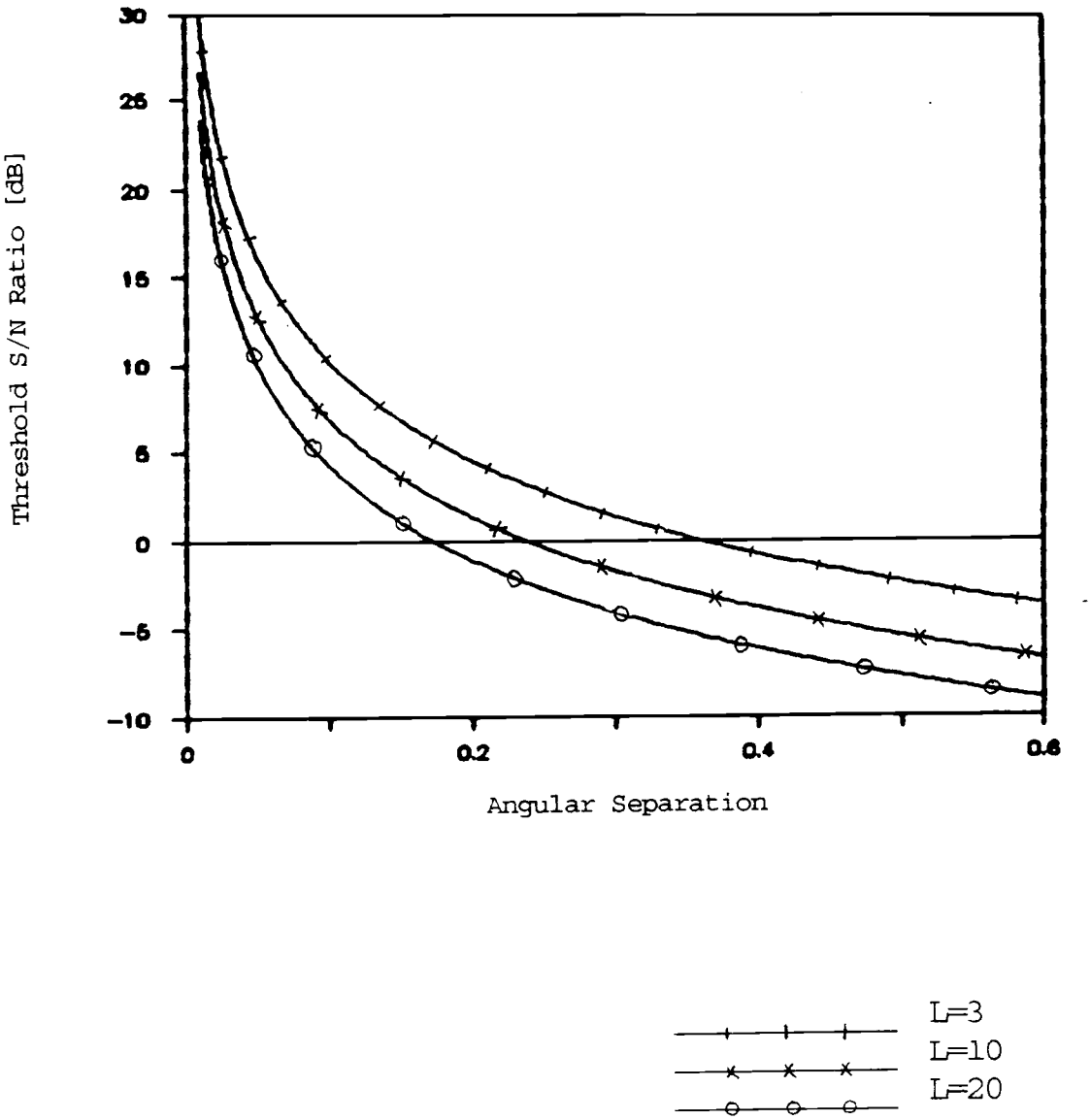

Fig.5-4. Array Threshold S/N Ratio for the SCM using Different Number of Sensors, when N=256.

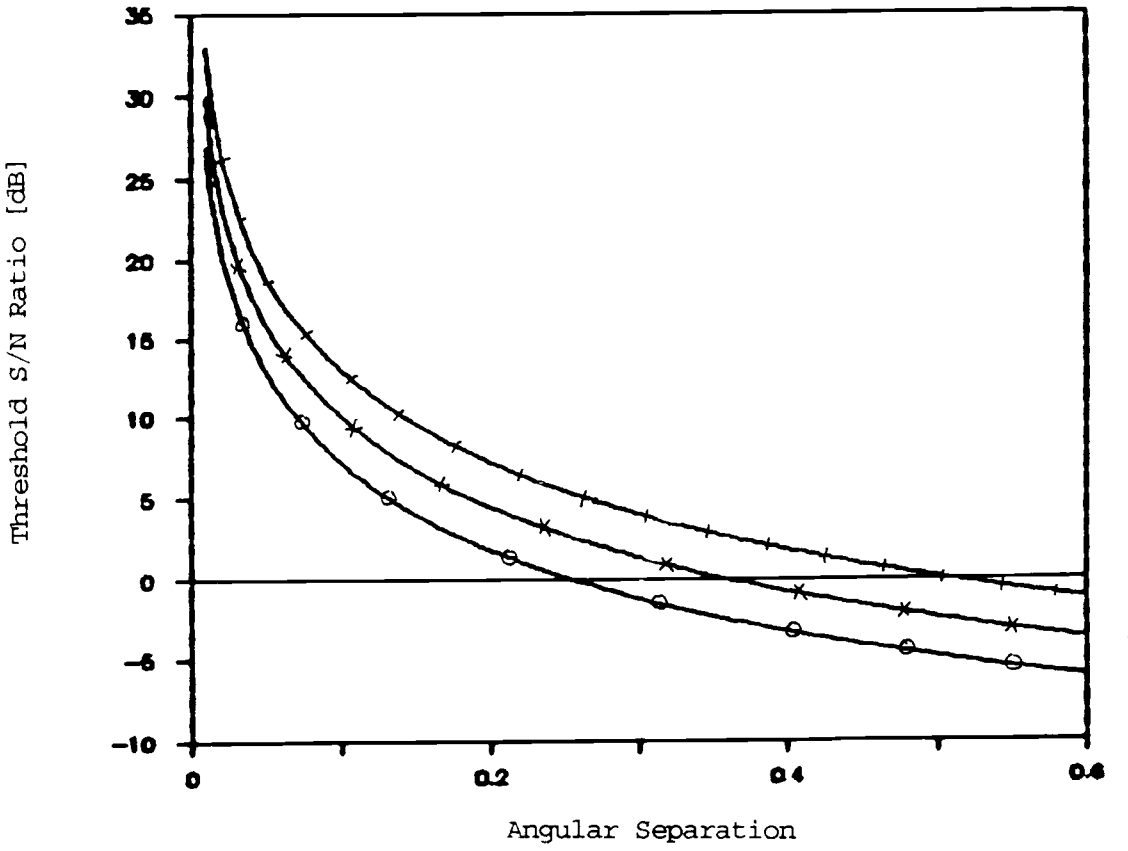

Fig.5-5. Array Threshold S/N Ratio for the SCM using Different Number of Data Points, when Q=3.

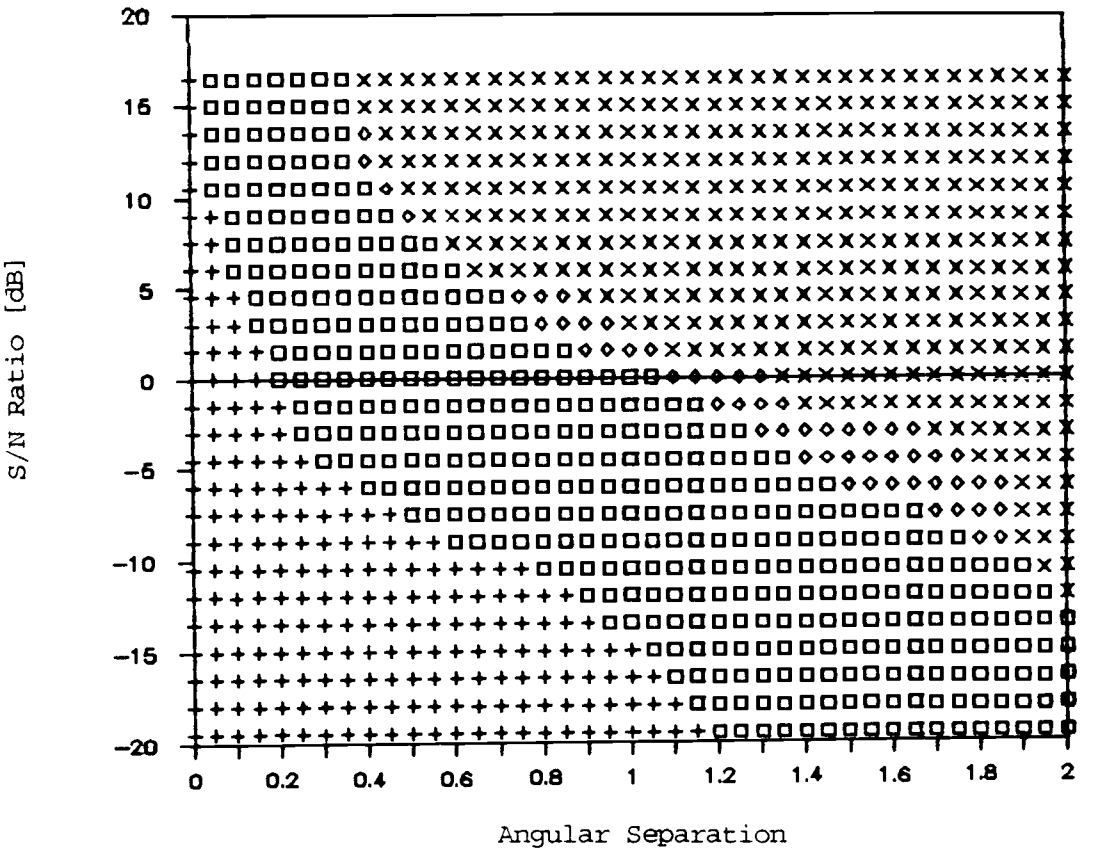

\+ Both FOM and SOM cannot resolve 2 sources directions
◇ Resolution superiority cannot be compared
□ SOM is superior to FOM
× FOM is superior to SOM

Fig.5-6. Comparisons of Resolution of Equipowered Multiple Sources between the SOM and FOM with respect to both S/N and Angular Separation, through 30 runs, Q=3 and M=2.

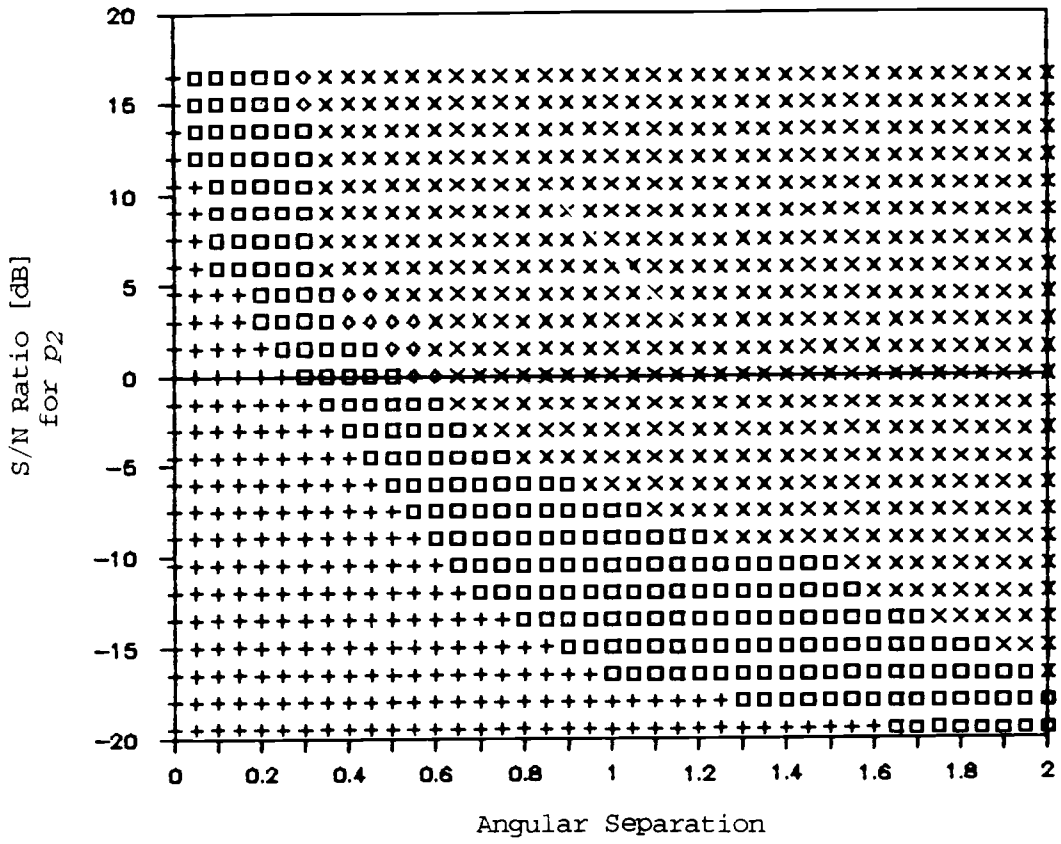

\+ Both FOM and SOM cannot resolve 2 sources directions
◇ Resolution superiority cannot be compared
□ SOM is superior to FOM
× FOM is superior to SOM

Fig.5-7. Comparisons of Resolution of Equipowered Multiple Sources between the SOM and FOM with respect to both S/N and Angular Separation, through 30 runs, Q=3 and M=2 (The Ratio of Stronger Signal Power and Weaker Signal Power is to be changed.).

Table 5-1. Array Threshold S/N Ratio and Resolution Probability in terms of Angular Separation of Two Equipowed Sources for the FOM and SOM, Q=3 and N=256.

direction angles		angular separation	FOM		SOM	
θ_1	θ_2	$2\omega_d$	ASNR [dB]	Res. Prob.	ASNR[dB]	Res. Prob.
5.00	7.00	0.1091			8.0	0.40
					9.0	0.45
					10.0	0.67
5.00	9.00	0.2177	16.0	0.28	2.0	0.27
			17.0	0.37	3.0	0.33
			18.0	0.55	4.0	0.52

Table 5-2. Comparisons of resolution between the SOM and ESPRIT.

	S/N [dB]	(ordinary) SOM	ESPRIT
8°, 13°	-3°	8.00°, 13.65°	cannot resolve
8°, 11°	0°	8.05°, 12.10°	10.29°, 17.28°
	12°	8.40°, 11.40°	9.05°, 13.52°
8°, 10°	18°	8.35°, 10.40°	9.20°, 11.94°

CHAPTER 6

CONCLUSION

One of the principle issues in array processing is the estimation of source signal direction angles of source signals impinging upon a sensor array which may be corrupted by noise. Eigenstructure-based methods yielding high resolution direction finding estimates comparable to any of the other proposed spectral estimates, including the Bartlett, ML, or AR methods, have been considered. In particular, this study has shown that the generalized eigenstructure algorithm efficiently handles cases in which the sensor noises are spatially correlated and for which correlation coefficients are known or can be estimated.

Problem areas continue to exist in situations such as very closely spaced source signals, low S/N ratios, spatially correlated noises without knowledge of the correlation coefficients, and non-Gaussian noises. The principal accomplishment of of this study was the introduction and careful analysis of a nonlinear second-order method (SOM) for consideration of these troublesome areas. The key idea of the SOM is to include information on all of the data points in correlation operations, at a constant lag, by the introduction of new data sequences, or second-order signals obtained by

auto-convolution of the original received data from each array sensor. Through an elaborate derivation procedure, it has been demonstrated that the SOM has a spatial spectral density matrix structure similar to that of the MUSIC. Thus, the same orthogonality test used with the MUSIC for the estimation of source direction angles can be performed for the SOM. The only difference between the two methods lies in the searching vector. All of the searching vector elements for the SOM become the squares of those for the MUSIC. This allows the SOM to double the effective aperture of the sensor array, theoretically offering twice the FOM resolution for closely spaced source signals. These findings have been confirmed by computer simulation for several different catagories, including single source detection at low S/N ratios with uncorrelated and correlated sensor noises, and closely spaced multiple sources with uncorrrelated and correlated Gaussian or non-Gaussian noises.

A revised SOM, based upon a different procedure for obtaining the second-order spatial spectral density matrix, has been developed for this study. Several computer simulations have indicated by means of statistical analysis that the revised SOM offers better resolvability than the ordinary SOM. Nontheless, it was difficult to compare both of the SOMs in terms of their reliability.

In situations where multiple source signals are well- separated, it cannot be claimed that the SOM definately offers a better method for estimating direction angles than the FOM, since the SOM offers much better rms. and std. of the direction error than the FOM, but the FOM shows the bias for direction angles which is slightly less than that of the SOM, regardless of the S/N ratios.

However, when the sources are very closely spaced and/or at relatively low S/N ratios, the SOM provides definite resolution advantages in comparison to the FOM. First, in terms of the angular separation, the theoretical derivations of the threshold S/N ratios were developed, along with comparisons of the FOM and SOM S/N ratios. These results were then verified by computer simulation with several runs at each angular separation. In all the cases, consistent agreement between the theory and the simulation results was clearly indicated. From these results, it may be readily stated that the difference between the SOM and FOM threshold S/N ratios becomes larger as the number of sensors is reduced. This indicates that the SOM can be used effectively, particularly in situations where there are only limited numbers of sensors for the resolution of very close angular separations of sources. Also, as expected, the threshold S/N ratios become gradually worse as the numbers of data points and sensors are reduced.

In addition, this study has demonstrated that the SOM can be combined with spatial smoothing techniques, which are used for the decorrelation of coherent source signals. In this respect, the results obtained from the use of the SOM have been found to be superior to those obtained with the use of the FOM. Also, the SOM has been compared with the ESPRIT which utilizes rotational invariance among signal subspaces.

In the future, the performance of real data analyses can be expected using the methods described in this study. These analyses will be used to demonstrate that the proposed ordinary and revised SOMs have the ability to effectively respond to the problem areas of closely spaced source signals, low S/N ratios, correlated noises between sensors where the correlation coefficients are not known, and uniformly distributed random noises.

BIBLIOGRAPHY

[1] H. Akaike, "Information Theory and an Extension of the Maximum Likelihood Principle," Proc. Second Int. Symp. on Information Theory, Suppl. to Problems of Control and Information Theory, 267-281 (1972).

[2] G. Bienvenu, "Influence of the Spatial Coherence of the Background Noise on High Resolution Passive Methods," Proc. IEEE ICASSP, Washingtion D.C., 306-309 (1979).

[3] G. Bienvenu and L. Kopp, "Optimality of High Resolution Array Processing Using the Eigensystem Approach," IEEE Trans. Acoust.,Speech, and Signal Processing, Vol. ASSP-31, 1235-1247 (1983).

[4] F. J. Bugnon and R. R. Mohler, "Nonlinear Processing with Mth-Order Signals," Nonlinear Time Series and Signal Processing, R. R. Mohler (ed.), Lecture Notes in Control and Information Series, Vol. 106, 119-129, Springer-Verlag, New York (1988).

[5] F. J. Bugnon, R. R. Mohler, and I. K. Rhee, "Nonlinear Second-Order Eigenstructure Method in Array Processing," Proc. Adv. in Communic. and Control Sys. (COMCON 88), Baton Rouge, 456-468 (1988).

[6] J. P. Burg, "The Relationship between Maximum Entropy and Maximum Likelihood Spectra, Geophysics, Vol. 37, 375-376 (1972).

[7] J. A. Cadzow, "A High Resolution Direction-of-Arrival Algorithm for Narrow-Band Coherent and Incoherent Sources," IEEE Trans. Acoust., Speech, and Signal Processing, Vol. 36, 965-979 (1988).

[8] J. Capon, "High Resolution Frequency Wavenumber Spectrum Analysis," Proc. IEEE, Vol. 57, 1408-1418 (1969).

[9] D. G. Childers, Modern Spectrum Analysis, IEEE Press, New York (1978).

[10] H. Cox, "Resolving Power and Sensitivity to Mismatch of Optimum (Line) Array Processors," J. Acoust. Soc. Am., Vol. 54, 771-785 (1973).

[11] F. S. Crawford,Jr., "Waves," Berkeley Physics Course, Vol. 3, McGraw-Hill, New York (1968).

[12] D. E. Dudgeon, "Fundamentals of Digital Array Processing," Proc. IEEE, Vol. 65, 898-904 (1977).

[13] E. J. Hannan and B. G. Quinn, "The Determination of the Order of an Autoregression," J. Roy. Stat. Soc., Ser. B, Vol. 41, 190-195 (1979).

[14] S. Haykin, ed., Nonlinear Methods of Spectral Analysis (2nd ed.) Springer-Verlag, New York (1983).

[15] S. Haykin, in S. Haykin (ed.), Array Signal Processing, Prentice-Hall, Englewood Cliffs, N.J. (1985).

[16] J. E. Hudson, Adaptive Array Principles. Stevenage, U. K.:Peter Peregrinus Ltd. (1981).

[17] D. H. Johnson, "The Application of Spectral Estimation Methods to Bearing Estimation Problems," Proc. IEEE, Vol. 70, 1018-1028 (1982).

[18] D. H. Johnson and S. R. Degraff, "Improving the Resolution of Bearing in Passive Sonar Arrays by Eigenvalue Analysis," IEEE Trans. Acoust., Speech, and Signal Processing, Vol. ASSP-30, 638-647 (1982).

[19] R. L. Kashyap, "Inconsistency of the AIC Rule for Estimating the Order of Autoregressive Models, IEEE Trans. Autom. Control, Vol. AC-25, 996-998 (1980).

[20] M. Kaveh and A, J. Barabell, "The Statistical Performance of the Music and the Minimum-norm Algorithms in Resolving Plane Wave in Noise," IEEE Trans. Acoust., Speech, and Signal Processing, Vol. ASSP-34, 331-341 (1986).

[21] S. M. Kay and S. L. Marple,Jr., "Spectrum Analysis - A Modern Perspective," Proc. IEEE, Vol. 69, 1380-1419 (1981).

[22] J. J. Komo, "Random Signal Analysis in Engineering Systems," Academic Press, Orlando, Florida (1987).

[23] R. T. Lacoss, "Data Adaptive Spectral Analysis Methods," Geophysics, Vol. 36, 661-675 (1971).

[24] S. L. Marple,Jr., "Frequency Resolution of Fourier and Maximum Entropy Spectral Estimates," Geophysics, Vol. 47, 1303-1307 (1982).

[25] S. L. Marple,Jr., "Digital Spectral Analysis with Applications," Prentice-Hall, Englewood Cliffs, N.J. (1987).

[26] N. L. Owsley, "Sonar Array Processing," in S. Haykin (ed.), Array Signal Processing, Prentice Hall, Englewood Cliffs, N.J. (1985).

[27] A. Paulraj, R. Roy, and T. Kailath, "Estimation of Signal Parameters via Rotational Invariance Techniques - ESPRIT," in Proc. 19th Asilomar Conf., Pacific Grove, CA (1985).

[28] A. Paulraj and T. Kailath, "Eigenstructure Methods for Direction of Arrival Estimation in the Presence of Unknown Noise Fields," IEEE Trans. Acoust., Speech, and Signal Processing, Vol. ASSP-34, 13-20 (1986).

[29] V. F. Pisarenko, "The Retrieval of Harmonics from a Covariance Function," Geoph. J. R. Astron.Soc.,Vol. 33, 347-366 (1973).

[30] M. Quirk and B. Liu, "On the Resolution of Autoregressive Spectral Estimation," Proc. IEEE Int. Conf. Acoust., Speech, and Signal Processing, 1095-1097 (1983).

[31] L. Rayleigh, "Investigations in Optics, with Special References to the Spectroscope," Philos. Mag. J. Sci., Ser. 5, Vol. 8, No. 49, 261-274 (1879).

[32] S. S. Reddi, "Multiple Source Location -- A Digital Approach," IEEE Trans. Aerosp. Electron. Syst., AES-15, 95-105 (1979).

[33] V. U. Reddy et al., "Performance Analysis of the Optimum Beamformer in the Presence of Correlated Sources and Its Behavior Under Spatial Smoothing," IEEE Trans. Acoust., Speech, and Signal Processing (1987).

[34] J. Rissanen, "Modeling by Shortest Data Description," Automatica, Vol. 14, 465-471 (1978).

[35] J. Rissanen, "Consistent Order Estimation of Autoregressive Processes by Shortest Description of Data," Analysis and Optimization of Stochastic Systems," Jacobs et al. (ed.), Academic Press, N.Y. (1980).

[36] E. Robinson and M. Silvia, "Digital Foundations of Time Series Analysis, Vol. 2, Wave-Equation Space-Time Processing," Holden-Day, San Francisco, CA (1981).

[37] R. Roy, A. Paulraj, and T. Kailath, "ESPRIT - A Subspace Rotation Approach to Estimation of Parameters of Cisoids in Noise," IEEE Trans. Acoust., Speech, and Signal Processing, Vol. ASSP-34, 1340-1342 (1986).

[38] E. H. Satorius and J. R. Zeidler, "Maximum Entropy Spectral Analysis of Multiple Sinusoids in Noise," Geophysics, Vol. 43, 1111-1118 (1978).

[39] R. O. Schmidt, "A Signal Subspace Approach to Multiple Source Location and Spectral Estimation," Ph.D dissertation, Stanford University, Stanford, CA (1981).

[40] R. O. Schmidt, "Multiple Emitter Location and Signal Parameter Estimator," IEEE Trans. Antennas Propag., Vol. AP-34, 276-280 (1986).

[41] G. Schwartz, "Estimating the Dimension of a Model," Ann. Stat., Vol. 6, 461-464 (1978).

[42] T. Shan, M. Wax, and T. Kailath, "On Spatial Smoothing for Direction-of-Arrival Estimation of Coherent Signals," IEEE Trans. Acoust., Speech, and Signal Processing, Vol. ASSP-33, No. 4, 801-811 (1985).

[43] T. Thorvaldsen, "Maximum Entropy Spectral Analysis in Antenna Spatial Filtering," IEEE Trans. Antennas Propag., AP-28, 552-560 (1980).

[44] M. Wax, T. J. Shan, and T. Kailath, "Spatio-Temporal Spectral Analysis by Eigenstructure Methods," IEEE Trans. Acoust., Speech, and Signal Processing, Vol. ASSP-32, 817-827 (1984).

[45] M. Wax and T. Kailath, "Detection of Signals by Information Theoretic Criteria," IEEE Trans. Acoust., Speech, and Signal Processing, Vol. ASSP-33, No. 2, 387-391 (1985).

APPENDICES

APPENDIX A

PLANE WAVE DESCRIPTION [26,27,28,29]

For the one-dimensional wave equation

$$(\partial^2 u/\partial x^2) = (1/c^2)(\partial^2 u/\partial t^2) \qquad \text{(A-1)}$$

where

c is the speed of propagation,

$u = u(x,t)$,

the variable t represents time and the variable x represents distance along the line in which the wave travels.

A general solution to this wave equation is

$$u = g(x - ct) \qquad \text{(A-2)}$$

where

g is an arbitrary twice differentiable function.

The wave in Eq.(A-2) produced by the Eq.(A-1) does not change its shape as it travels.

We now consider the sinusoidal wave or harmonic wave varying in space and time as

$$u(x,t) = A \exp[j(\omega t - kx)] \qquad \text{(A-3)}$$

where A is a positive constant indicating the amplitude of the harmonic wave of Eq.(A-3), the quantity ω is called the angular frequency, k is said to be the spatial frequency or angular wavenumber. In the case of more

than one dimension, subscripts x, y, and z are used to indicate that k_x, k_y, and k_z are spatial frequencies with respect to the x-axis, y-axis, and z-axis, respectively.

To show that Eq. (A-3) is a solution to Eq. (A-1) rewrite Eq. (A-3) as

$$u(x,t) = A \exp[j(\omega t - kx)]$$
$$= A \exp[-jk(x - (\omega/k)t)] \qquad \text{(A-4)}$$

Then, we can easily see that Eq. (A-4) is of the form $g(x-ct)$ provided that $(\omega/k)=c$, which is the condition under which the sinusoidal wave of Eq. (A-3) is a solution to Eq. (A-1).

A sinusoidal wave traveling in the positive x-direction can be written as

$$u(x,t) = \exp[j(\omega t - kx)] \quad (k > 0,\ \omega > 0)$$

while a sinusoidal wave traveling in the negative x-direction can be written as

$$u(x,t) = \exp[j(\omega t + kx)] \quad (k > 0,\ \omega > 0).$$

In the case of a simple harmonic time dependence, we can separate the x and t dependence as

$$u(x,t) = g(x)\exp(j\omega t) .$$

Considering the sinusoidal wave for fixed angular frequency ω_o and spatial frequency k_o as

$$u(x,t) = \exp[j(\omega_o t - k_o x)] \qquad \text{(A-5)}$$

we have the temporal Fourier transform of Eq. (A-5) as

$$U(x,w) = \int_{-\infty}^{\infty} \exp[j(\omega_o t - k_o x)] \exp(-j\omega t)\, dt$$

$$= \delta(\omega-\omega_o) \exp(-jk_o x) \qquad \text{(A-6)}$$

while the spatial Fourier transform of Eq.(A-5) as

$$U(k,t) = \int_{-\infty}^{\infty} \exp[j(\omega_o t - k_o x)] \exp(jkx)\, dx$$

$$= \delta(k - k_o) \exp(j\omega_o t) \qquad \text{(A-7)}$$

where

$$\delta(\omega-\omega_o) = \int_{-\infty}^{\infty} \exp[-j(\omega-\omega_o)\, t]$$

$$\delta(k-k_o) = \int_{-\infty}^{\infty} \exp[j(k-k_o)\, x] \ .$$

For the case of finitely limited time and space, a sinusoidal wave has the form

$$u(x,t) = \begin{cases} \exp[j(\omega_o t - k_o x)] & -T \le t \le T,\ -L \le x \le L \\ 0 & \text{elsewhere.} \end{cases} \qquad \text{(A-8)}$$

Then, the temporal Fourier transform of Eq.(A-8) is

$$U(x,\omega) = \int_{-T}^{T} \exp[j(\omega_o t - k_o x)]\ \exp(-j\omega t)\, dt$$

$$= \exp(-jk_o x) \int_{-T}^{T} \exp\{-j(\omega-\omega_o)]\, dt$$

$$= (2T)\,((\sin((\omega-\omega_o)T))/((\omega-\omega_o)T))\,\exp(-jk_ox) \quad \text{(A-9)}$$

while the spatial Fourier transform of Eq. (A-8) is

$$U(k,t) = \int_{-L}^{L} \exp[j(\omega_o t - k_o x)]\,\exp(jkx)\,dx$$

$$= \exp(j\omega_o t) \int_{-L}^{L} \exp[j(k-k_o)x]\,dx$$

$$= (2L)\,((\sin((k-k_o)L))/((k-k_o)L))\,\exp(j\omega_o t). \quad \text{(A-10)}$$

The graphs of the magnitudes of Eq. (A-9) and (A-10) are shown in Fig. A.2. From the graphs, we can see that although the major contribution comes from the frequencies and wavenumbers around ω_o and k_o, respectively, they take infinite number of frequencies to represent a sinusoidal wave of finite extent. As T becomes larger, the height of the main lobe (which equals $(2\pi/T)$) becomes smaller. In the limit as $T \to \infty$ we obtain the delta function $\delta(\omega-\omega_o)$. Also, the longer the harmonic wave is in space, the smaller the range of wavenumbers is required to specify the wave.
In the limit as $L \to \infty$ we obtain the delta function $\delta(k-k_o)$.

In summary, we have the resolution limits $\Delta\omega = (2\pi/T)$ for frequency and $\Delta k = (2\pi/L)$ for wavenumber. These results often hold for other waves, i.e., waves that

are non-sinusoidal, and have important consequences in wave propagation.

For the one-dimensional case we have

$$u(x,t) = \exp[j(\omega t - kx)]$$

traveling along the x-axis with a velocity $(dx/dt)=c$ equal to the phase velocity $c_p = (\omega/k)$. Now in three-dimensions a sinusoidal wave has the form

$$u(x,y,z,t) = \exp[j(\omega t - k_x x - k_y y - k_z z)]$$

$$= \exp[j(\omega t - \mathbf{k}\cdot\mathbf{r})] \ . \qquad \text{(A-11)}$$

Defining $\varphi = \varphi(x,y,z,t) = \omega t - \mathbf{k}\cdot\mathbf{r}$

$$= \omega t - k_x x - k_y y - k_z z \ , \qquad \text{(A-12)}$$

we have

$$\mathbf{k}\cdot\mathbf{r}(t) = \omega t - \theta = \text{constant} \qquad \text{(A-13)}$$

for a given φ and fixed t .

Therefore,

$$\mathbf{k}\cdot\mathbf{r} = \text{constant}$$

represents a plane perpendicular to the direction of $\mathbf{k}$ (see Fig. A-1).

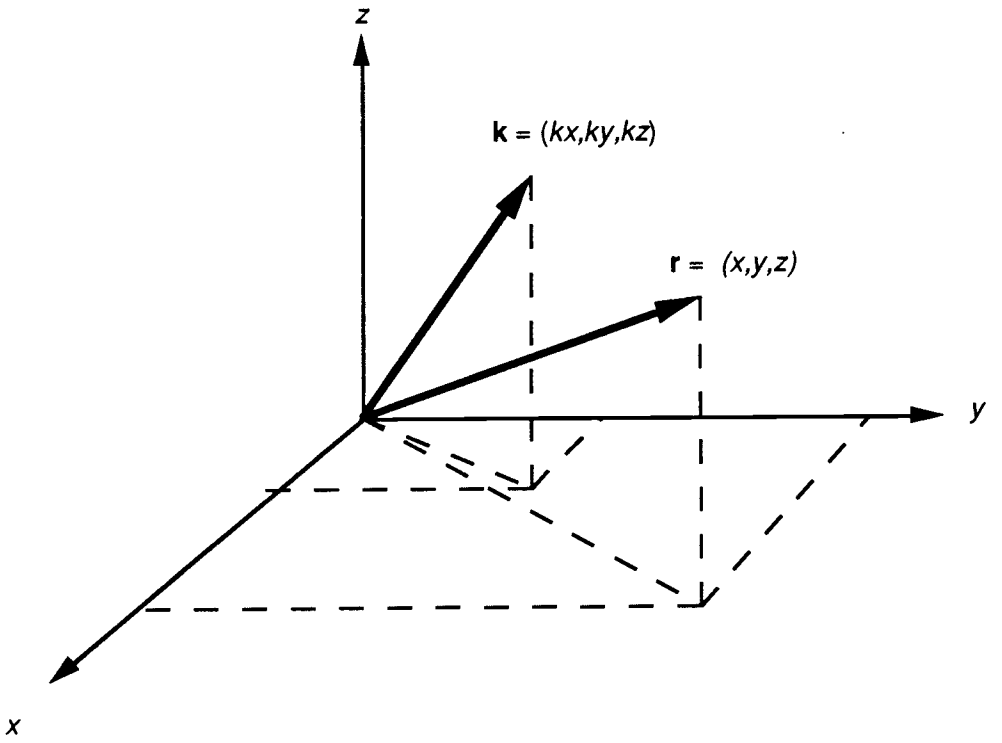

Fig. A-1 Graphical Expression for $\mathbf{k}\cdot\mathbf{r}$.

$$k = |\mathbf{k}| = (k_x^2 + k_y^2 + k_z^2)^{1/2}$$

$$r = |\mathbf{r}| = (x^2 + y^2 + z^2)^{1/2} .$$

There are other planes in space for which the value of the complex exponential

$$\exp[-j(\mathbf{k}\cdot\mathbf{r}(t))] \qquad \text{(A-14)}$$

is the same. An example of giving the value of Eq. (A-14) is the plane

$$\mathbf{k}\cdot\mathbf{r}'(t) = \omega t - \varphi + 2\pi = \text{constant} . \qquad \text{(A-15)}$$

This is so because harmonic functions whose planes differ by 2π have the same value.

The distance between the planes given by Eq. (A-13)

and (A-15) is

$$(\mathbf{k}/k)\cdot\mathbf{r}' = (\mathbf{k}/k)\cdot\mathbf{r}$$

$$= ((\omega t - \varphi + 2\pi)/k) - ((\omega t - \varphi)/k)$$

$$= (2\pi/k) = \lambda$$

where $(\mathbf{k}/k)$ is a unit vector in the direction of $\mathbf{k}$, and λ is the wavelength of the sinusoidal wave.

Thus the surfaces, for which the complex exponential Eq.(A-14) has the same value, are a set of planes perpendicular to the direction of $\mathbf{k}$ and separated by the wavelength λ of the harmonic wave of Eq.(A-11). For this reason, the sinusoidal wave

$$\exp[j(\omega t - \mathbf{k}\cdot\mathbf{r})]$$

is said to be a plane wave and the plane surfaces are referred to as the wavefronts.

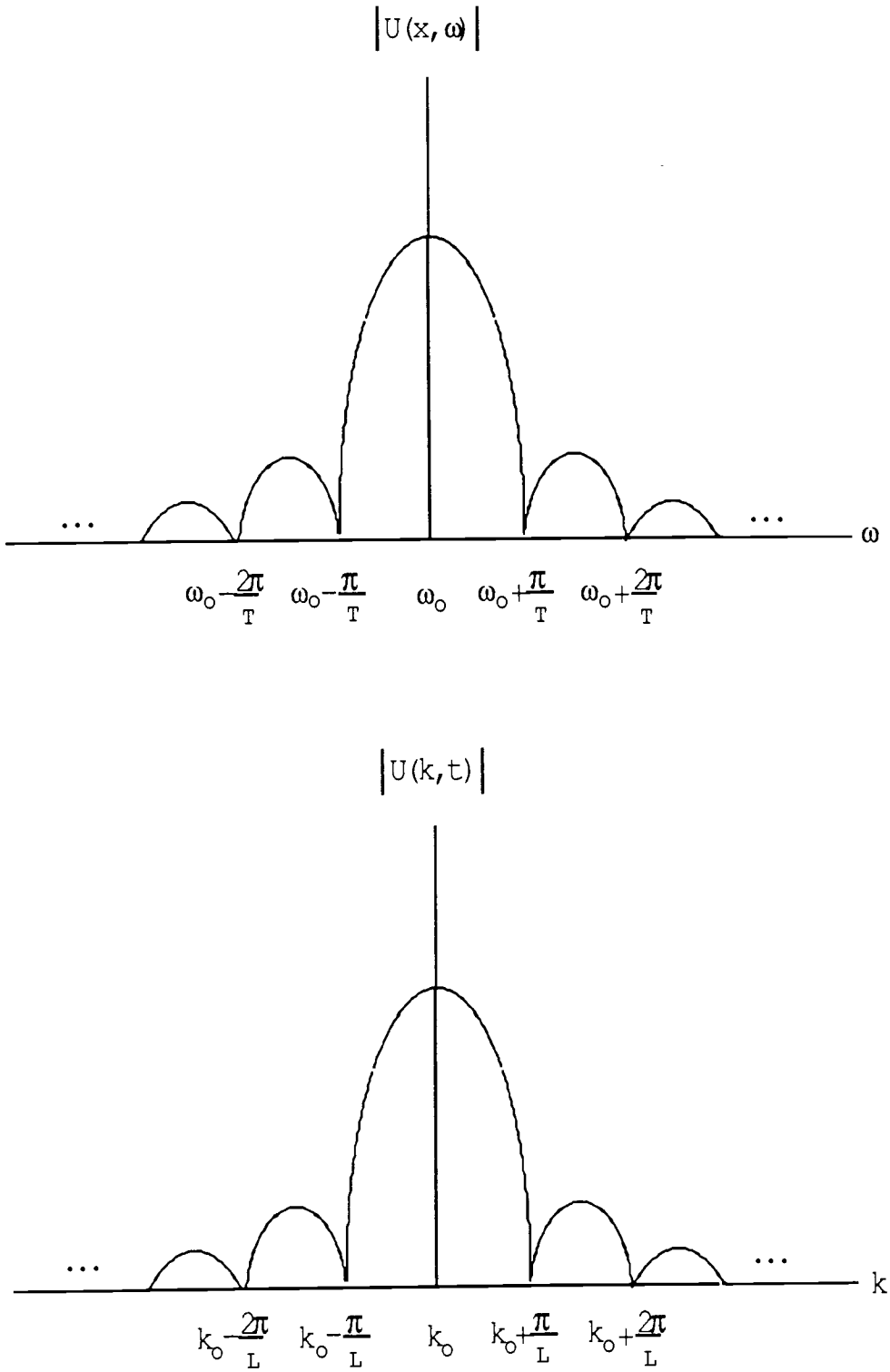

Fig. A-2 Magnitudes of Eq. (A-9) and Eq. (A-10), respectively.

APPENDIX B

EXPRESSION FOR GENERALLY CORRELATED NOISES [25]

This appendix shows how to obtain correlated random noises instead of statistically independent random noises. The correlated random noises can be derived from statistically independent ones by a linear transformation. For $\mathbf{X}^T = [X_1(t), \cdots, X_Q(t)]$ which is an Q x 1 Gaussian random vector with $\mu_{\mathbf{X}}{}^T = [0, \ldots, 0]$ and $\mathrm{Cov}(\mathbf{X}) = \mathbf{I}$ as possibly obtained from the program of Gaussian random number Generator, an Q x 1 Gaussian random vector $\mathbf{Y}$ with $\mu_{\mathbf{Y}}{}^T = [\mu_1, \mu_2, \ldots, \mu_Q]$ and $\mathrm{Cov}(\mathbf{Y}) =$

$$\begin{pmatrix} \sigma_{11} & \sigma_{12} & \cdots & \sigma_{1Q} \\ \sigma_{21} & \sigma_{22} & \cdots & \sigma_{2Q} \\ \vdots & \vdots & & \vdots \\ \sigma_{1Q} & \sigma_{2Q} & \cdots & \sigma_{QQ} \end{pmatrix}$$

can be obtained by the linear transformation

$$\mathbf{Y} = \mathbf{TX} + \mu_{\mathbf{Y}} \tag{B-1}$$

where

$\mathbf{T}$ is a lower triangular matrix given as

$$\mathbf{T} = \begin{bmatrix} t_{11} & 0 & . & . & 0 \\ t_{21} & t_{22} & . & . & 0 \\ . & . & & . & . \\ . & . & & . & . \\ t_{q1} & t_{q2} & . & . & t_{qq} \end{bmatrix}$$

Eq. (B-1) is valid only if Cov(**Y**) is a positive definite matrix, but it is sufficient to obtain a modified **T** if Cov(**Y**) is only positive semi-definite matrix. The elements of **T** are obtained by

$$\text{Cov}(\mathbf{Y}) = \mathbf{T}\ \text{Cov}(\mathbf{X})\,\mathbf{T}^T = \mathbf{T}\mathbf{I}^T\mathbf{T} = \mathbf{T}\mathbf{T}^T.$$

Going across the first row of **T** and the first column of $\mathbf{T}^T$ yields the element

$$t_{11}^2 = \sigma_{11} \quad \text{or} \quad t_{11} = (\sigma_{11})^{1/2}$$

and across the first row of **T** and the ith column of $\mathbf{T}^T$ gives the element

$$t_{11}t_{i1} = \sigma_{i1} \quad \text{or} \quad t_{i1} = \sigma_{i1} / (\sigma_{11})^{1/2}.$$

Going across the second row of **T** and the second column of $\mathbf{T}^T$ yields

$$t_{21}^2 + t_{22}^2 = \sigma_{22} \quad \text{or} \quad t_{22} = (\sigma_{22} - t_{21}^2)^{1/2}$$

and across the second row of **T** and the ith column of $\mathbf{T}^T$ gives

$$t_{21}t_{i1} + t_{22}t_{i2} = \sigma_{i2} \quad \text{or} \quad t_{i2} = (\sigma_{i2} - t_{21}t_{i1})/t_{22}\ .$$

This is continued for the third row, fourth row, up to Qth row. Combining these results, the t_{ij}'s are obtained as

$$t_{i1} = \sigma_{i1} / (\sigma_{11})^{1/2} , \quad i = 1,. . .,Q \tag{B-2}$$

$$t_{jj} = (\sigma_{jj} - \sum_{k=1}^{j-1} t_{jk}^2)^{1/2} \tag{B-3}$$

$$t_{ij} = 0 , \quad i = 1,. . .,j-1 \tag{B-4}$$

$$t_{ij} = \frac{\sigma_{ij} - \sum_{k=1}^{j-1} t_{jk}t_{ik}}{t_{jj}} , \quad i = j+1,. . .,Q \tag{B-5}$$

for $j = 2,. . .,Q$.

This method of obtaining correlated random noises from statistically independent random noises is called "the square root method" or "Cholesky's method". This method can be used for any random noises with the given mean vector and covariance matrix, not even for the Gaussian random noises.

Example B.1 Let $\mathbf{X}$ be a 3 x 1 real Gaussian random vector with $\mu_x = [0,0,0]$ and $\mathrm{Cov}(\mathbf{X}) = \mathbf{I}_3$. Then, a 3 x 1 real Gaussian random vector with $\mu_y{}^T = [0,0,0]$ and

$$\text{Cov}(\mathbf{Y}) = \begin{bmatrix} 1 & \rho & \rho \\ \rho & 1 & \rho \\ \rho & \rho & 1 \end{bmatrix},$$

where $0 \leq \rho < 1$, can be obtained as follows:

The t_{ij}'s are calculated as

$$t_{11} = \sigma_{11} / (\sigma_{11})^{1/2} = 1 ,$$

$$t_{21} = \sigma_{21} / (\sigma_{11})^{1/2} = \rho ,$$

$$t_{31} = \sigma_{31} / (\sigma_{11})^{1/2} = \rho ,$$

$$t_{22} = (\sigma_{22} - t_{21}^2)^{1/2} = (1 - \rho^2)^{1/2} ,$$

$$t_{32} = (\sigma_{32} - t_{21} t_{31}) / t_{22} = (\rho - \rho^2) / (1 - \rho^2)^{1/2} ,$$

$$t_{33} = (\sigma_{33} - t_{31}^2 - t_{32}^2)^{1/2}$$

$$= (1 - \rho^2 - (\rho^2 (1 - \rho)^2 / (1 - \rho^2)))^{1/2} ,$$

to yield

$$\mathbf{T} = \begin{bmatrix} t_{11} & 0 & 0 \\ t_{21} & t_{22} & 0 \\ t_{31} & t_{32} & t_{33} \end{bmatrix}.$$

Then, using Eq.(B-1), the correlated random matrix $\mathbf{Y}$ is obtained as

$$\mathbf{Y} = \begin{bmatrix} Y_1 \\ Y_2 \\ Y_3 \end{bmatrix} = \begin{bmatrix} t_{11} & 0 & 0 \\ t_{21} & t_{22} & 0 \\ t_{31} & t_{32} & t_{33} \end{bmatrix} \begin{bmatrix} X_1 \\ X_2 \\ X_3 \end{bmatrix}$$

$$= \begin{pmatrix} t_{11}X_1 \\ t_{21}X_1 + t_{22}X_2 \\ t_{31}X_1 + t_{32}X_2 + t_{33}X_3 \end{pmatrix} .$$